

INFORMATION TO USERS

This reproduction was made from a copy of a document sent to us for microfilming. While the most advanced technology has been used to photograph and reproduce this document, the quality of the reproduction is heavily dependent upon the quality of the material submitted.

The following explanation of techniques is provided to help clarify markings or notations which may appear on this reproduction.

1. The sign or "target" for pages apparently lacking from the document photographed is "Missing Page(s)". If it was possible to obtain the missing page(s) or section, they are spliced into the film along with adjacent pages. This may have necessitated cutting through an image and duplicating adjacent pages to assure complete continuity.
2. When an image on the film is obliterated with a round black mark, it is an indication of either blurred copy because of movement during exposure, duplicate copy, or copyrighted materials that should not have been filmed. For blurred pages, a good image of the page can be found in the adjacent frame. If copyrighted materials were deleted, a target note will appear listing the pages in the adjacent frame.
3. When a map, drawing or chart, etc., is part of the material being photographed, a definite method of "sectioning" the material has been followed. It is customary to begin filming at the upper left hand corner of a large sheet and to continue from left to right in equal sections with small overlaps. If necessary, sectioning is continued again—beginning below the first row and continuing on until complete.
4. For illustrations that cannot be satisfactorily reproduced by xerographic means, photographic prints can be purchased at additional cost and inserted into your xerographic copy. These prints are available upon request from the Dissertations Customer Services Department.
5. Some pages in any document may have indistinct print. In all cases the best available copy has been filmed.

**University
Microfilms
International**

300 N. Zeeb Road
Ann Arbor, MI 48106

8306719

Dejbakhsh, Haydeh

NUCLEAR SPECTROSCOPY OF NEUTRON-RICH ODD-A NUCLEI

The University of Oklahoma

PH.D. 1982

**University
Microfilms
International** 300 N. Zeeb Road, Ann Arbor, MI 48106

**UNIVERSITY OF OKLAHOMA
GRADUATE COLLEGE**

**NUCLEAR SPECTROSCOPY OF NEUTRON-RICH
ODD-A NUCLEI**

**A DISSERTATION
SUBMITTED TO THE GRADUATE FACULTY
in partial fulfillment of the requirements for the
degree of
DOCTOR OF PHILOSOPHY**

**BY
HAYDEH DEJBAKHSH**

Norman, Oklahoma

December 1982

**NUCLEAR SPECTROSCOPY OF NEUTRON-RICH
ODD-A NUCLEI**

APPROVED BY

Robert J. Beatty

Ryan J. Dreyer

W. S. Eickbush

John D. Haffner

Charles W. Terrell

DISSERTATION COMMITTEE

PREFACE

The work described here in this thesis was done at the Brookhaven National Laboratory, New York, and the University of Oklahoma, under the supervision of Dr. Robert F. Petry. The experiment was done with the assistance of Dr. M. Shmid from the BNL group. During the period October 1979 to June 1982 the author spent a great deal of time at the laboratory and acknowledges the support of all members of the BNL nuclear physics group throughout her work.

The author believes this work is original and has not been submitted previously for a degree at the university.

TABLE OF CONTENTS

| | Page |
|--|------|
| PREFACE | iii |
| LIST OF TABLES | vii |
| LIST OF FIGURES | viii |
| ACKNOWLEDGEMENTS | xi |
| Chapter | |
| I. INTRODUCTION | 1 |
| II. THEORETICAL CONSIDERATIONS | 15 |
| 2.1. Introduction | 15 |
| 2.2. Gamma Transitions | 15 |
| 2.3. Single Particle Shell Model | 20 |
| 2.3.1. A Shell Model Description of Nuclear Deformation | 24 |
| 2.4. Collective Nuclear Motion | 29 |
| 2.5. Interacting Boson Model | 34 |
| 2.5.1. Transitional Nuclei | 40 |

| | Page |
|--|-------------|
| III. EXPERIMENTAL CONSIDERATIONS | 43 |
| 3.1. Introduction | 43 |
| 3.2. THE BNL Facility TRISTAN | 43 |
| 3.2.1. Ion Source and Target | 45 |
| 3.2.2. Mass Separator | 50 |
| 3.2.3. Moving Tape Collector | 51 |
| 3.3. Experimental Arrangement | 53 |
| 3.3.1. Singles and Multiscale Systems | 54 |
| 3.3.2. Coincidence Electronics | 57 |
| 3.3.3. Data Acquisition System | 61 |
| 3.4. Experimental Procedures | 63 |
| 3.4.1. Source Optimization | 63 |
| 3.4.2. Intensity and Energy Determination Procedures | 64 |
| 3.4.3. Beta Decay Half-Lives | 65 |
| IV. DATA ANALYSIS | 69 |
| 4.1. Introduction | 69 |
| 4.2. Peak Identification and Half-Lives | 71 |
| 4.3. Energies and Intensities | 75 |
| 4.3.1. Statistical Errors | 77 |
| 4.4. Gamma-Gamma Coincidences | 81 |

| | Page |
|--|-------------|
| 4.5. Construction of Level Schemes | 82 |
| 4.6. Spin and Parity Assignments | 82 |
| V. EXPERIMENTAL RESULTS | 85 |
| 5.1. ^{89}Sr | 85 |
| 5.2. ^{145}Cs | 119 |
| 5.3. ^{147}La | 146 |
| VI. DISCUSSION | 157 |
| 6.1. Introduction | 157 |
| 6.2. The Onset of Deformation in $A \sim 100$ Region | 157 |
| 6.3. The Onset of Deformation in $A \sim 150$ Region | 165 |
| 6.4. Conclusion | 174 |
| REFERENCES | 176 |
| APPENDIX A | 183 |
| APPENDIX B | 188 |

LIST OF TABLES

| | Page |
|---|------|
| 3.1. Half-Lives of the Isobaric Chain $A=99$ | 66 |
| 3.2. Half-Lives of the Isobaric Chains $A=145,147$ | 66 |
| 5.1. Measured Energies and Intensities of γ -Ray Transitions in ^{90}Sr β -Decay | 93 |
| 5.2. Comparison of Gamma-Ray Intensities in ^{90}Sr Decay with Previous Work | 98 |
| 5.3. Coincidence Relationships of γ -Rays Studied in ^{90}Sr Decay . . | 100 |
| 5.4. Energies and Intensities of the γ -Ray Transitions in ^{145}Cs Decay | 127 |
| 5.5. Coincidence Relationships of γ -Rays Studied in ^{145}Cs Decay . | 132 |
| 5.6. Measured Energies and Intensities of γ -Rays in ^{147}La Decay . . | 149 |
| 5.7. Coincidence Relationships of γ -Rays Studied in ^{147}La Decay . | 153 |

LIST OF FIGURES

| | Page |
|--|------|
| 1.1. Chart of the Nuclides | 2 |
| 1.2. Level Systematics for the Sm Isotopes [taken from Ref. 45] | 8 |
| 1.3. Level Systematics of Even-Even Mo, Zr, Sr Isotopes [taken from Ref. 45] | 11 |
| 2.1. Cascade Transition | 19 |
| 2.2. Shell Model Diagram of Nuclear Level System with Spin-Orbit Coupling [taken from Ref. 47] | 22 |
| 2.3. Experimental Spectra of ^{20}O and ^{20}Ne . In the ^{20}Ne spectrum levels with heavy lines belong to the rotational band [taken from Ref. 1] | 26 |
| 2.4. Single Particle Levels Appropriate to a Description of Nuclei in the $A=100$ Region | 28 |
| 2.5. The Ground-State Rotational Band of ^{169}Dy [taken from Ref. 59] | 33 |

| | Page |
|--|------|
| 2.6. The Low-Energy States of ^{108}Pd [taken from Ref. 26] | 33 |
| 2.7. Nilsson Diagram for Protons or Neutrons with the $Z \leq 50$ | 35 |
| 2.8. An Example of $SU(5)$ Symmetry: $^{110}_{48}\text{Cd}$, $N=7$ [taken from Ref. 6] | 39 |
| 2.9. An Example of an $SU(3)$ Symmetry: $^{156}_{64}\text{Gd}$, $N=12$ [taken from Ref. 6] | 39 |
| 2.10. An Example of an $O(6)$ Symmetry: $^{196}_{78}\text{Pt}$, $N=6$ [taken from Ref. 6] | 39 |
| 3.1. Schematic Diagram of TRISTAN at the HFBR | 44 |
| 3.2. Schematic Diagram of the Positive Surface Ionization Source at TRISTAN | 46 |
| 3.3. Direct Production Rates of Nuclides Measured at TRISTAN [taken from Ref. 73] | 48 |
| 3.4. Fission Product Yield from ^{235}U for Thermal Neutron Fission | 49 |
| 3.5. Moving Tape Collector System and Two Detector | 52 |
| 3.6. Block Diagram of Gamma Single Electronics | 55 |
| 3.7. Electronic Setup of the Gamma-Gamma Coincidence System | 58 |

| | Page |
|---|---------|
| 3.8. A Gated Time Spectrum Showing the FWHM of the Coincidence Peak | 60 |
| 3.9.a. Structure of the Data Acquisition System | 62 |
| 3.9.b. Gamma-Gamma-Time Coincidence Analyzer Interface | 62 |
| 4.1. Structure of the Data Analysis System at BNL | 70 |
| 4.2. Decay Curve of the 536-keV Transition in ^{90}Sr Decay with and without Correction for ^{90}Y Decay | 73 |
| 4.3. Efficiency Curve for a Ge(Li) Detector | 78 |
| 5.1. Decay Curve of ^{90}Sr Transitions | 86 |
| 5.2 a-f. Gamma Spectrum from ^{90}Sr Decay | 87-92 |
| 5.3. Peak Fitting for the 120-130-keV Region in Gamma Spectrum of ^{90}Sr | 96 |
| 5.4. Decay Scheme of ^{90}Sr | 99 |
| 5.5 a-c. Spectrum in Coincidence with the 125-keV Transition in ^{90}Sr | 103-105 |
| 5.6 a-d. Spectrum in Coincidence with the 536-keV Transition in ^{90}Sr | 108-111 |

| | Page |
|---|---------|
| 5.7. Spectrum in Coincidence with the 462-keV Transition in ^{88}Sr . | 113 |
| 5.8. Spectrum in Coincidence with the 1198-keV Transition in ^{88}Sr . | 116 |
| 5.9. Spectrum in Coincidence with the 1619-keV Transition in ^{88}Sr . | 117 |
| 5.10. Spectrum in Coincidence with the 1744-keV Transition in ^{88}Sr | 118 |
| 5.11. The Decay Curve of the 175-keV Transition in ^{145}Cs | 120 |
| 5.12 a-e. Gamma Spectrum from ^{145}Cs Decay | 121-125 |
| 5.13 a,b. Decay Scheme of ^{145}Cs | 130-131 |
| 5.14 a-c. Spectrum in Coincidence with the 112-keV Transition in ^{145}Cs | 135-137 |
| 5.15 a-c. Spectrum in Coincidence with the 175-keV Transition in ^{145}Cs | 140-142 |
| 5.16 a-c. Spectrum in Coincidence with the 199-keV Transition in ^{145}Cs | 143-145 |
| 5.17. Decay Curves of Some ^{147}La Transitions | 147 |
| 5.18. Gamma Spectrum from ^{147}La Decay | 148 |
| 5.19. Decay Scheme of ^{147}La | 152 |

| | Page |
|---|------|
| 5.20. Spectrum in Coincidence with the 117-keV Transition in ^{147}La | 155 |
| 6.1. Systematics of E_{2^+} versus Neutron Number in the $A \simeq 100$ Region | 159 |
| 6.2. Level Systematics for Odd-A Yttrium Isotopes | 160 |
| 6.3. Nilsson Diagram for Protons or Neutrons with the $Z \leq 50$ | 162 |
| 6.4. Level Systematics for Odd-A Nuclei with $N=60$ | 164 |
| 6.5. Experimental and Calculated Ground-State Rotational Band in the ^{90}Y [Lohngren-Josef data] | 166 |
| 6.6. Systematics for Odd-A Ba Isotopes | 168 |
| 6.7. Systematics of Odd-A Cerium Isotopes | 169 |
| 6.8. Systematics for $N=89$ Isotones | 170 |
| 6.9. Nilsson Diagram for Neutrons, $82 \leq N \leq 126$ | 172 |
| B-1. Function Used for Peak Fitting | 190 |
| B-2. An Example of Peak Fitting for 530–537-keV Region in ^{90}Sr Decay | 191 |

| | Page |
|---|------|
| 5.20. Spectrum in Coincidence with the 117-keV Transition in ^{147}La | 155 |
| 6.1. Systematics of $E_{2_1^+}$ versus Neutron Number in the $A \simeq 100$ Region | 159 |
| 6.2. Level Systematics for Odd- A Yttrium Isotopes | 160 |
| 6.3. Nilsson Diagram for Protons or Neutrons with the $Z \leq 50$. . . | 162 |
| 6.4. Level Systematics for Odd- A Nuclei with $N=60$ | 164 |
| 6.5. Experimental and Calculated Ground-State Rotational Band in the ^{90}Y [Lohngren-Josef data] | 166 |
| 6.6. Systematics for Odd- A Ba Isotopes | 168 |
| 6.7. Systematics of Odd- A Cerium Isotopes | 169 |
| 6.8. Systematics for $N=89$ Isotones | 170 |
| 6.9. Nilsson Diagram for Neutrons, $82 \leq N \leq 126$ | 172 |
| B-1. Function Used for Peak Fitting | 190 |
| B-2. An Example of Peak Fitting for 530–537-keV Region in ^{90}Sr Decay | 191 |

ACKNOWLEDGEMENTS

The author would like to express her appreciation and thanks to any individual who helped me through the past few years. In particular I would like to thank:

Dr. R. F. Petry for suggesting the topic of the thesis and for his involvement, support and guidance throughout the project.

Dr. R. F. Casten, for his guidance and useful discussions on nuclear structure theory.

Dr. M. Shmid, for his help and contributions during experiments and running TRISTAN and also many political discussions and arguments.

All TRISTAN group members at BNL who kept the machine and computer facility running, and also computer experts and operators at the University of Oklahoma.

And finally I would like to thank my parents, Mr. and Mrs. Dejbakhsh, who by their encouragement and support made possible for me that which is rarely accessible to any woman in that nation.

NUCLEAR SPECTROSCOPY OF NEUTRON-RICH

ODD-A NUCLEI

CHAPTER I

INTRODUCTION

In the present work the beta decays of three neutron-rich odd-A nuclides were studied. These nuclides are ^{99}Sr , ^{145}Cs , and ^{147}La , and are shown in the chart of nuclides in Figure 1.1. These nuclides are obtained as fission products of ^{235}U , and as the figure shows they lie far from the line of beta stability. The study of the decay of these nuclides is difficult because of the low fission yield, short half-lives, and difficulty in producing them. Therefore, little or no work has previously been performed on them. Fission produces a large group of neutron-rich isotopes, and the technology has become available in recent years to construct an on-line fission product mass separator, which could separate rare isotopes and produce sources pure and strong enough for detailed spectroscopic investigation. The activity for the present work was produced by the on-line mass separator TRISTAN at Brookhaven National Laboratory.

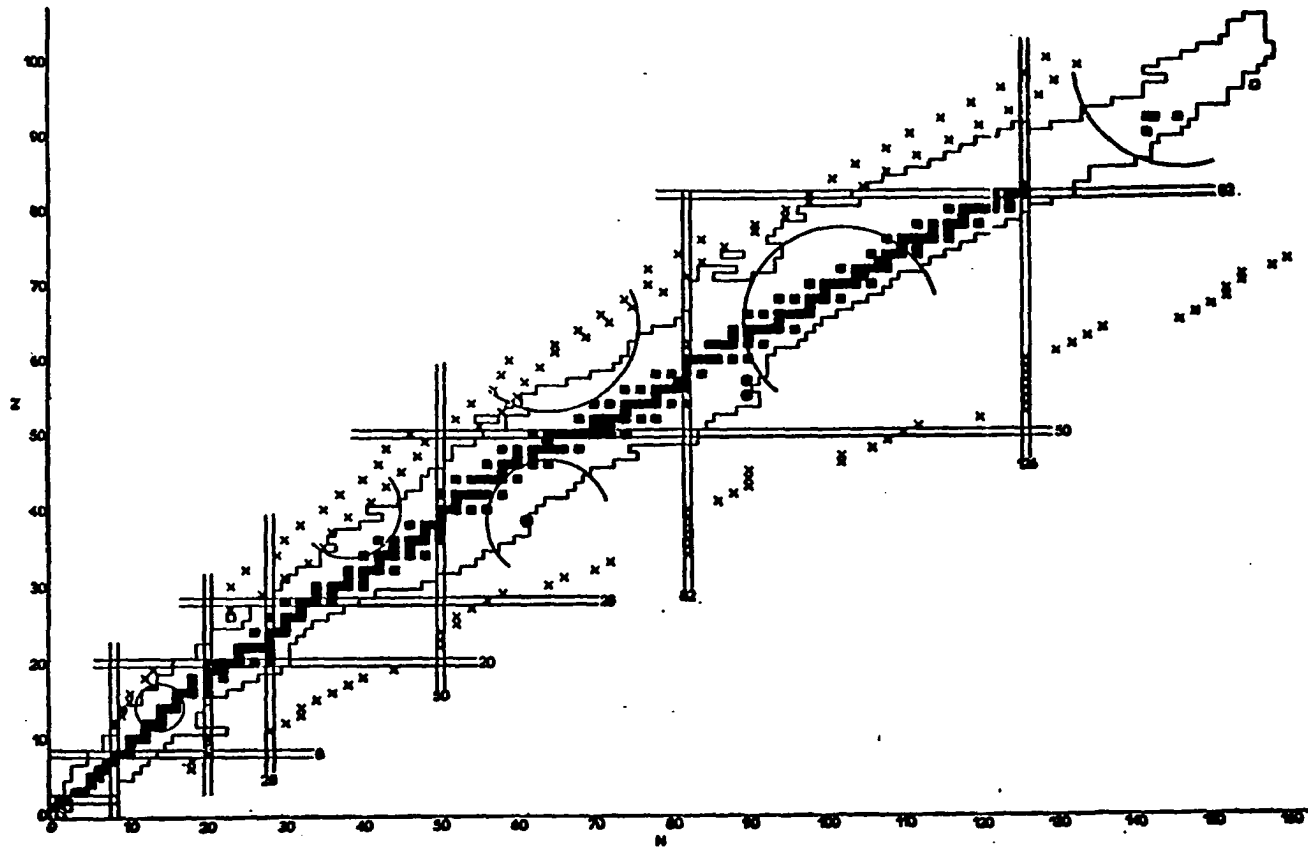


Figure 1.1. Chart of the Nuclides, Showing ^{89}Sr , ^{145}Cs and ^{147}La Place with Solid Circle in the Chart, Particle Drip-Line Predictions, Magic Nucleon Numbers and The Region of Deformation .

Since the first International Conference on Nuclei Far From Stability was held in Lysekil, Sweden, in 1966, a great deal of progress has been made in this field which has expanded our knowledge and understanding of nuclear structure. The need and reasons for studying these nuclei were discussed by I. Bergstrom at that conference.¹⁴ The purposes of the conference were to examine the scientific justification for studying these nuclides and to review new ways of producing them. The argument for justifying the study of nuclides far from stability is that the study of these nuclides leads to information on new doubly magic regions, new regions of deformation, highly excited states populated by beta decay, Q values on the edges of the mass shell, and delayed neutron and proton emission.

For concrete knowledge about the nucleus, experimental information is necessary, and the study of different radioactive decay modes provides a useful tool for investigating nuclear properties. These nuclides can be produced by fission, spallation or heavy ion reactions. The means of producing nuclides far from stability were discussed at that conference, and the on-line isotope separator system (ISOL) was one approach which was considered. At that time only two such systems were in existence, ISOLDE at Cern in Geneva and TRISTAN at Ames, which was scheduled to begin operation later that year. It was hoped that this conference would stimulate the activities in this field. Since then the subject of nuclei far from stability has been the topic of several international conferences. The

most recent one was at Helsingor, Denmark (1981).³³ A new generation of on-line isotope separators, along with new experimental techniques, is in operation at different reactors and accelerators around the world. The name and location of these (ISOL) systems can be found in reference 84. At the third conference³⁰ on nuclei far from stability, the progress which had been made in developing the on-line system, as well as target ion sources to produce the new nuclei was discussed. Also the fast progress which has been made in this field was reported. Because of the decision to close the reactor at Ames, it was decided to move TRISTAN to Brookhaven National Laboratory in 1978. TRISTAN now is on-line at the High-Flux Beam Reactor. It has been upgraded and a new target ion source has been developed for this system. The results of studies done on TRISTAN were reported at the Fourth Conference at Helsingor.⁷¹ In this conference it was reported that progress in technology made it possible to study the nuclei very far from stability with half-lives as short as 50 msec. It showed the advancement which has been achieved in nuclear spectroscopy.

The reason for studying nuclides far from beta stability is to advance the knowledge and understanding of nuclear systematics to aid in the development of nuclear structure theories as applied to transitional regions. Present knowledge of nuclear physics leads one to believe that a nucleus consists of many nucleons, each interacting with all the others, and moving within a complex structure. Many nuclear models have been

proposed, each with a certain set of parameters. In the successful models most properties of a nucleus can be extracted from these parameters.

In the shell model nucleons are assumed to move in stationary orbits with fixed angular momentum. These orbits form a series of discrete energy levels. Whenever there is a large gap in the spacing of the energy levels, corresponding discontinuities appear in certain nuclear properties such as binding energy, capture cross-section, and angular momentum. The groups of levels between these gaps are known as shells. In a shell model, the nucleons in a closed shell are considered to be paired together to form an inert core with zero angular momentum, and all properties of the nucleus are due to particles in unfilled shells. The shell model has been most successful for nuclei with only a few nucleons beyond closed shells. In the simplest form of the shell model, called the single particle shell model (SPSM), no interaction among the particles outside closed shells is assumed. This model applies only to odd-A nuclides, and it is assumed that the nuclear properties are due only to the last unpaired nucleon. In a more realistic form of the shell model, the residual interactions among the particles outside the closed shells are properly taken into account. This model is a basis for all nuclear theory, and it is assumed to be an exact microscopic model.

For nuclei with nucleon numbers midway between closed shells, the lowering states often are described fully as collective in nature, which is to say that single particles move in their orbits in a correlated manner to form a constant or slowly changing shape. In the Bohr-Mottelson²⁰ collective model the nucleus is treated as a deformable liquid drop. Nuclei with a few particles outside a closed shell are described as vibrating about a spherical equilibrium shape. As the number of nucleons outside the closed shell is increased, which means going away from the closed shell, the sphere becomes deformed and after passing through the transitional region the nucleus is considered to be a permanently deformed rotating spheroid. This model gives good agreement with experimental data for near spherical and well deformed nuclei. For nuclei in the transitional region the model does rather poorly because the nuclear shape is not well defined, and the calculation is based on the perturbation of one of these limiting cases. The single-particle shell model predictions of static quadrupole moments for nuclei are completely off. Therefore this model cannot describe the deformed nuclei and cannot be appropriate for all nuclei, because the approximation would seem to be unreasonable in the presence of a strong short range nucleon-nucleon force. The Bohr-Mottelson liquid-drop model can describe properties of deformed nuclei very well, but it can hardly predict the discontinuities associated with the magic numbers. These two models do poorly in transitional regions, so it is clear that in the prediction

of even a main feature of nuclear structure, a model must be considerably more complicated than either of these extreme cases (spherical and deformed nuclei). A classical example of a deformed region is the rare-earth region with $A=150$ to 190 . It has been studied very well because the line of stability passes through the middle of this region (see Figure 1.1). The solid squares in figure 1.1 show the stable nuclides. Since these nuclides are on or close to the stability line their half-lives are long enough to make the access and investigation of them easier. The lowering of the 2_1^+ level energies in even-even nuclei and the increase in the ratio of the 4_1^+ to 2_1^+ states are the main characteristics of the deformed nuclides. The large quadrupole moments are another feature. The Sm isotopes are a classic example of a transition between a vibrational spectrum (^{148}Sm) and the spectrum of a good axial rotor (^{156}Sm). In the vibrational limit the 0_2^+ , 4_1^+ and 2_2^+ levels lie quite close together at approximately twice the energy of the 2_1^+ state. The rotational limit is quite different and 0_2^+ and 2_2^+ lie relatively high in spectrum. Figure 1.2 shows the lowering of 2_1^+ states in Sm isotopes. The ratio of 4_1^+ to 2_1^+ energy levels has been increased. This experimental data shows the clear and smooth shape transition in Sm isotopes as a function of neutron numbers. Figure 1.2 shows that the transition occurs for neutron number $N=88$ to 90 for Sm isotopes. In the rare-earth region nuclei with proton number $Z=58$ to 64 , the transition occurs for neutron number $N=88$ to 90 . It has become

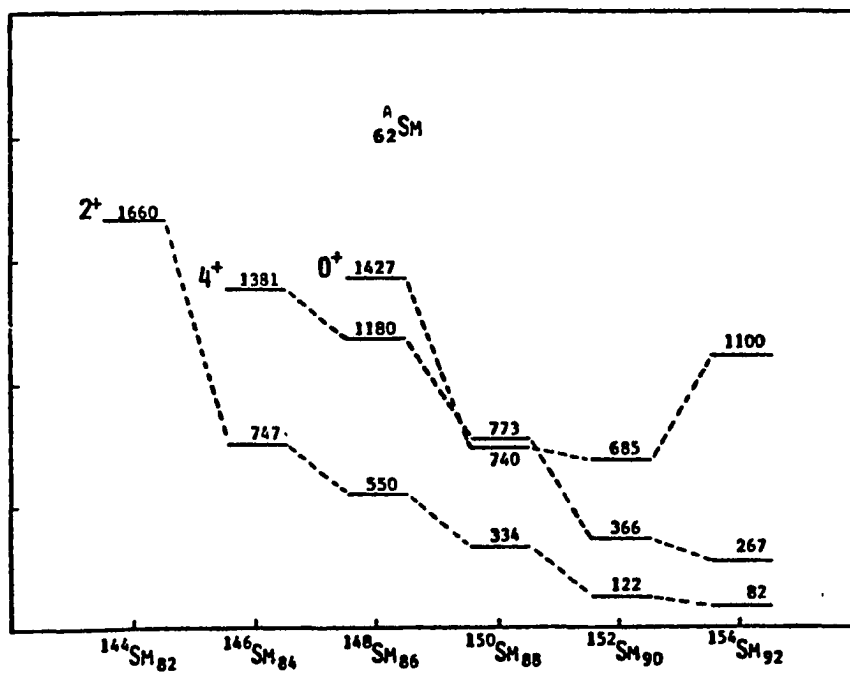


Figure 1.2. Level Systematics for the Sm Isotopes [Ref. 45]

clear that the development of a model which can do well in transitional nuclei as well as in extreme cases is very important. The experimental information of transitional nuclides is extremely helpful for such a development.

In recent years a new model has been proposed by Arima and Iachello.³⁸ This model tries to describe the collective structure of nuclei with $A > 100$ over a very broad region. In this model, particles outside closed shells are coupled together in pairs to form bosons which then can interact with each other. The model is called the Interacting Boson Model (IBM). The model is based on group theory, and the group structure corresponds to a unitary group $SU(6)$. In three special cases an analytic solution to the Hamiltonian exists, corresponding to the subgroups $SU(5)$, $SU(3)$, and $O(6)$. The $SU(5)$ and $SU(3)$ symmetries correspond to an anharmonic vibrator and an axial rotor respectively (cases studied by Bohr and Mottelson), and $O(6)$ corresponds to the γ -unstable model of Wilets and Jean.⁸³ One of the main features of this model is the fact that it can treat shape transitions from one limiting case to another, for example the transition from the $SU(5)$ limit to the $SU(3)$ limit. The Hamiltonian for transitional nuclei is solved numerically. The IBM appears to describe the transitional nuclei as easily as those in the limiting cases; this is one of the most important features of the IBM. This model gives good agreement with experimental results in transitional nuclei in the mass 150 region.³⁸

Deformation in s - d shell nuclei with $8 < Z < 20$ and $8 < N < 20$ has been known for quite some time.⁸³ Because the number of nucleons outside the closed shell is small, shell model calculations are possible. Careful investigation of this region revealed the origin of deformation. In 1962 Talmi⁷⁸ showed that $1d_{5/2}$ and $1d_{3/2}$ spin-orbit partner orbitals played an important role in deforming the nucleus in the $(2S-1d)$ shell. The nuclear deformation in the $(2S-1d)$ shell arises from the $T=0$ component of nuclear forces. In other words, when protons and neutrons simultaneously occupied the spin orbit partner orbital with a very large spatial overlap, such as the $1d_{5/2}$ and $1d_{3/2}$, then n - p interaction, which is responsible for deformation, overcomes the n - n and p - p pairing forces which favor sphericity. The n - p interaction provides the necessary condition for deformation in this region.

A few years ago a new region of deformation was discovered for nuclei in the mass region of $A \sim 100$.^{12,70} The experimental data for Zr and Mo isotopes exhibit a clear and smooth shape transition as a function of the neutron number similar to that observed in the rare earth region. The new region at one end includes nuclei like ^{88}Sr , ^{90}Zr and ^{92}Mo that can be described in terms of simple shell-model configurations,¹³ and at the other end it also includes excellent examples of rotational nuclei like ^{100}Sr , ^{102}Zr , and ^{104}Mo . Figure 1.3 shows the systematics of these isotopes. The systematics show the drastic lowering of the 2_1^+ energy level and the increase in the 4_1^+ to 2_1^+ energy ratio especially for ^{98}Zr to ^{100}Zr and ^{96}Sr

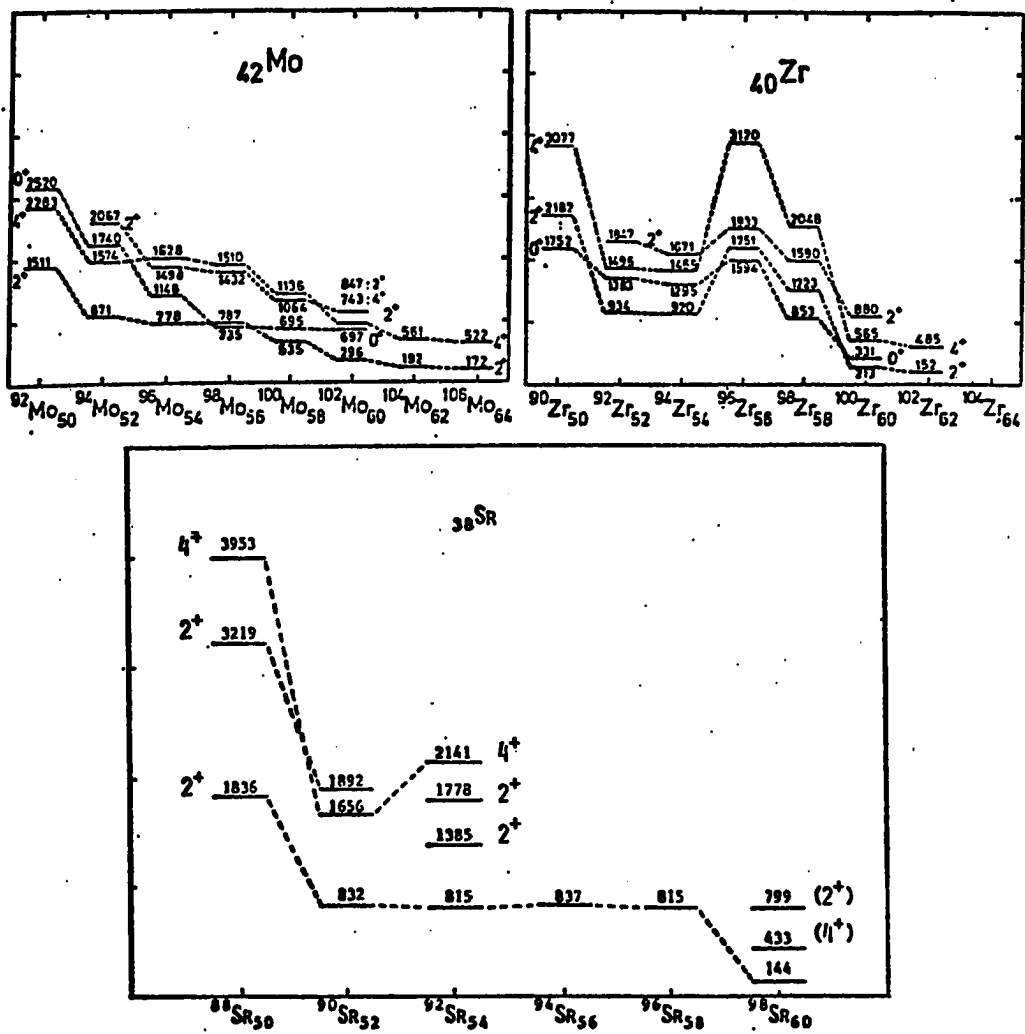


Figure 1.3. Level Systematics of Even-Even Mo, Zr, Sr Isotopes [Ref. 45]

to ^{98}Sr . As was mentioned earlier for Sm isotopes this transition was very smooth (see Figure 1.2).

Microscopic shell model calculations have been carried out in this region by Federman and Pittel.^{31,32} As in the *s-d* shell nuclei they succeeded in explaining the shape transition in terms of the residual neutron-proton force. They postulate that even in neutron-rich nuclei, deformation arises from the $^3\text{S}_1$ component of the *n-p* force, and they demonstrated (for Zr and Mo isotopes) that the *n-p* interaction is largest and most effective in its deforming tendency when the particles are in spin-orbit partner orbits of large spatial overlap. In such orbits the *n-p* force effectively counteracts the *n-n* and *p-p* forces which are responsible for sphericity. Thus in this region the shell model calculation seems to describe the systematics in Zr and Mo isotopes and suggests the relation between the strength of the *n-p* interaction and the onset of deformation. It is of great interest that the same mechanism has also been shown to be important for nuclear deformation in the framework of the interacting boson model.⁹ Therefore it is very important to test the model in the new region in which no information or very little has been available.

Most of the experimental data and theoretical calculations in this region are for even-even nuclei ($^{98-98}\text{Sr}$, $^{88-98-100}\text{Zr}^{42}$ and also $^{102-104}\text{Mo}^{24}$). There is not much information on odd-*A* nuclei in this region, and for a

better understanding of the transitional region more spectroscopic work is needed. Experimental data is needed on odd- A nuclei such as ^{89}Y , which lies in the transitional region having a sharp transition from spherical to deformed shape when the number of neutrons goes from 58 to 60 (such as $^{98}_{46}\text{Zr}$ to ^{100}Zr and $^{96}_{38}\text{Sr}$ to ^{98}Sr). ^{89}Y can be viewed as a proton hole and the deformed ^{100}Zr core, or a proton particle and a ^{98}Sr core. In either case, one can expect to observe the characteristics of a deformed nucleus for ^{89}Y . The study of the beta decay of ^{99}Sr to levels of ^{89}Y provides detailed information on the level structure of ^{89}Y . Since the level structure of ^{95}Y and ^{97}Y is known, a clear picture of the single particle states is contained in the systematics of these odd- A nuclides.

The two other nuclei studied in this work, ^{145}Cs and ^{147}La , lie in another interesting region around $A \sim 150$. The study of the beta decay of ^{145}Cs to levels in ^{145}Ba and of the beta decay of ^{147}La to levels in ^{147}Ce will extend the knowledge in level systematics for $N = 89$ isotones to more neutron-rich isotopes just below the rare earth region. The slow regular decrease of the first excited 2^+ levels in the even-even nuclei in this transitional region around $N = 89$ suggests that the deformation appears very progressively, and a smooth behaviour of some levels in neighbouring odd nuclei may also be observed.

In Chapter II the theoretical aspects of this study will be discussed. Chapter III is devoted to the mass separator facility and the experimental setup and procedure. Analysis of the data will be explained in Chapter IV, and the results of the experiment are given in Chapter V. Experimental results and conclusions are discussed in Chapter VI.

CHAPTER II

THEORETICAL CONSIDERATIONS

2.1 Introduction

This thesis is an experimental result presentation, and a detailed theoretical discussion is out of place. However, since the theory is the basis for the interpretation of experimental results the general discussion of the gamma transitions and nuclear structure theory necessary for interpreting the results of this work is given in this chapter.

2.2 Gamma Transitions

In this section an introduction to multipole radiation is given. A full discussion of the theory is given by Jackson³⁹ and Sakurai⁶² where a full quantum mechanical treatment of the problem is undertaken. Any distribution of electric charge produces an electric potential which at a large distance R can be written as follows:

$$V = 4\pi \sum_{\lambda, \mu} \frac{1}{2\lambda + 1} \left[\int Y_{\lambda\mu}^*(\theta', \phi') r'^{\lambda} \rho(r') dv' \right] \frac{Y_{\lambda\mu}(\theta, \phi)}{R^{\lambda+1}} \quad (2.1)$$

The first term ($\lambda = \mu = 0$) is just the net charge, the second ($\lambda = 1, \mu = 0, 1$) and third ($\lambda = 2, \mu = 0, 1, 2$) terms are known as dipole and

quadrupole terms respectively. The series rapidly converges due to its $1/R^n$ dependence. Electric radiation fields are produced by the oscillations of such a charge distribution and magnetic radiation is caused by oscillations in the current density. These oscillations can be expressed as the sum of oscillations in each term of the expansion and the resulting radiation can be thought of as being made of various associated multipole components. In particular a given term in the expansion may be predominant and the radiation can be described as being of that multipolarity.

Now consider the de-excitation of an excited nucleus by γ -ray emission. The transition probability between the initial and final states is given by Fermi's golden rule

$$T = \frac{2\pi}{h} |\langle I_f m_f | H_{\text{int}} | I_i m_i \rangle|^2 \frac{d\rho}{dE} \quad (2.2)$$

For an electric or magnetic transition of multipolarity λ the relevant operators for H_{int} are given by:

$$H_{\text{int}} = \mathcal{J}_N \bar{A}_{\lambda\mu}^{(\pi)} \quad (2.3)$$

where \mathcal{J}_N is the nuclear current operator, $\pi = E$ or M for electric and magnetic transitions respectively, λ is the total angular momentum, μ is the z component of λ , and $\bar{A}_{\lambda\mu}^{(\pi)}$ are given by

$$\bar{A}_{\lambda\mu}^{(M)} = i^\lambda \frac{\bar{\lambda}}{(\lambda(\lambda+1))^{1/2}} j_\lambda(\kappa r) Y_{\lambda\mu}(\theta, \phi) \quad (2.4)$$

$$A_{\lambda\mu}^{(E)} = \frac{i^\lambda}{\kappa} \frac{\vec{\nabla} \times \vec{\lambda}}{(\lambda(\lambda+1))^{1/2}} j_\lambda(\kappa r) Y_{\lambda\mu}(\theta, \phi) \quad (2.5)$$

where $j_\lambda(\kappa r)$ are spherical Bessel functions, κ is the transition energy (in units of mc^2) and $Y_{\lambda\mu}$ are spherical harmonics.⁷¹

We are now considering individual quanta and it can be shown⁷¹ that a γ -ray related to the operator $A_{\lambda\mu}^{(\pi)}$ will carry away angular momentum λ with z component μ . Conservation of angular momentum implies that in the transition between two states with known spin quantum number $I_i m_i$ and $I_f m_f$, only those specific $A_{\lambda\mu}^{(\pi)}$ operators have non-zero matrix elements for which

$$|I_i - I_f| \leq \lambda \leq I_i + I_f$$

and

$$\mu = m_f - m_i.$$

In the case of electric transitions the 2λ -pole operators will only connect states of opposite parities and for magnetic transitions states of the same parity are connected by odd λ . [Nuclear states are assumed to have definite parity—the strong force conserves parity.] In the SPSM the *single particle* transition matrix elements for electric transitions are approximately 10^2 of the order of magnitude greater than that of magnetic transitions of the same multipolarity.⁷¹

We usually need only to consider the lowest multipole order al-

lowed by conservation of angular momentum and parity, because the magnitude of the probability drops by $\sim 10^3$ order from one multipole to the next higher multipole. The E_1 , M_1 and E_2 are the dominant multipolarities, but in some cases due to angular momentum selection rule some of these multipolarities may be forbidden.

It can be seen that the operators $A_{\lambda\mu}^{(\pi)}$ have explicit dependency on the direction of the emission of the gamma-ray with respect to the nuclear spin axis through the $Y_{\lambda\mu}(\theta, \phi)$. The γ - γ directional correlation experiment is based on the above fact. Performance of this type of experiment can lead to the spin assignments for some low-lying states in the nuclei. To do the angular correlation experiment the nuclei must decay through a cascade of two or more radiations. The correlation function $W(\theta)$ depends on the spins of the states involved I_i, I, I_f and on the multipolarities of the transitions γ_1 and γ_2 (see Figure 2.1). When an excited nucleus decays to its ground state through a cascade of two gamma-rays, the probability of the second gamma-ray being emitted at an angle θ with respect to first one is given by:

$$W(\theta) = \sum_k B_k(\gamma_1) A_k(\gamma_2) P_k(\cos \theta) \quad (2.6)$$

where P_k is the k^{th} order of Legendre polynomial. $B_k(\gamma_1)$ is dependent on the initial and final spin (I_i, I_f) of transitions concerned and $A_k(\gamma_2)$ is dependent on the multipole mixing ratio. A measurement of $W(\theta)$ provides

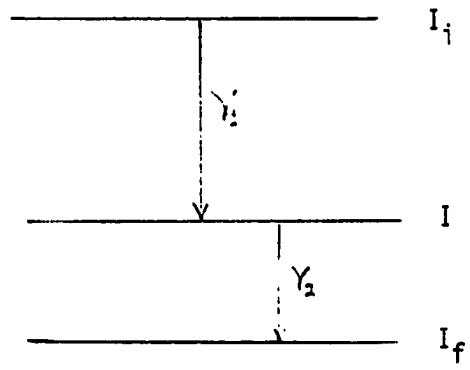


Figure 2.1. Cascade Transition

information on these quantities. The above picture is for the simplest case. If the intermediate state decays through different transitions the calculation becomes more complicated. A detailed discussion of angular correlations is outside the scope of this study; however, the interested reader is referred to reference 4.

2.3 Single Particle Shell Model

In the early history of nuclear physics the basic problems of nuclear structure were attacked with a relatively crude approximation. The reasons for this lie partly in the complexity of many particle structures and the incomplete knowledge of the nuclear forces. It was quite surprising that a very simple nuclear model turned out to be quite successful describing some of the nuclear properties of a great variety of nuclei. This approximate description of nuclear structure is the single-particle shell model (SPSM).

In this model the individual nucleons are considered to move in stationary orbits and are paired off in such a way that the values of nuclear parameters are determined only by a single unpaired nucleon. The model contains no correlated or collective motion of several nucleons and no reference to two body forces between nucleons. Furthermore, it applies only to odd- A nuclei. If each nucleon moves in a permanent orbit with fixed angular momentum, the force can be described by means of a central potential $v(r)$. In a central potential, the orbital angular momentum of each nucleon

is a constant of motion. For each quantum number L there is a series of energy levels, which is associated with quantum number n corresponding to the number of nodes of the radial wave function. For each level, there are $2L + 1$ degenerate substates corresponding to different orientations of the angular momentum, and according to the exclusion principle, each of the substates can contain at most two nucleons of each type. Wherever there is a large gap in the spacing of the energy levels, discontinuities appear in nuclear properties, such as binding energy, capture cross section, and angular momentum. The number of nucleons corresponding to these gaps or shells are called "magic". When only a central force is assumed, except for the first three the SPSM magic numbers were not the ones that were found in the experimental data. This leads to the need for an additional term originating from a spin-orbit interaction in the potential. The new Hamiltonian is written as:

$$H = H_0 + v_1(r)\vec{L} \cdot \vec{S} = \frac{-\hbar^2}{2m}\nabla^2 + V(r) + v_1(r)\vec{L} \cdot \vec{S} - cL^2. \quad (2.7)$$

The first term in the Hamiltonian is kinetic energy, the second term $V(r)$ is the central potential, the $\vec{L} \cdot \vec{S}$ term is the spin-orbit coupling, and the L^2 term only flattens the potential depth. This Hamiltonian then leads to magic numbers which are in agreement with experimental data. The energy levels of the first 126 nucleons in the simple shell model is given in Figure 2.2.

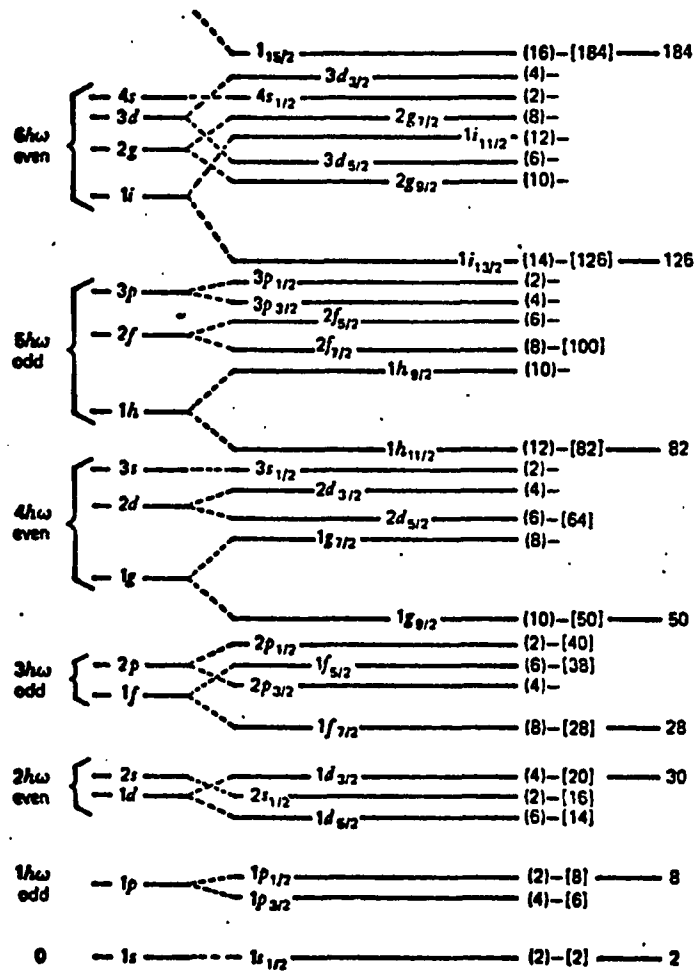


Figure 2.2. Shell Model Diagram of Nuclear Level System with Spin-Orbit Coupling [Ref. 47]

In the shell model, the nucleons in the ground state are assumed to be paired so that the nuclear properties are due to unpaired nucleons. The neutron and proton states fill independently. In this kind of system, every even-even nuclide has zero spin, and every odd- A nuclide has the angular momentum of the unpaired particle. For odd-odd nuclides, the prediction of angular momentum is not possible, because it is not obvious which of the different possible resultants from the coupling of the j -vectors of the two unpaired particles has the lowest energy. This model provides understanding of the parities and angular momenta of low-lying states of various odd- A nuclei.

In order to extend the shell model to more realistic calculation all particles outside a major closed shells (valence nucleons) must be included in the calculation with residual interaction among them. The interaction potential v_{ij} between valence particles in a shell is not necessarily the same as that in a free-particle system. A large part of the actual interaction is accounted for in the single particle shell model potential, which represents the average effect on one nucleon of all the other nucleons.

At this point it is convenient to discuss the symmetry of the nucleon wave function. The nucleon is represented as a particle of isospin $\frac{1}{2}$, which can exist in two states, the proton p and the neutron n , according to whether the i -spin points "up" or "down". The Fermion wave function, which is the product of space, spin, and i -spin functions, should be an-

tisymmetric under the interchange of all coordinates of any pair of nucleons as required by the exclusion principle.

Each particle has available only two i -spin states, and hence at most two particles can be in a given space state with same (n, l, j, m) . Thus there may be space-spin symmetric pairs which must be antisymmetric, in i -spin, which is a $T = 0$ state. When space-spin part of wave function is antisymmetric the i -spin wave function must be symmetric, which is a $T=1$ state. $T=1$ interactions are n - n or p - p pairing interaction which tend to produce a spherical nuclear shape. The $T=0$ or n - p interaction, because it is space antisymmetric, tends to produce a non-spherical nuclear shape.

2.3.1 A Shell Model Description of Nuclear Deformation

In a series of papers from 1977 through 1979 Federman and Pittell²⁹⁻³² tried to give a unified shell model description of nuclear deformation valid throughout the periodic table. The concept of deformation has been used to describe the collective properties of heavy nuclei.²⁰ It is generally known that deformation in neutron-rich heavy nuclei arises from the long-range (quadrupole) part of the effective nuclear force. But such a picture is not really microscopic. Unfortunately, any further microscopic insight into the structure of deformation in heavy nuclei (the insight that would accompany a shell-model study) is hindered by the complexity of the problem. It is therefore very convenient that deformation was observed in the region of light nuclei, namely in the $(2s-1d)$ shell, in which microscopic

shell-model calculations are possible. An example can show what has been learned about deformation from the $(2s - 1d)$ shell nuclei. The nucleus ^{20}Ne is a classical example of a rotational nucleus in the $(2s - 1d)$ shell. It consists of two neutrons and two protons outside the doubly magic ^{16}O core. By comparing the spectrum of ^{20}Ne with the one of ^{20}O , which has four neutrons outside ^{16}O , the evidence for deformation becomes clear (see Figure 2.3). The low-lying spectrum of ^{20}Ne looks rotational, but the one for ^{20}O shows no collective trend. This would indicate that the deformation in the light nuclei is due to the $T=0$ neutron-proton interaction. This will be explained in more detail in the next paragraph. When comparing the properties of ^{20}Ne and ^{20}O , it is clear that nuclear deformation arises from the isoscalar component of the nuclear force from $^3\text{S}_1$ component. In the $(2s - 1d)$ shell, for example, $T=0$ correlations between nucleons in the $1d_{5/2}$, $1d_{3/2}$ spin-orbit partner orbit and stretch-configuration correlation between nucleons in identical orbitals have been responsible for building up deformation in this region.

Some years ago a new region of deformation was discovered for nuclei in the mass region of $A \sim 100$, especially for the Zr and Mo isotopes. The nuclei in this region have the advantages of being both neutron-rich, like the heavy deformed nuclei, and still manageable for shell-model calculations. Federman and Pittel showed that the same picture based on the n - p correlation is valid also in this region. Their conclusions provide

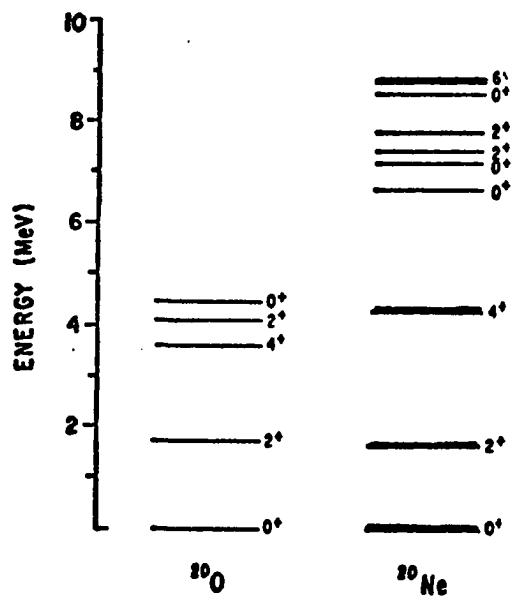


Figure 2.3. Experimental Spectra of ^{20}O and ^{20}Ne .
 In the ^{20}Ne spectrum levels with heavy lines belong to the
 ground state rotational band
 [taken from Ref. 1].

a unified description of nuclear deformation that seems to be valid for all regions in the periodic table, although the arguments for the $A \sim 150$ region are only qualitative since SM calculations are not possible. How can the shell model qualitatively tell about this $A \sim 100$ region of deformation? In Figure 2.4 the relevant single particle levels appropriate to a description of the Zr-Mo region are shown. In the purely independent-particle picture of these nuclides the $1g_{9/2}$ proton orbit is empty and $1g_{7/2}$ neutron orbit does not begin to fill until after $N=62$. However, the residual interaction between valence nucleons can modify the occupation probabilities of these orbitals. In this situation as neutron pairs are added (*e.g.*, the ^{95}Y , ^{97}Y , ^{99}Y sequence) the occupation of $1g_{7/2}$ neutron orbital increases and the strong overlap in the wavefunctions for spin orbit partner orbitals increases the probability for filling the $1g_{9/2}$ proton orbital. This n - p interaction is sufficiently strong to break the pairing correlations through a kind of polarization effect. This is analogous to the situation in the $(2s, 1d)$ shell which leads to deformation in the light deformed region. The n - p correlations thus provide the mechanism for deformation in the Zr and Mo isotopes. In heavier nuclei the situation is different. Because there are many close-lying orbitals for both neutrons and protons and shell effects are less important. Although the interaction between an arbitrary neutron-proton pair may not be as strong as the pairing interaction, the $(n$ - $p)$ interaction may still be dominant if there

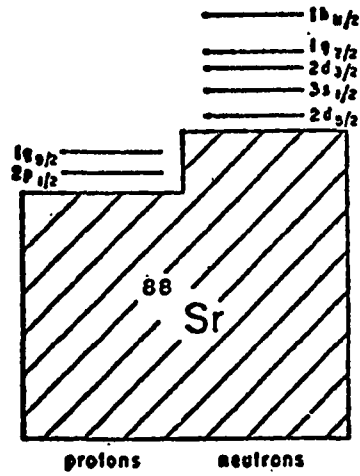


Figure 2.4. Single Particle Levels Appropriate to a Description of Nuclei in the $A=100$ Region

are a large number of valence protons and neutrons. The pairing interaction contributes to the total energy an amount which is roughly proportional to the number of valence protons plus neutrons ($N_p + N_n$), but the n - p interaction can be felt by any pair of neutrons and protons, and so it contributes to the total energy by amount roughly proportional to ($N_p \times N_n$). Therefore, even though the n - p interaction is not in general as strong as the pairing interaction, it can dominate for large N_p and N_n . Also, there are strong overlapping neutron and proton orbits which are available to valence nucleons in heavy nuclei, for example the $1h_{11/2}$ proton and $1h_{9/2}$ neutron in the rare-earth region. Qualitatively these partner orbits begin to fill very near the observed onset of deformation in the heavy regions. But the effect of partner orbitals may not be as important for deformation in heavy nuclei as for the lighter deformed regions. There has not been any quantitative investigation for heavy nuclei due to complexity of the problem. But the relative importance of these partner orbitals and the effect of single particle orbitals for producing deformation needs quantitative study.

2.4 Collective Nuclear Motion

The large quadrupole moments and the energy-level structure of some nuclei can neither be explained with the shell model nor in terms of a spherical drop of condensed matter. They require the assumption of collective motions and nonspherically symmetric deformations of the

potential well in which the individual independent particles move. The study of the collective motion of the center of mass may help us to understand some of the problems that arise in the study of the shell model. The nucleons at each moment form a pattern in space generally assumed to be ellipsoidal. The motion is collective if this pattern changes very slowly or is permanent. The particles move through many circuits of their orbits, but in a sufficiently correlated manner so that at all times the overall space pattern is essentially the same or slowly changing. Such a motion may be characterized by the coupling of particle motion and surface motion. Because the surface is distorted at some moment the potential felt by a particle is not spherically symmetric. In the nearly spherical nuclei, there is only a very weak coupling of this type. The particles have no directional correlation, and the resultant average shape is spherical. A nonspherical equilibrium shape may be thought of as arising as a result of the opposing tendencies of the outer nucleons to polarize the nuclear core and of the core to resist this polarization and maintain a spherical shape. This model was worked out by Bohr and Mottelson.²⁰

A spherical nucleus in the simplest model may be assumed to be a charged liquid drop, with its excitation modes arising from small oscillation about the equilibrium spherical shape. Shape changes can occur only under assumption of incompressibility (volume conservation). Bohr and Mottelson²⁰ developed a description of collective quadrupole states in

nuclei in terms of the concept of shape and its deformations. In this approach, one describes the nuclear surface by its radius:

$$R = R_0 \left[1 + \sum_{\mu} \alpha_{\mu} Y_{2\mu}(\Omega) \right] \quad (2.8)$$

and a crucial role is played by the five shape variables α_{μ} and the average radius R_0 . Instead of α_{μ} , one may employ an equivalent set of variables $\beta, \gamma, \theta_1, \theta_2, \theta_3$ (Bohr variables), by going from the laboratory frame to the body-fixed frame. Originally the Bohr and Mottelson model was mostly used for nuclei with a stable deformation with axial symmetry. However, it has been extended to other situations either in purely phenomenological fashion by Gneuss and Greiner³⁵ or in a more microscopic way by Kumar.⁴⁴ The motion in this model was described as oscillations of the nucleus as a whole around the equilibrium shape and rotations with preservation of shape and internal structure. Such oscillations and rotations are typically collective motions. For large deformations in nuclei away from magic numbers, the rotational states are lower in energy than the vibrational ones. In the case that the nucleus is rotating about an axis perpendicular to the axis of symmetry, the ground state rotational band has been seen. The energies at the levels in these bands follow closely the simple formula

$$E(J) = AJ(J + 1) + BJ^2(J + 1)^2. \quad (2.9)$$

The coefficients A and B (in keV) are determined from the first two excited

states. From the generally small value of B it has been realized that the energy can be approximated by the formula

$$E(J) = A'J(J + 1). \quad (2.10)$$

The ground state rotational band of ^{169}Dy spectrum is shown in Figure 2.5 along with a calculation based on Eq. (2.10).

The nucleus as a whole can oscillate as well as rotate, and the resulting collective vibrations are equivalent to the surface waves of the old liquid drop model. Dipole collective oscillations, which correspond to a displacement of the whole nucleus, cannot occur because of conservation of momentum, and the simplest oscillations have a quadrupole character. The excitation energies of the vibrational levels are evenly spaced. A typical example of a spectrum of an almost harmonic vibrator is provided by ^{108}Pd and is shown in Figure 2.6. The collective model has had considerable success in giving a description of deformation in heavy nuclei.

Further study and understanding of deformed odd- A nuclei became possible when a fundamental paper on this subject was written by Nilsson *et al.*⁵¹ He considered axially symmetric nuclei with a definite deformation. His Hamiltonian for this system consists of a simple harmonic oscillator potential and a spin-orbit term which contains a function of the coordinate which is not spherically symmetric. The energy eigenvalues for protons or neutrons $Z \leq 50$ as a function of the deformation parameter ϵ is

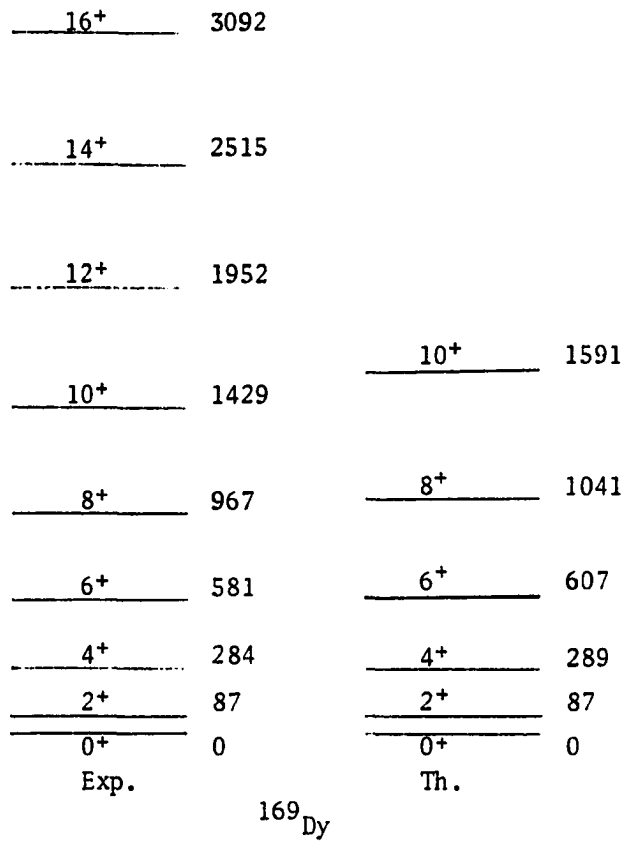


Figure 2.5. The Ground-State Rotational Band of ^{169}Dy [Ref. 59]

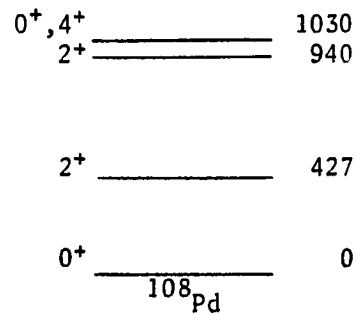


Figure 2.6. The Low-Energy States of ^{108}Pd [Ref. 26]

shown in Figure 2.7. The single particle energy levels and the removal of degeneracy of the SPSM levels can be seen in Figure 2.7 as a function of deformation also. It can be seen in this figure that the single J shells split into orbitals that are characterized by the projection of J onto the symmetry axis of the nucleons. J is no longer a good quantum number for $\epsilon \neq 0$ and is replaced by the projection quantum number K . This extension of the shell model to the deformed nuclei was very successful in describing the intrinsic non-collective states of these nuclei.²²

2.5 The Interacting Boson Model

The interacting boson model of Iachello and Arima^{4,5,7,38} is a different attempt to provide a unified description of the collective states of many nuclei. As mentioned earlier, it emphasizes the inherent symmetries of the nucleus rather than its geometrical properties. The microscopic basis for the model is currently being studied by Pittel *et al.*⁵⁸ and Otsuka^{9,54} and they hoped to be able to demonstrate the direct connection with the shell model, thus bridging the gap between the collective and single particle description of nuclei.

The basic model treats nucleons outside closed shells of an even-even nucleus as being paired together to form bosons with angular momentum $L=0$ and angular momentum $L=2$, known as s and d bosons. Bosons with higher angular momentum have been introduced, the $L=3$ f boson

to describe certain negative parity states, and the $L=4$ g boson, but most calculations have been done with only s and d bosons. The total number of bosons in a nucleus N is a constant and is made of N_π proton bosons and N_ν neutron bosons, where N_π is the number of pairs of protons or proton holes outside the nearest closed shell and similarly for N_ν . When the model called IBM1 was first introduced, there was no distinction between proton bosons and neutron bosons. Treating proton bosons and neutron bosons differently was brought up first by Arima *et al.*,^{8,54} and it has not yet been studied as completely as the IBM1.⁴ This second approach is called IBM2.

The Hamiltonian of IBM1⁵ can be written as:

$$H = \epsilon_s s^\dagger s + \epsilon_d \sum_m d_m^\dagger d + V \quad (2.11)$$

Where $s^\dagger s$ and $d^\dagger d$ are the boson creation and annihilation operators, and ϵ_s , ϵ_d are the s boson state and the d boson state energies, the sum is over the five $(2L+1)$ components of the d bosons state, and V is the interaction potential between bosons (boson interaction).

The five components of the d state, together with the single component of the S state span a vector space which provides a basis for the representation of the group $SU(6)$. The only representations allowed for bosons are the totally symmetric ones belonging to the partition N of $SU(6)$.

In the case where $\epsilon = \epsilon_d - \epsilon_s$ is much larger than the interaction potential V , the Hamiltonian is invariant under the transformation among the five components of the $L=2$ state. The eigenvalues and eigenstates depend only on the number of d bosons, and an approximately unbroken symmetry exists from the decomposition of $SU(6) \supset SU(5) \otimes U(1)$. Thus, the Hamiltonian and the energy eigenvalues are given by:

$$H = \epsilon_d d^\dagger d \quad (2.12)$$

$$E = n_d \epsilon \quad (2.13)$$

This is simply the spectrum of an harmonic oscillator. Figure 2.8 shows an example of $SU(5)$ symmetry.

Another symmetry case occurs when the boson energy ϵ is small and of the same order of magnitude as the matrix element of the interaction potential. This is especially true when eigenenergies ϵ_s, ϵ_d and the interaction matrix elements correspond to a quadrupole-quadrupole interaction

$$v = -\kappa \sum_{i,j} Q_i Q_j \quad (2.14)$$

where Q_i is the quadrupole moment of the i^{th} boson symmetry occurs, with a representation space for the groups $SU(6) \supset SU(3) \supset O(3)$. In the $SU(3)$ limit, the eigenvalue problem can be solved analytically. The Hamiltonian can be written:

$$H = -k \sum_{i,j} Q_i \cdot Q_j - k' \sum_{i,j} L_i \cdot L_j \quad (2.15)$$

where Q and L operators are given by:

$$Q = (d^\dagger s + s^\dagger d)^{(2)} + \chi (d^\dagger d)^{(2)} \quad (2.16)$$

$$L = (d^\dagger d)^{(1)} \quad (2.17)$$

The eigenvectors are characterized by quantum numbers:

$$| \lambda, \mu, \kappa, L, M \rangle$$

where (λ, μ) labels the representations of $SU(3)$, L and M are the angular momentum and its component on z direction and κ is another quantum number needed for state identification. The energy eigenvalues are given by:

$$E(\lambda, \mu, L) = \left(\frac{3}{4} k - k' \right) L(L+1) - kC(\lambda, \mu) \quad (2.20)$$

where $C(\lambda, \mu)$ is given by:

$$C(\lambda, \mu) = \lambda^2 + \mu^2 + \lambda\mu + 3(\lambda + \mu)$$

The $L(L+1)$ term in the energy eigenvalues is the same as those in the axial rotor limit of the geometrical model of Bohr and Mottelson.¹⁸ In this limit the 2^+ states of the β and γ vibrations are degenerate. A typical example of $SU(3)$ symmetry is the ^{156}Gd spectrum which is shown in Figure 2.9.

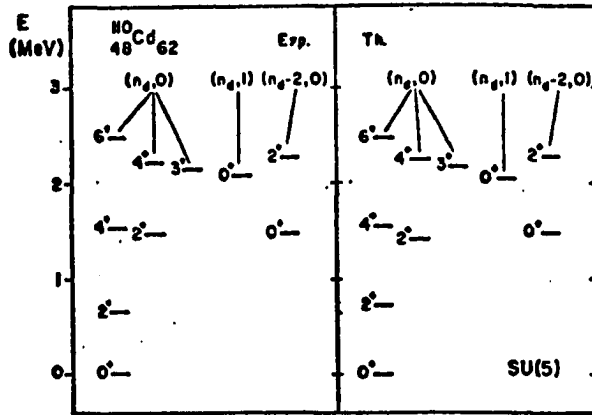


Figure 2.8. An Example of $SU(5)$ Symmetry: $^{110}_{48}\text{Cd}$, $N=7$ [Ref. 6]

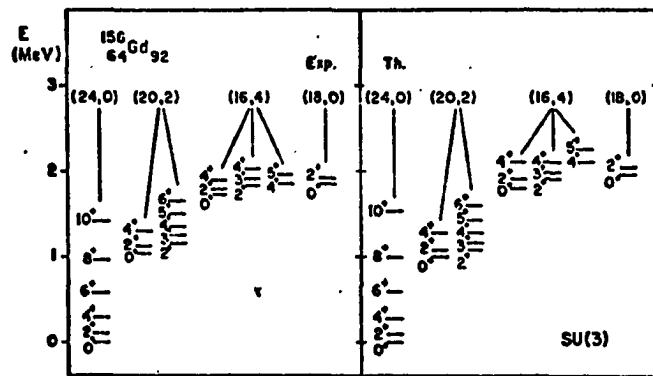


Figure 2.9. An Example of an $SU(3)$ Symmetry: $^{156}_{64}\text{Gd}$, $N=12$ taken from [Ref. 6]

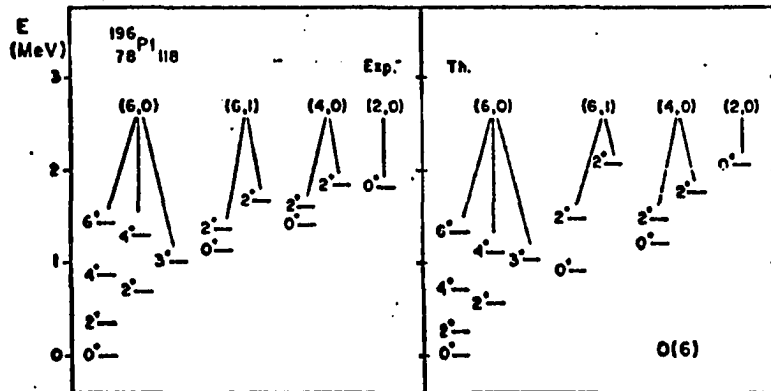


Figure 2.10. An Example of an $O(6)$ Symmetry: $^{196}_{78}\text{Pt}$, $N=6$ [taken from Ref. 6]

A third limiting case in this model was found to be $O(6)$ by Arima and Iachello.⁸ The Hamiltonian for this case is written by:

$$H = -k'' \sum_{i,j} P_i \cdot P_j \quad (2.19)$$

where P is the pairing operator. This limiting case corresponds to the triaxial rotor with $\gamma = 30^\circ$ or the γ unstable model. An example of the limiting case of $O(6)$ symmetry is the ^{196}Pt spectrum shown in Figure 2.10. Figures 2.8–2.10 demonstrate the excellent agreement between the experimental data and theoretical calculation for a wide variety of nuclei. The ability to account for the character and properties of such a broad range of nuclides is an unprecedented achievement for a model. It does this with a minimum of parameters, which usually vary smoothly across the region. In addition its ability to treat simply but successfully complex transitional regions is another feature of this model.

2.5.1 Transitional Nuclei

For a nucleus between any of the limiting cases, an analytical solution is not possible. In order to describe these “transitional” nuclei, the general Hamiltonian must be diagonalized numerically. The Hamiltonian can be written as:

$$\mathcal{H} = \epsilon n_d - kQ \cdot Q - k'L \cdot L - k''P \cdot P \quad (2.20)$$

The $P \cdot P$ pairing operator between bosons defined as:

$$P \cdot P = \frac{5}{2} [(d^\dagger d^\dagger)^{(0)}(dd)^{(0)} + \frac{1}{2} (s^\dagger s^\dagger)^{(0)}(ss)^{(0)}]^{(0)} \\ + \frac{5}{2} [(d^\dagger d^\dagger)^{(0)}(ss)^{(0)} + (s^\dagger s^\dagger)^{(0)}(dd)^{(0)}]^{(0)}$$

It is convenient to divide transitional nuclei into four different classes:

1. Nuclei with spectra intermediate between the $SU(5)$ and $SU(3)$ limit.
2. Nuclei with spectra intermediate between the $SU(3)$ and $O(6)$ limit.
3. Nuclei with spectra intermediate between the $O(6)$ and $SU(5)$ limit.
4. Nuclei with spectra intermediate among all three limiting cases.

Nuclei in the 4th group of transition are the most difficult to treat, because they require the use of all the operators in Eq. (2.20). The nuclei belonging to the transitional group of 1, 2 and 3 are easier to study. The transitional nuclei of group 1 were studied by Scholton, Iachello and Arima.⁶⁵ A study of the transitional nuclei in group 3 was done by Casten and Cizewski.²³ All the studies performed so far seem to indicate that the interacting boson model is able to account reasonably well for all situations observed in collective low-lying spectra of medium-mass and heavy nuclei. However, the interacting boson model provides a description of energy spectra and other properties in terms of some parameters that are fixed nucleus by nucleus. In a more fundamental approach, one would like to relate the parameters appearing in the boson Hamiltonian and other

operators to a microscopic theory of the nucleus, especially to the shell model.²⁶

The success and limitations of the interacting boson model for even-even nuclei brought about the attempt to investigate the odd- A nuclei based on this model. The interacting boson fermion model (IBFM) was developed a few years ago (1978).^{60,61} The Hamiltonian in this model consists of a boson part, a fermion part, and the interaction between them:

$$H = H_B + H_F + V_{BF} .$$

The solution to this problem is complex because of the interaction between bosons and fermions. Most of the study was done for unique parity orbits for which there was no interaction among the fermions. It has been quite successful for describing the level structure of odd- A nuclei such as odd- A Europium isotopes.⁶⁶ There have not been any IBFM calculations for odd- A nuclei performed in the light deformed or transitional regions in lower mass ranges. It is hoped that as more and more experimental data became available for lighter deformed region, theoretical calculations will be made for these nuclei also.

CHAPTER III

EXPERIMENTAL CONSIDERATIONS

3.1. Introduction

The nuclides studied in this work were produced by the on-line fission product mass separator TRISTAN at Brookhaven National Laboratory (BNL). The mass separator is operating on-line to the High Flux Beam Reactor (HFBR). A description of the system is given in Section 3.2. The various experimental configurations of gamma multi-scaling, coincidence and data collection systems are discussed in Section 3.3. Finally, the experimental procedures are described in Section 3.4.

3.2. The BNL TRISTAN Facility

On-line isotope separation is an essential tool for studying individual nuclei far from the beta stability line with very short half-lives, on the order of a second or less. The BNL on-line isotope separator TRISTAN is a facility which is connected to a fission source placed at an external beam port of the High Flux Beam Reactor.

The layout of the on-line mass separator is shown in Figure 3.1. The facility consists of a thermal neutron beam provided by the reactor,

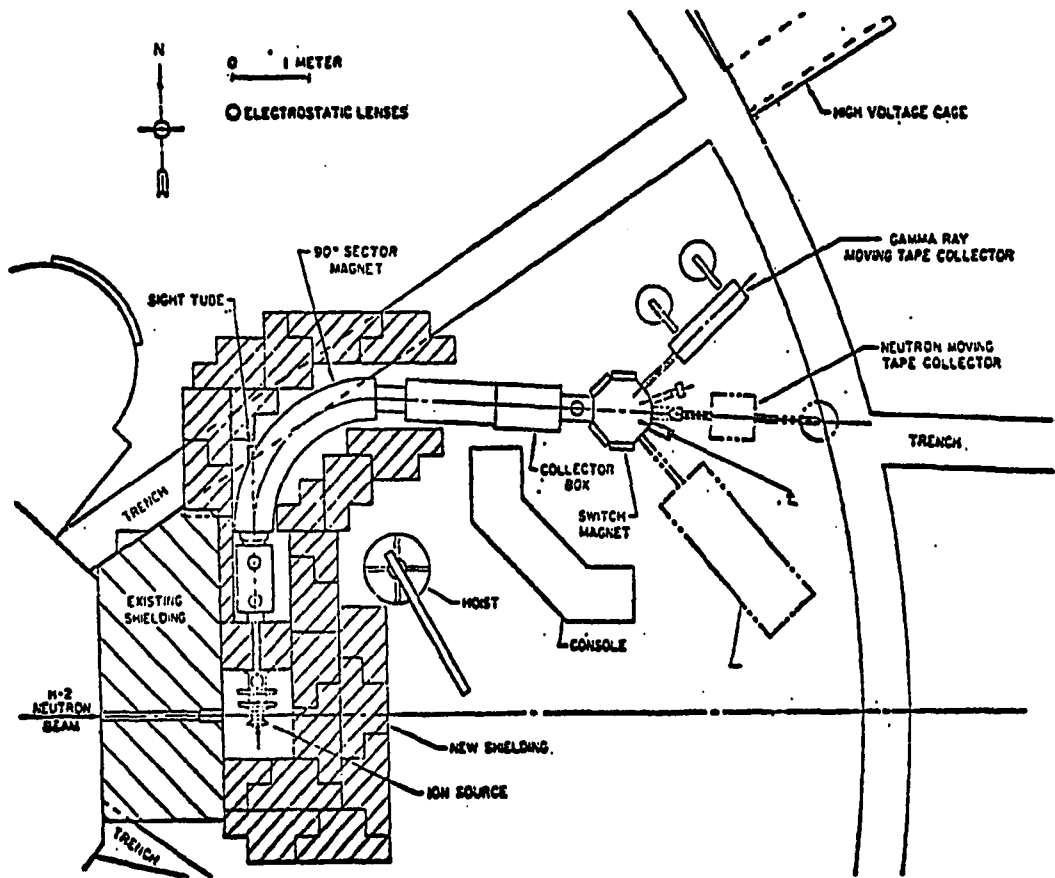


Figure 3.1. Schematic Diagram of TRISTAN at the EFBR

an integral target ion-source system, an extractor, lenses to focus the beam, a magnetic separator, and a switch magnet to guide the beam into one of the experimental stations. The mass separated ion beam is deposited on mylar tape in the Moving Tape Collector (MTC). A brief description of the system and ion-source which produced the nuclides in this study is given below. The full description of the system and the different types of ion-sources which have been developed is given in other references.^{25,34,48,77}

3.2.1. Ion Source and Target

The HFBR provides an external thermal neutron beam with a flux of 1.5×10^{10} neutrons per square centimeter per second on the target in the ion-source. The fission products are produced when thermal neutrons are absorbed by uranium-235 nuclei in the target. The nuclides in this study were produced by a positive surface ionization ion source which has been successfully operational since December 1980.

The ion source is a surface ionization type developed for TRIS-TAN to operate at temperatures as high as 2500° C.^{2,3,72,74} A diagram of the present version of the target ion-source can be seen in Figure 3.2. The target consists of graphite cloth impregnated with ~ 5 g of uranium-235 in the chemical form UO_2 inserted in a tantalum cylinder. The tantalum cylinder forms the heating chamber of the ion source, and it is exposed to the neutron beam. The fission products diffuse out of the target surface and pass into the ionizing chamber, where they are ionized on the surface

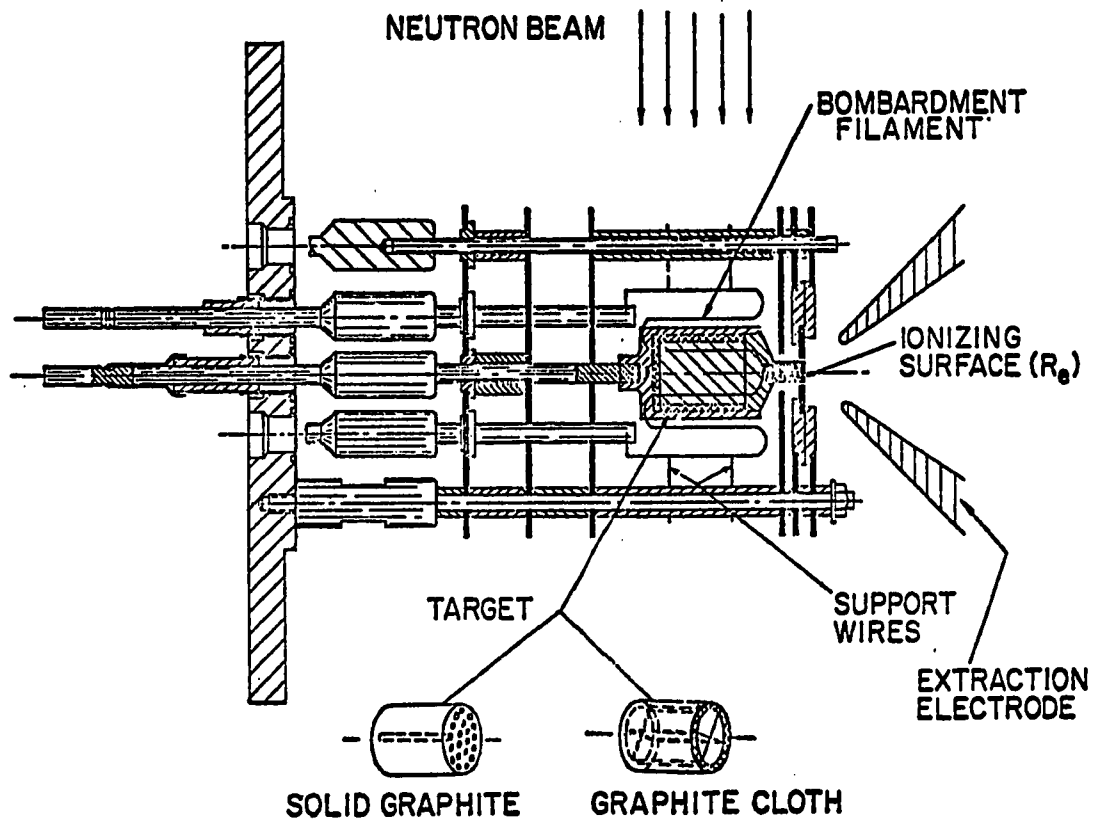


Figure 3.2. Schematic Diagram of the Positive Surface Ionization Source at TRISTAN

of a hot rhenium wire and extracted into the mass separator. This is effectively a chemical separation of the fission products, and also a few elements are ionized due to the relatively low ionization potential required for the surface ionization to occur.

Ion beams of the alkali elements Rb and Cs at the target temperature of 2000° C were obtained with a very short delay time between production and diffusion of the ions from the target surface. The alkaline earth elements (Sr and Ba) are produced with lower efficiency due to higher ionization potential and longer delay time. Using the Re wire as the surface ionization element increases the ionization efficiency for Sr and Ba. The direct production for masses in the range of $A = 141$ to 150 and $A = 84$ to 99 is shown in Figure 3.3. The production rate is not only a function of temperature and delay time for any element, it only depends on fission fragment yield (Figure 3.4) and the half-life of the nuclide. Figure 3.3 only shows elements which were extracted directly from separator. Other elements (such as La) were produced as daughter products.

The activity levels for ^{89}Sr and ^{147}La were low due to very low fission yields and production rates. In addition, the activity level dropped off considerably for these nuclides over a period of 400 hours, Cs by a factor of 20, Sr by a factor of 13, and Ba by a factor of 2. The behaviour of the ion-source made it especially difficult to do these experiments. But the

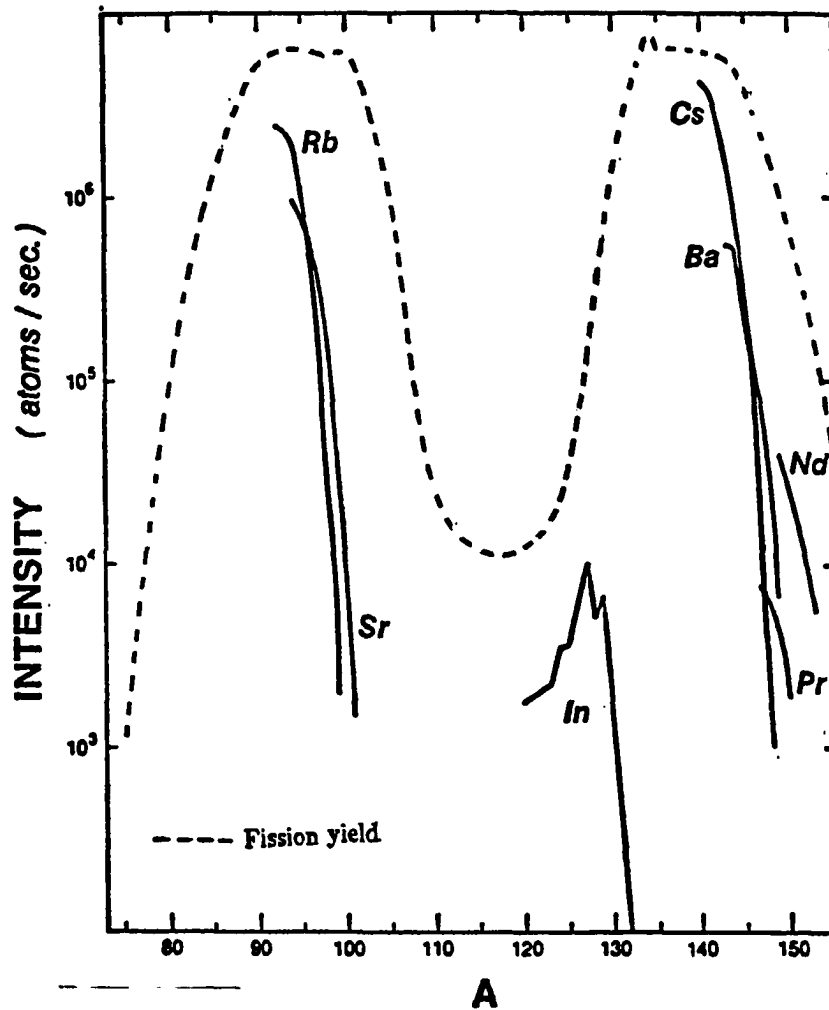


Figure 3.3. Direct Production Rates of Nuclides Measured at TRISTAN
[taken from Ref. 73]

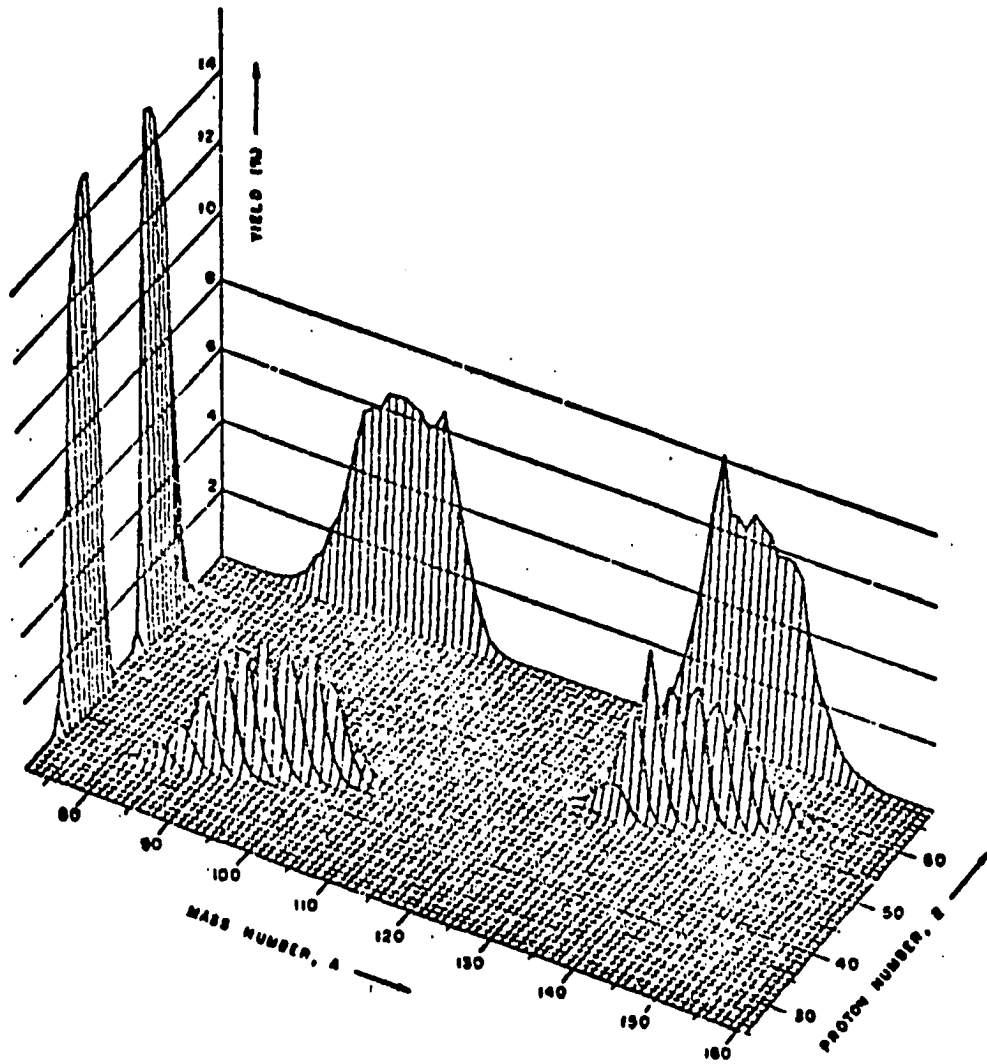


Figure 3.4. Fission Product Yield of ^{235}U for Thermal Neutron Fission

activity level for ^{145}Cs was high enough for a successful experiment even after a period of 400 hours of ion-source life.

3.2.2. Mass Separator

After extraction from the ion source the ions are accelerated to 50 KeV and then passed through an electrostatic cylindrical compression lens to focus the beam before it enters the 90° analyzing magnet. The mass separated ion beams from the magnet enter a collector box where stable isotopes can be visually focused on a fluorescent screen. At this stage the beam of interest can be positioned on a slit which is aligned with the entrance of the switch magnet. Two parallel copper strips on opposite sides of the slit provide feedback signals with which to stabilize the beam position. The separated ion beam passes through an electrostatic quadrupole lens before entering the switch magnet, which directs the beam to one of the experimental stations. For experiments in this study the beam was directed to the $+45^\circ$ station where the MTC (Figure 3.5) is placed. Delayed neutron and time of flight experiments are performed at the 0° station, perturbed angular correlation experiments are performed at the -45° station, and the -22.5° station has been reserved for a future laser spectroscopy experiment.

3.2.3. Moving Tape Collector

In the MTC the beam is deposited on aluminized mylar tape. The tape is 12.5mm wide and 0.03mm thick and each reel carries 600m of tape. The whole tape system is housed in a vacuum box mounted vertically under the source collection point and is maintained at a pressure of about 5×10^{-6} Torr. (The remainder of the separator except the ion source is maintained at a pressure of less than 1×10^{-6} Torr by four different turbo pumps.) The deposited activity can be placed in front of the detectors and later moved by means of the tape moving system. A stepping motor drives the MTC in a continuous or discontinuous (step) mode. In all of the present experiments the step mode was used to move the tape.

The purpose of the MTC is to enhance the activity of the nuclide under study relative to other nucleides with the same mass. The operating cycle consists of the time of collecting the beam, the time of deflecting the beam, the time of counting the deposited source, and the delay time. The cycle is controlled by the Daughter Analysis System (DAS) which controls the collection time of the beam, the delay or deflection time, the counting time, and the rate of tape motion. The determination of all these parameters depends on the half-life of the nuclide to be optimized compared to the other members of the isobaric chain. The procedure for this optimization and the parameters related to it are detailed in Section 3.4.1 and Appendix A.

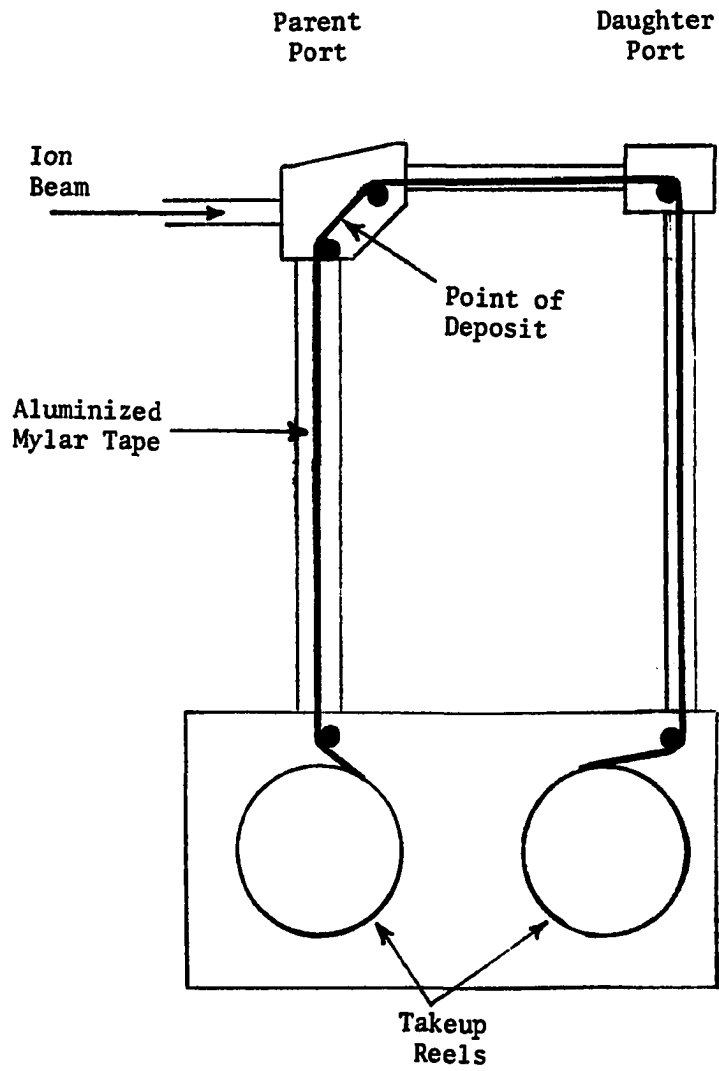


Figure 3.5. Moving Tape Collector System

The detectors can be placed at two different places, one at the point of deposit (called the parent port), and the other downstream (called the daughter port) as shown in Figure 3.5. Depending on the half-life of the nuclide under investigation and the type of experiment, the experiments were performed at one of these ports. Details of the MTC system are shown in Figure 3.5. A full description of this system is given by Norman *et al.*⁵²

3.3. Experimental Arrangement

Most of the present measurements have been performed at the parent port of the MTC with two Ge(Li) detectors, though some measurements were performed at the daughter port. Figure 3.5 shows the detector arrangement at the parent port. In this study three different types of measurements were performed:

1. **Gamma Singles Spectra:** When each gamma-ray is detected, the system puts it in a different channel according to its energy, and keeps track of the number of gamma-rays detected in every channel. Each gamma-ray was distributed over several channels, due to finite resolution of the system. For a specific energy with a very large number of counts the distribution was almost gaussian. In order to eliminate background some of the singles spectra were beta gated, which means imposing a coincidence relation on the singles spectrum, *i.e.*, by allowing detection of a gamma-ray to be processed only if there is a simultaneous detection of a beta by the beta detector. Because the gamma-ray background is not in coincidence with

beta emission from the source, they will not be counted. An example of a beta gated gamma-singles spectrum is shown in Figure 5.2.

2. Gamma-multiscale spectra: timed sequences of gamma singles spectra.
3. Gamma-gamma coincidences: simultaneous measurement of two singles energy spectra with different detectors with a determined time relationship between them.

The Ge(Li) detectors used for detection of gamma-rays were large in volume and had an intrinsic efficiency of $\approx 20\%$ for photon detection, with typical resolution of 2.0–2.3 keV. In the case of low energy gamma-ray measurements a Low-Energy Photon Spectrometer (LEPS) was used because it has a very thin window to reduce absorption at low energies and a very high resolution for low energies.

3.3.1. Singles and Multiscale System Electronics

The general block diagram of the electronics used to obtain gamma singles measurements is shown in Figure 3.6. The electronics and computer used for the data collection are situated in a room some distance away from the experimental area, and it is necessary to run long cables from the detectors to the system. (These are shown by broken lines in Figures 3.6 and 3.7.) During the initial testing it was found that no worsening in the resolution of the detectors occurred because of transmission through these cables.

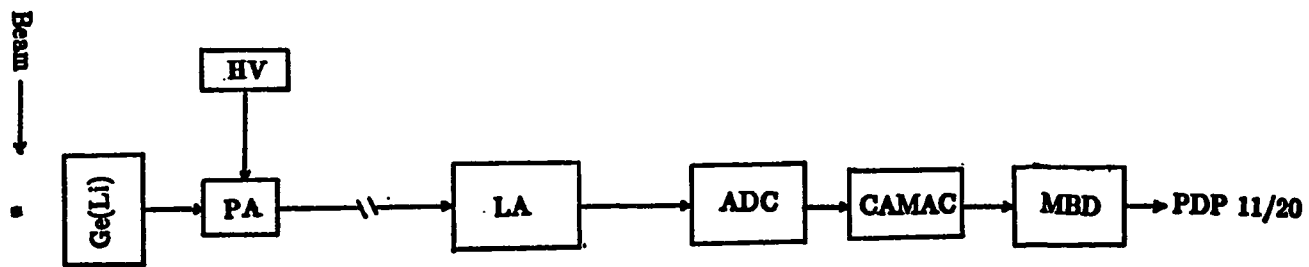


Figure 3.6. Block Diagram of Gamma Single Electronics

The output signals from the detector preamplifiers were fed into the Linear Amplifier (LA), and the outputs of the amplifiers were fed to an Analog to Digital Converter (ADC). All ADC's were capable of processing 8192-channel spectra. The ADC output is transmitted to a CAMAC interface and then to a Micro-Programmed Branch Driver (MBD) which stores the data in a one-megaword memory. In order to eliminate the room background and Pb x-rays (from gamma-rays scattered by the Pb shielding) from the gamma-singles spectra, some of the gamma singles were beta gated. In the case of beta-gated singles only those gamma-rays were processed which were detected simultaneously with beta radiation from the source. The set up for beta-gated singles is similar to that for gamma singles except for use of a coincidence circuit to satisfy the condition of a simultaneous detection of gamma and beta radiations.

When an experiment runs for more than a day, gain and zero shifts in the system due to temperature and the voltage fluctuations may become significant. In order to avoid this problem all experimental channels were stabilized. To stabilize the experimental channel, the stabilizing unit sets window on high-stability pulser peaks and checks the pulse height distribution in the window. For any pulser peak which drifts out of the window, due to gain and/or baseline shifts the stabilizer adds a correction to the digitized pulse height information in the ADC. Two reference peaks (pulser peaks) are needed to compensate for both gain and baseline shift.

The stabilization works very well provided the pulser is very stable.

Gamma multiscaling is another type of singles measurement which involves the recording of a time sequence of spectra. In most multiscale measurements for this work the activity was collected for a preset time at the parent port, the beam was deflected electrostatically, and a signal was sent to the multiscale clock that controlled the collection of 16 spectra in sequence for a preset duration. This generated 16, 8192-channel spectra collected in consecutive time bins, which could be used to determine the half-life of many of the gamma lines in the spectrum. It also generated a spectrum which was time integrated over all channels. All 17 spectra were stored in a one megaword memory interfaced to a PDP 11/20 computer.

3.3.2. Coincidence Electronics

The layout of the electronics used for all gamma-gamma coincidence experiments is shown in Figure 3.7. The preamplifier signals from each Ge(Li) detector are split into two outputs labeled Energy (E) and Timing (T). The energy outputs of each detector were fed into linear amplifiers and the unipolar outputs of the amplifiers were fed into ADC's. The outputs of the ADC's were routed to the PDP 11/20 computer via a CAMAC interface. The timing outputs from the amplifiers were shaped

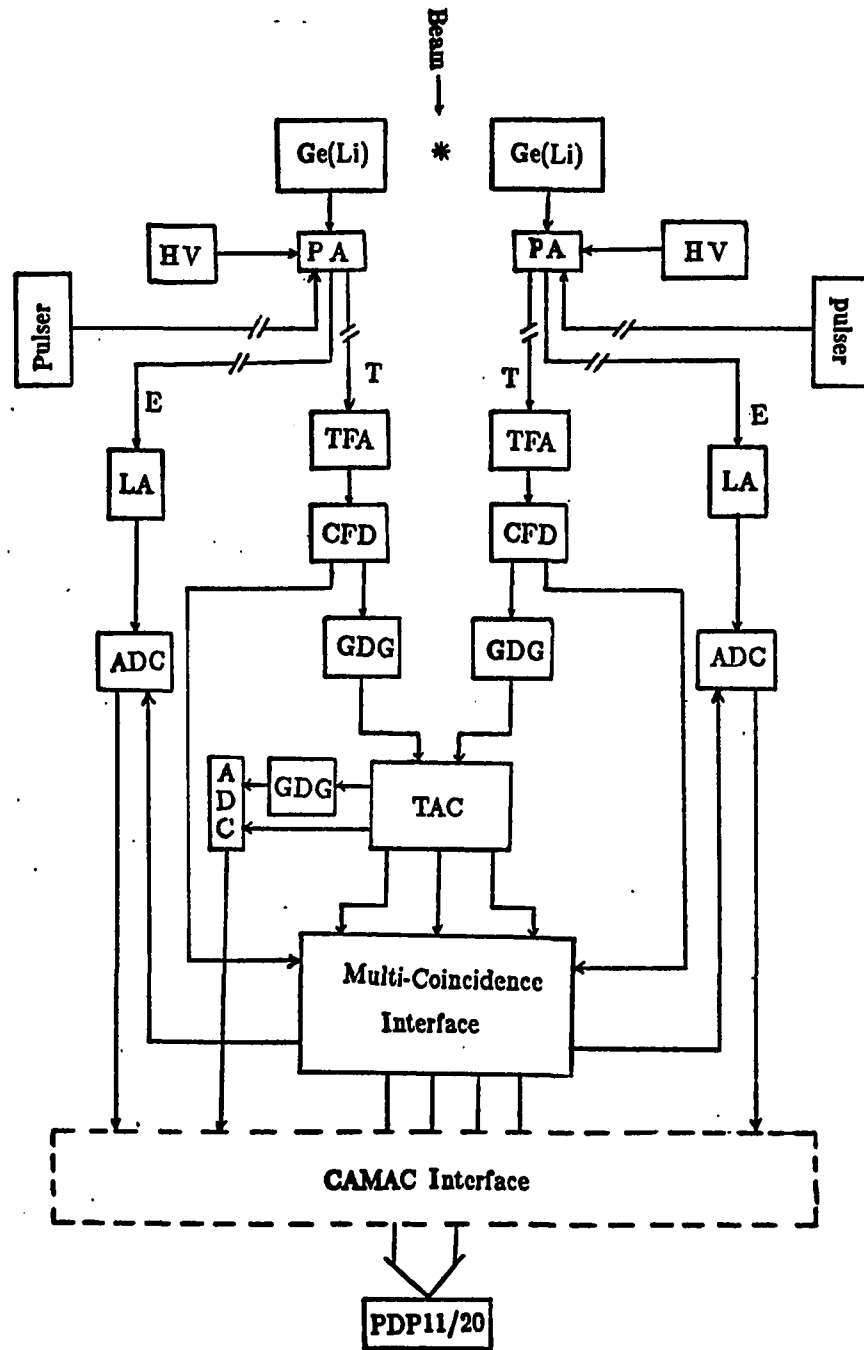
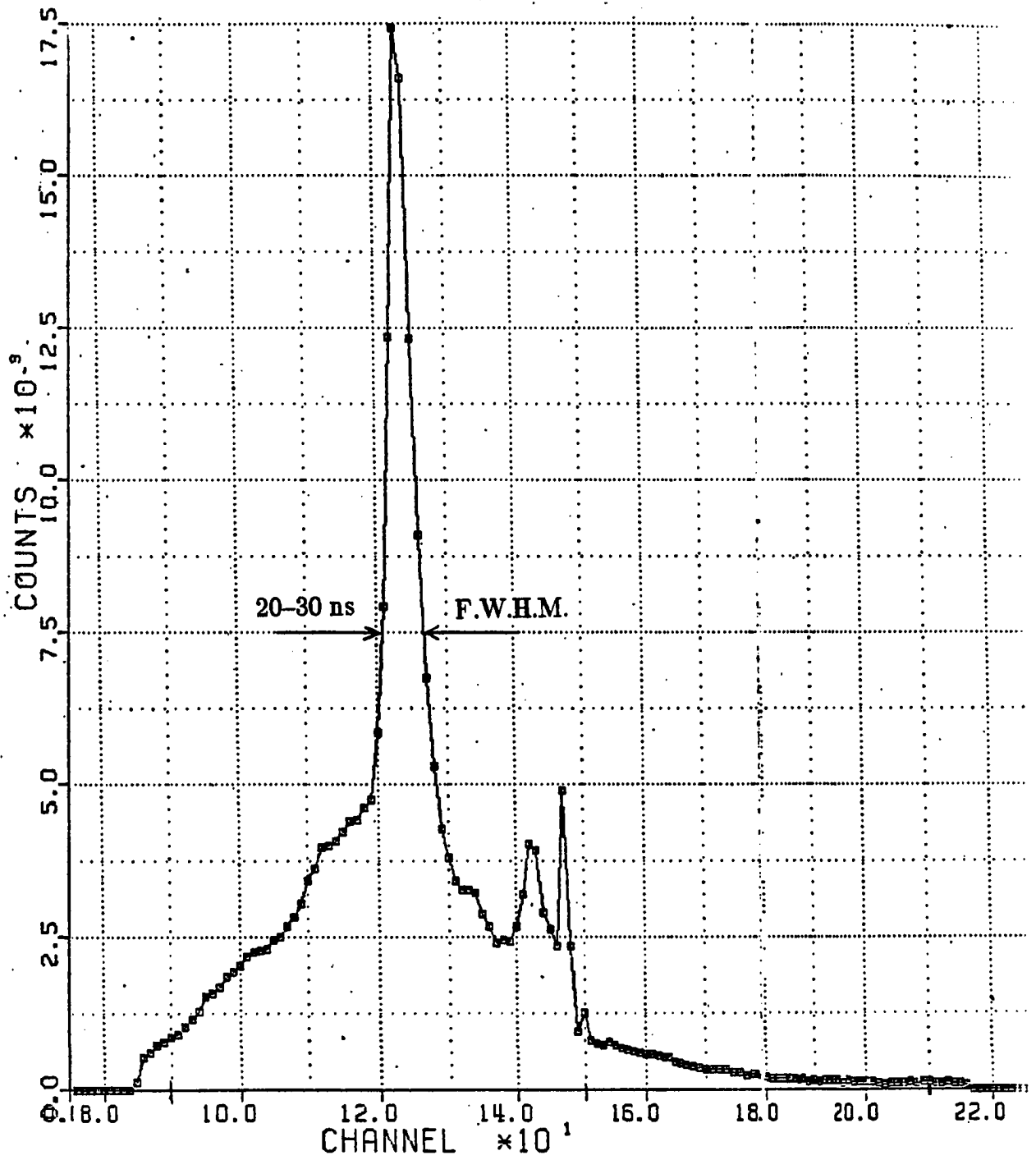


Figure 3.7. Electronic Setup of the Gamma-Gamma Coincidence System

by Timing Filter Amplifiers (TFA) to pick up the timing information and then fed into Constant Fraction Discriminators (CFD). The positive logic outputs from the CFD's were fed into a Multi-Coincidence Interface (MCI), and the fast negative outputs of the CFD were fed into Gate and Delay Generators (GDG). One output of a GDG was used as a start pulse for an Ortec 476 Time to Amplitude Converter (TAC). The output from the second GDG was delayed by 32 ns and used as a stop pulse for the TAC. The output of the TAC, which has a height proportional to the time difference between the start and stop pulses was passed into an ADC. A window was set on the TAC output in order to limit the time difference between events in the two detectors to a preset value of 50 to 100 nsec. The energy ADC's were used in the 8192-channel mode, and the resulting coincidence matrix was 8192 by 8192 channels. The time difference between these two events was a third dimension of this matrix. The Full Width Half Maximum (F.W.H.M.) resolution of the time spectrum was found to be 20-30 ns. Figure 3.8 shows a time spectrum from one of the experiments. The outputs of the ADC's were fed into a computer which wrote the coincidence events on magnetic tape. [A more detailed description of this type of coincidence circuit is given in reference 53.]



3.8. A Gated Time Spectrum Showing the FWHM of the Coincidence Peak

3.3.3. The Data Acquisition System

The data acquisition system is built around a PDP11/20 computer. This was connected to the various data channels by a the CAMAC interface system (see Figure 3.9.a). In order to provide an efficient use of the CAMAC dataway the CAMAC operations are controlled by a Microprogrammed Branch Driver (MBD). The MBD is a fast microprocessor (70 ns cycle time) which is capable of multiplexing up to eight separate channels of CAMAC input information and which determines priorities among the various data channels.

The principle modules of the multicoincidence interface are shown schematically in Figure 3.9.b. After a coincidence output has been detected, the information is loaded into a status register which sends a signal to the MBD. The MBD code reads out the ADC's together with the corresponding TAC output. The code stores these three words in the buffer in the MBD memory, and when the buffer of 256 events is full the events are transmitted to the PDP11/20 buffer directly out to the magnetic tape. Other processing is carried out by the computer such as two global energy spectra, a time spectrum, and sorting to produce a sample gated spectra.

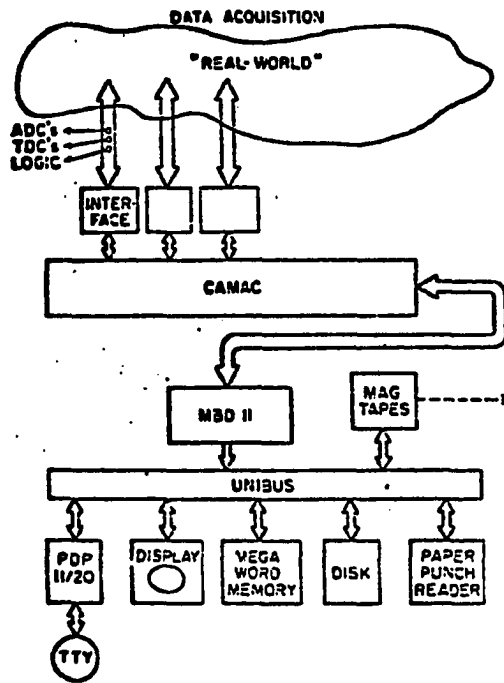


Figure 3.9.a. Structure of the Data Acquisition

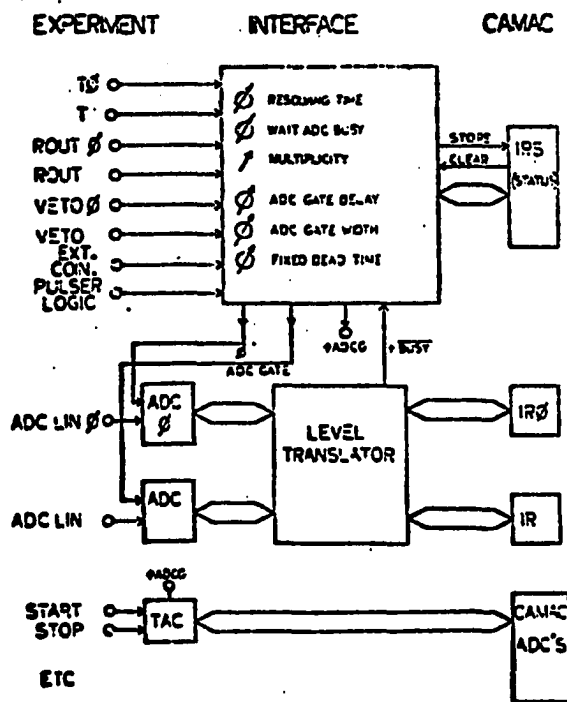


Figure 3.9.b. Gamma-Gamma-Time Coincidence Analyzer Interface

3.4. Experimental Procedure

3.4.1. Source Optimization

In order to carry out the experiments and get the best possible results, the moving tape cycle was set to give the highest counting rate possible for the nuclide of interest while at the same time giving the lowest counting rate possible for the other members of the isobaric chain. The optimum conditions for the source buildup were determined by solving the differential equations governing the activity level for each member of an isobaric chain. For example, for a chain of four decays which ends a long-lived or stable isobar the equations are given below:

$$\begin{aligned}\frac{dN_1}{dt} &= R_1 - \lambda_1 N_1 & \frac{dN_2}{dt} &= R_2 + N_1 \lambda_1 - N_2 \lambda_2 \\ \frac{dN_3}{dt} &= N_2 \lambda_2 - N_3 \lambda_3 & \frac{dN_4}{dt} &= N_3 \lambda_3 - N_4 \lambda_4 \\ \frac{dN_5}{dt} &= N_4 \lambda_4 & & \text{(stable end of chain)}\end{aligned}$$

where N_i is the number of nuclei for i^{th} isobar, λ_i is the corresponding decay constant, and R_1 and R_2 are the rates at which the first and second elements are being deposited by the beam (primary production is assumed only for the first two members of the chain since this is the case in the experiments under consideration). These equations are easily solved for the activity $\lambda_i N_i$ of each isobar. The solution of these equations for the special case of ^{90}Sr is given in Appendix A.

A computer program was written to evaluate the solutions of

these equations and produce a table of source strength against time for $A = 99$ and $A = 145$. The solutions helped to decide the best cycles for the experiments.

The MTC cycles were set according to the above consideration and also by restrictions in the multiscale code for selecting multiscale spectrum times. According to the cycle time which was determined by factors mentioned above, for each case the source was allowed to build up for a fixed period of time (deposit or accumulation time), then the beam was deflected and the source counted for an appropriate fixed period of time (counting time) after which the source was quickly moved away from the counting region. Details of the cycles for each case studied will be given in Section 3.4.3.

3.4.2. Intensity and Energy Determination

The energy and intensity of each gamma transition are two important quantities which must be determined very carefully in each study. To determine the relative intensities of each transition, the intrinsic efficiency of the detectors must be known as a function of gamma-ray energy. This is done by using standard sources of known intensity. Such an efficiency curve must be determined for each detector used. A singles spectrum of standard sources mixed with the spectrum from each radioactive nuclide in this study was taken to allow an energy calibration of the gamma rays to be carried out. Such a mixed spectrum containing gamma lines with

well-known energies facilitates the precision determination of transition energies. The primary energy region studied in each experiment was approximately 100 keV to 2.5 MeV. In addition, separate singles spectra for higher energies (up to 5 MeV) were taken, and a separate measurement for low energy was performed with an energy range of 5 keV to 500 keV.

3.4.3. Beta Decay Half-Lives

The ^{90}Sr produced by TRISTAN is short-lived and decays by β^- decay through ^{90}Y , ^{90}Zr , and ^{90}Nb to long-lived ^{90}Mo . ^{145}Cs and ^{147}Cs are also short-lived and decay by β^- decay through Barium, Lanthanum, Cerium, and Praseodymium. Tables 3.1 and 3.2 show the half-lives in each isobaric chain.

The half-lives measured in this work were determined by computing the area under clean (uncontaminated) individual peaks with very good statistics for each time bin to obtain activity versus time. The exponential function governing the decay of radioactive nuclei would appear as a straight line in semi-log plot. The slope of these straight lines were determined by least square fitting and give the half-lives of the nuclei.

Table 3.1. Half-Lives of Isobaric Chain of $A = 99$.

| | $T_{1/2}$ | |
|----|-------------------|-------------------------|
| Rb | 59.0 ± 4.0 | <i>ms</i> (reference b) |
| Sr | 0.266 ± 0.006 | <i>s</i> This work |
| Y | 1.50 ± 0.08 | <i>s</i> (reference a) |
| Zr | 2.1 ± 0.1 | <i>s</i> (reference a) |
| Nb | $15.0 \pm$ | <i>s</i> |
| | $2.6 \pm$ | <i>ms</i> |
| Mo | $66.0 \pm$ | <i>hr</i> |

Table 3.2. Half-Lives of Isobaric Chain of $A = 145, 147$.

| | $A = 145$ | | $A = 147$ | |
|----|-----------------|--------------------|-----------------|--------------------|
| | $T_{1/2}$ | | $T_{1/2}$ | |
| Cs | 0.54 ± 0.02 | <i>s</i> This work | 0.21 ± 0.01 | <i>s</i> This work |
| Ba | 4.31 ± 0.5 | <i>s</i> (ref d) | 0.72 ± 0.07 | <i>s</i> (ref c) |
| La | 24.8 ± 3.1 | <i>s</i> (ref d) | 4.48 ± 0.08 | <i>s</i> This work |
| Ce | 2.98 ± 0.10 | <i>m</i> (ref d) | $55.0 \pm$ | <i>s</i> |
| Pr | $5.98 \pm$ | <i>hr</i> | $13.0 \pm$ | <i>m</i> |

Half-life curves of a few gamma-lines belonging to ^{89}Sr are shown in Figure 5.1.

In the study of the decay of ^{89}Sr a one-second cycle (or 1/16 second per channel) was chosen, in order to look at the growth as well as the decay of this nucleus. The reason for looking at the growth for the $A=99$ case was to attempt to see the Rb precursor. The beam was collected for 0.4 second while the multiscale system was counting, then deflected for 0.6 second while the multiscale system continued to count. The system recorded 16 time sequence spectra, each one corresponding to 1/16 second of cycle time.

In the case of ^{145}Cs , only the decay portion of the cycle was recorded because there was no precursor. Since it was decided to do measurements for ^{145}Cs and ^{145}Ba simultaneously, a 2-second cycle was chosen to give the best possible activity level for both nuclei, even though this was not the optimum cycle for either. Because of the longer half-life in this case the detector for the multi-scale channel for the ^{145}Cs experiment could be set half-way between the parent port and daughter port. The purpose was to avoid losing beam time by deflecting the beam and letting the source decay while counting for multiscale system. In this way one could get as many coincidence events as possible in the period scheduled for this experiment. The source was deposited for two seconds then moved quickly to half-way between the parent port and daughter port for the multiscale

experiment. The coincidence experiment was running continuously at the parent port without any interruption, as was the multiscale measurement in its own station. The same procedure as mentioned earlier was used to determine the half-life of ^{145}Cs .

For ^{147}La the longer half-life permitted the experiment to be performed at the daughter port to avoid any deflection of the beam and the consequent loss of beam time. The cycle was an 8 second collection period (this was long enough for buildup of ^{147}La) after which the source was moved to the midway point and left to decay for 8 seconds (by then most of the ^{147}Cs and ^{147}Ba had decayed). Finally the source was moved to the daughter port for an 8 second count. The same procedure as mentioned earlier was used to determine the half-life of ^{147}La .

CHAPTER IV

DATA ANALYSIS

4.1. Introduction

Nuclear spectroscopy experiments produce large amounts of data, which must be analyzed very carefully. The two most important quantities are the energy and intensity of each gamma ray in spectrum. Therefore, the above quantities must be determined as accurately as possible. For data analysis at BNL a PDP-11/34 computer is available with an on-line VERSATEC printer/plotter and a VT105 display terminal for interactive graphics (see Figure 4.1). The author also used a VAX-11/780 computer at The University of Oklahoma (OU) for data analysis. In order to carry out the analysis computer programs have been developed at BNL and at OU. Computer codes available for data analysis at BNL have the capability of printing, plotting, gain shifting and adding spectra together, scanning the event-mode tapes, interactive least-square fitting of calibration points and decay curves, and precision fitting of gamma lines in the various singles spectra. Some of the programs used at OU were adapted from Iowa State University programs, which were modified for use on the VAX. Programs

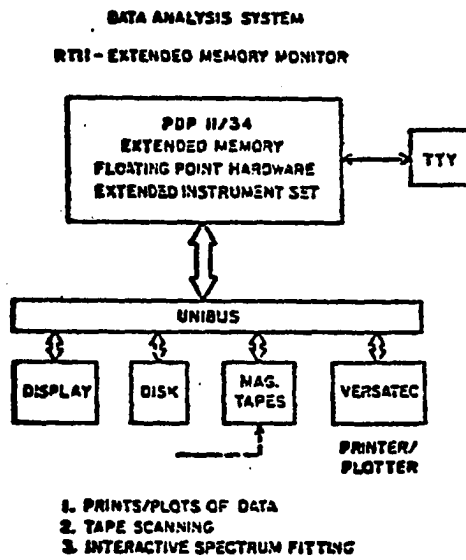


Figure 4.1. Structure of the Data Analysis System at BNL

at O.U. perform all the functions mentioned for the BNL programs except scanning event-mode tapes. A list and short description of programs used to analyze the data are given in Appendix B.

4.2. Peak Identification and Half-Lives

The sixteen time sequence spectra in the GMS data were sorted by using the computer code DLK. As mentioned earlier data for ^{90}Sr consisted of two parts, growth and decay. Since the decay of this nucleus was of interest the decay portion were summed in two groups for initial analysis. The gamma line's decay rates were compared in these two spectra, and the decay rate of a known gamma line such as the 125 keV line was used as a reference. This procedure helped in the assignment of the gamma transitions to members of the isobaric chain. The plot of the integrated sum of all sixteen spectra (which will be referred to as the total sum later) was taken also, and is the spectrum which was used for energy and intensity determination. For ^{145}Cs the spectra were summed into four different groups. The first and last sum spectrum were compared the same way as mentioned above, and the 175-keV gamma transition was used as a reference peak. In addition to comparison of decay rates in summed spectra the decay curves were obtained for identification of all gamma transitions in spectrum. The total sum spectrum was used to determine the placement of windows that were set on the peaks of interest and on the background above or below the peaks. A computer code used these windows to obtain the corrected areas

(background was subtracted from the number of counts under the peak) of the peaks in each of the sixteen time bins. Plots of these data were used to identify the peaks in spectrum from their decay behaviour. In order to identify the background and contamination peaks several different techniques were used. In one of these techniques the spectrum of the nuclide under study was compared with a background spectrum taken with no source. Almost all of the background activities observed were those associated with reactor background from neutron absorption such as ^{60}Co , ^{40}K , ^{41}Ar and ^{137}Cs . Also during the experiment the gamma transitions belonging to prompt Ge and Al neutron capture were observed. There was no observable contamination from adjacent masses. Another type of contamination for some transitions happened when two members of the isobaric chain under study had transitions of the same energy. This kind of mixture made the half-life of that transition different than any half-life in the isobaric chain. One transition in ^{90}Sr was found to be contaminated due to presence of ^{90}Y (536 keV, see Figure 4.2). In the case of ^{145}Cs there were at least 20 transitions from ^{145}Ba which had nearly the same energy as a transition in ^{145}Cs . ^{147}La has a few transitions with the same energy as ^{147}Ba . These transitions could be identified and assigned to a new nucleus by their coincidence relationships with those transitions which were uniquely identified by their half-life.

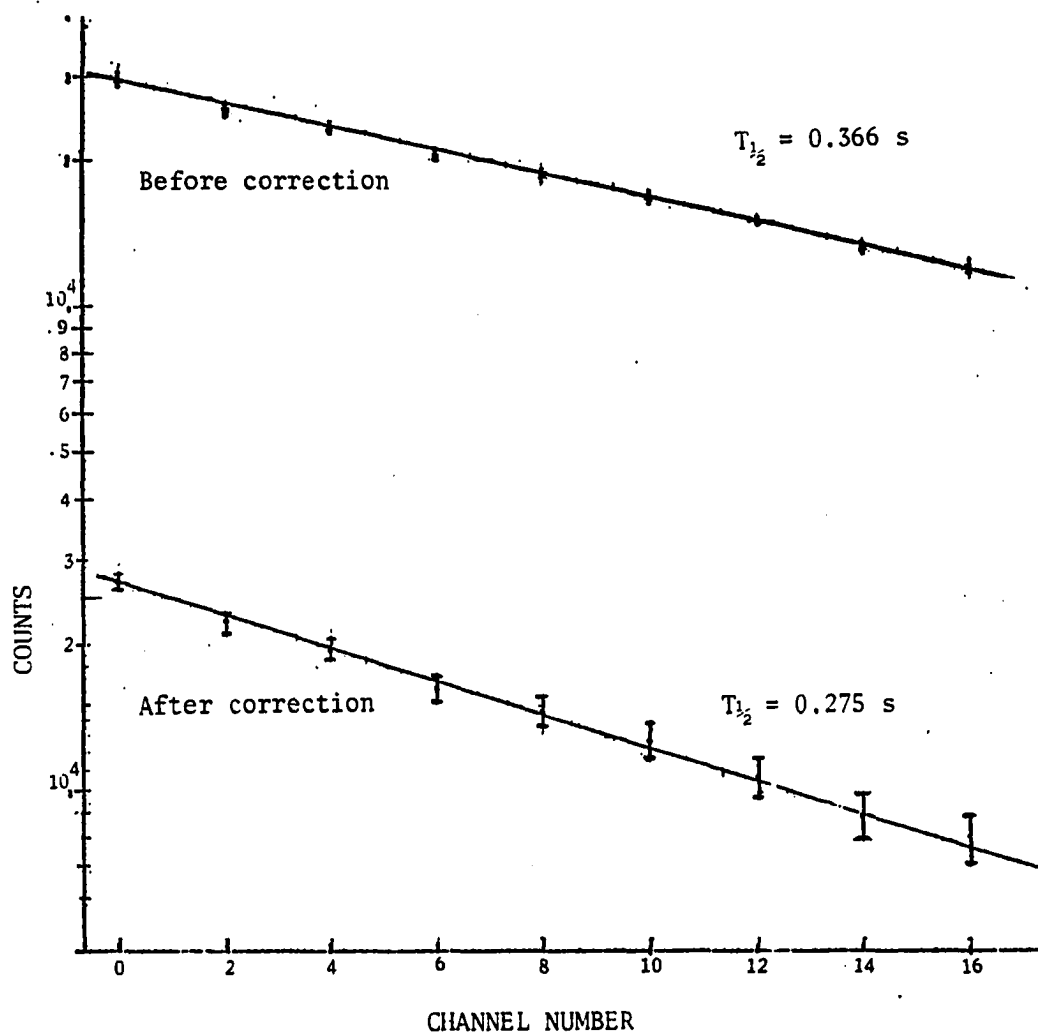


Figure 4.2. Decay Curve of 536-keV Transition in ⁸⁹Sr Decay with and without Correction for ⁹⁰Y Decay

When the beta-decay energy available for a nuclide is greater than the neutron binding energy in the daughter nucleus, it is possible for the beta transition to populate high-energy states in the daughter nucleus that are above the neutron binding energy. In this case neutron emission from these levels competes with γ -ray emission and populates levels in isotopes one mass number lower. Such a delayed neutron emission effectively mixes two isobaric chains and can lead to confusion in the γ -ray spectrum, especially since the γ -rays in the lower mass nucleus will have the same beta decay lifetime as those in the nuclide of interest.

Both ^{90}Rb and ^{145}Cs are delayed neutron precursors, and transitions associated with ^{98}Sr and ^{144}Ba were identified in the respective spectra. When transitions from delayed neutrons had the same energy as transitions belonging to nuclei under study it made the analysis very complicated. This was the case in ^{145}Cs where the 199-keV transition had the same energy as the strongest transition in ^{144}Ba . This made a precise intensity determination impossible, because the intensity of the gamma transition from delayed neutron emissions is not known. These transitions were very weak in ^{90}Sr , however, and did not cause problems in the analysis.

Two procedures were used for determination of the half-life in ^{90}Sr . In one case several strong peaks were fitted in all sixteen spectra using the computer code SKEWGAUS to get the area under the peak for each time bin. The slope of the exponential decay functions were determined

by least square fitting with a computer code, and from this the half-life was determined. In the other procedure mentioned earlier in this section, gates were set for each peak of interest on the total sum spectrum, and the GMS data were sorted using these gates. The background was subtracted from each peak, providing the net number of counts for each peak in each time bin. Least square fitting was used to determine the half-life from these data also. The half-lives of ^{145}Cs and ^{147}La were obtained only through the second procedure. The weighted average of these values for each nucleus was determined and used as the reported half-life.

4.3. Energies and Intensities

Gamma singles spectra were then used for determination of energies and intensities of gamma transitions in each case of the present study. As mentioned in section 3.4.2, three different types of gamma singles were taken, a singles spectrum of standard sources, a singles spectrum of standard sources with unknown (mixed spectrum), and the unknown alone. Gamma rays belonging to standard sources in these spectra had very well determined energies. These have been used to get an accurate relation between energy and channel number. This relation was used to assign an accurate energy to some of the strong gamma transitions with very good statistics belonging to the unknown spectrum. These energies in turn were used to calibrate the unknown spectrum to determine the energy of every peak in the spectrum. To accomplish the energy determinations the

centroid of each peak must be determined very accurately. This has been done using the codes PEAKFIND⁶³ and SKEWGAUS⁶⁴ at OU or ATP at BNL, which also provide an area for each peak that allows determination of relative intensities. A brief explanation of the above programs is given in Appendix B. The actual energy and intensity determinations were done by using the code DRUDGE.

The procedure for determining the energy using the code DRUDGE is as follows: A weighted least square straight line for the energy as a function of channel number was obtained for the mixed spectrum, using standard source peaks which were well defined. The nonlinearity of the system with respect to this least square line was obtained for the mixed spectrum. The difference between known energies of standard source lines (called true energies) and the energies from the least square line defines the nonlinearity corrections for the system. These nonlinearity corrections were used to determine the energies of some of the well defined lines which were present in both the mixed and the unknown spectra. The energy of these peaks were used as true energies in the unknown spectrum. A weighted least square straight line for energy as a function of channel number was obtained for the unknown spectrum, using peaks for which true energies were determined. Then new nonlinearity correction was obtained for the unknown spectrum, which was used to determine the energy of each gamma line of interest in the spectrum. In the case of very weak lines which

were observed only in coincidence spectra the energies were determined by using strong lines in the same coincidence spectrum as calibration points.

The absolute efficiency of a gamma-ray detector consists of the intrinsic efficiency of the detector times the solid angle subtended by the detector. In order to eliminate the necessity of determining the solid angle intercepted by detector, only relative efficiencies were determined. A relative efficiency curve for gamma detection was obtained from the calibration spectrum using the peak areas and known relative intensities of gamma rays from the calibration sources. A sample curve plotted on a log-log scale is shown in Figure 4.3. The computer code DRUDGE was used to convert the peak areas in the unknown spectrum into relative intensities. The normalization used was 100 for the most intense transition in the spectrum. For the very weak lines which were observed only in a coincidence spectrum as mentioned earlier, there was no way of extracting the relative intensity directly. An upper limit estimate is given in the tables from the singles spectra.

4.3.1. Statistical Errors

The statistical spread of values for the count in each individual channel of energy is governed by a Poisson distribution.^{16,17} The Poisson distribution provides an analytical form appropriate to a case which describes the probability distribution in terms of average number of counts per unit

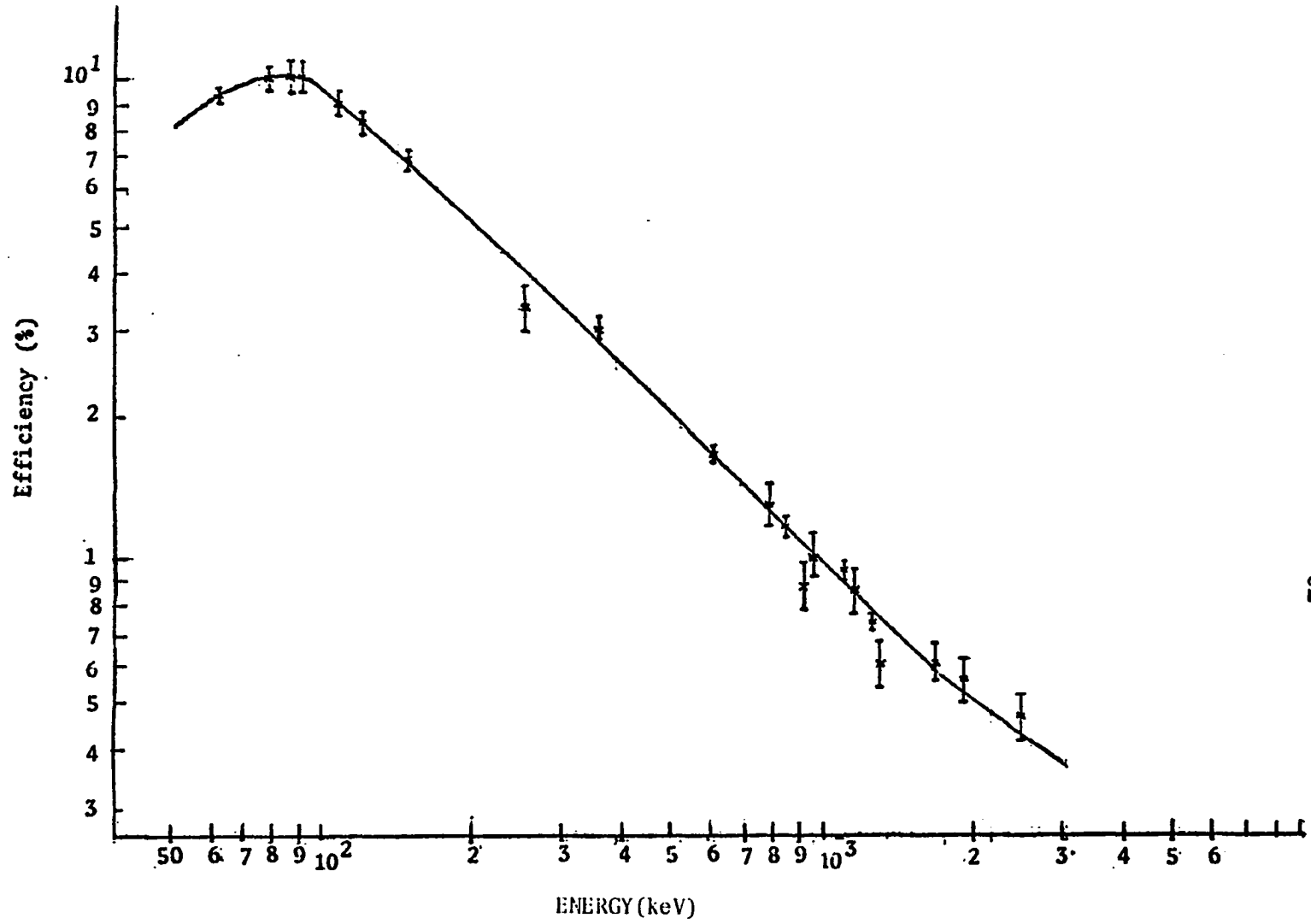


Figure 4.3. Efficiency Curve for a Ge(Li) Detector

time. That is to say the standard deviation for a count of N is \sqrt{N} . Mean values for each quantity measured in this work were obtained from a weighted average of the contributions:

$$\bar{x} = \frac{\sum_i W_i x_i}{\sum_i W_i}. \quad (1)$$

The x_i are the individual data points and \bar{x} is the weighted average of them, where the weights W_i are given:

$$W_i = \frac{1}{\sigma_i^2}. \quad (2)$$

The error on \bar{x} , assuming the x_i are independent, is given by propagation as

$$\sigma^2 = \frac{1}{\sum_i W_i}. \quad (3)$$

where σ is the uncertainty in \bar{x} due to the uncertainties in the individual values x_i .

In the case of least square fitting of measured values to a functional form, the goodness of fit for the function parameters is determined by application of a χ^2 test. χ^2 is defined to be:

$$\chi^2 = \sum_{i=1}^n \frac{1}{\sigma_i^2} [Y_i - Y(x_i)]^2. \quad (4)$$

Examination of the χ^2 indicates whether the actual spread of values of data correspond to that which would be predicted by the parent Poisson distribution. The expectation value of χ^2 is equal to the number of degrees

of freedom ($n - p$) where n is the number of points and P the number of parameters. The variance of the fit (minimum χ^2 divided by the number of degrees of freedom) should be close to 1 for a good fit, if the following assumptions are valid: the Y_i have a normal probability distribution, the W_i are the correct weights for this distribution, the function Y is the correct representation of the Y_i , and no approximations are made in solving for the minimum value of χ^2 . For the case of calibration and decay curve fitting the errors on the final values were estimated by the simple propagation errors of the various contributions. Errors in energy determination were due to errors in peak centroids obtained from the fitting programs. The error in a centroid was smallest for very good fits with variance very close to one. The errors for energies were on the order of a few tenths of a keV. Errors in half-life were due to errors in peak areas propagated through the least square fit to the logarithm of the data points. The time could be considered exact, therefore the error in time was neglected. In the case of ^{90}Sr the error came from the fitting procedure. In the other cases it was just the difference in number of counts under the peak and under the background gate, which is simply square root of the sum of the square of the errors for each number of count. The source of error in the intensities was more complicated because the error was due to error in areas and also the error in the relative efficiencies.

4.4. Gamma-Gamma Coincidences

The data collection system produces magnetic tapes of individual coincidence events between two gamma rays. Each event consists of two words containing the two energy channel numbers (E_1 , E_2) and a third derived from the TAC output which contains the time relationship between events. Thus the coincidence data consists of three dimensional arrays, two for detector energy output and one for timing information between them.

To obtain the global energy spectra a gate was set on the time spectrum in order to set a time requirement on the events, and then the data were searched to find all those events in energy channel 2 that were in coincidence with something in energy channel 1, and vice versa. The plots of these spectra were obtained and peaks were identified according to their energies. These spectra were then used to select peak and background gates for all peaks of interest. The data were then read again, this time producing a spectrum of all peaks in coincidence with the individual peaks of interest. The scanning of the tape was done by a computer code DLE which had the capability of processing up to 32 gates simultaneously.

These spectra have been plotted and analyzed to identify the gamma transitions in coincidence with the gamma ray of interest (see Table 5.3). If the peak in the coincidence spectrum had very poor statistics, it was identified only as a possible coincidence; otherwise it was called definite coincidence. In cases of very weak lines coincidence statistics were improved

by setting gates in both directions and summing the resulting spectra. To accomplish this it was necessary to first gain shift one of the spectra before summing.

4.5. Construction of the Level Scheme

A review of the literature was completed before attempting to construct a level scheme. At the beginning of the experiment no information was available in the literature on ^{88}Sr and ^{145}Cs , but a level scheme had been proposed for ^{147}La .^{18,36} From this review and the singles and coincidence results of this work, a level scheme was constructed for each nucleus under study. The final decision on whether a proposed level was accepted depended on several factors:

1. Number of transitions populating and depopulating the levels.
2. How many of these transitions had definite coincidence relation.
3. How many of these transitions had definite coincidence relations.
4. Energy match of the cascade sum.

A level with only one transition but with definite coincidence support was accepted; it was disregarded if no coincidence support was available.

4.6. Spin and Parity Assignments for Levels

The determination of spins and parities for nuclear levels is made with a variety of techniques. Ground state spins can be measured in a direct way by on-line laser spectroscopy and on-line atomic resonance techniques.

Once the spin and parity (I^π) of a ground state is known, the I^π of excited states connected to the ground state by a gamma transition can be inferred if the multipolarity of the gamma ray can be determined. (Multipolarities are generally determined from conversion electron measurements.) The I^π for other excited state sometimes can be inferred both from gamma-ray multipolarities and gamma-ray branching ratios. The basis for these determinations are the gamma ray selection rules discussed in Chapter II.

Another technique for determining I^π for excited states is the measurement of the gamma-gamma angular correlations which would allow spin assignments of some of the low-lying excited states where cascade transitions exist and at least two of the level spins are known. The spin and parity of some low-lying levels also can be obtained in an indirect way using the deduced beta feeding and beta branching ratios. To calculate the beta branching ratio, the beta feeding to the ground state must be determined. In a saturation or equilibrium situation where $N_1\lambda_1 = N_2\lambda_2 = N_3\lambda_3 = \dots$ (see Appendix A), the activity of all members of the chain is equal. When the absolute intensity of a gamma-ray transition in one of the daughter products of the isobaric chain is known, it can be used to determine the ground-state beta feeding. For the case where two members of an isobaric chain are primarily produced, the ratio of these two activities must be known for a determination of the ground-state beta feeding. For determination of the beta feeding to the excited state gamma-ray intensity balances

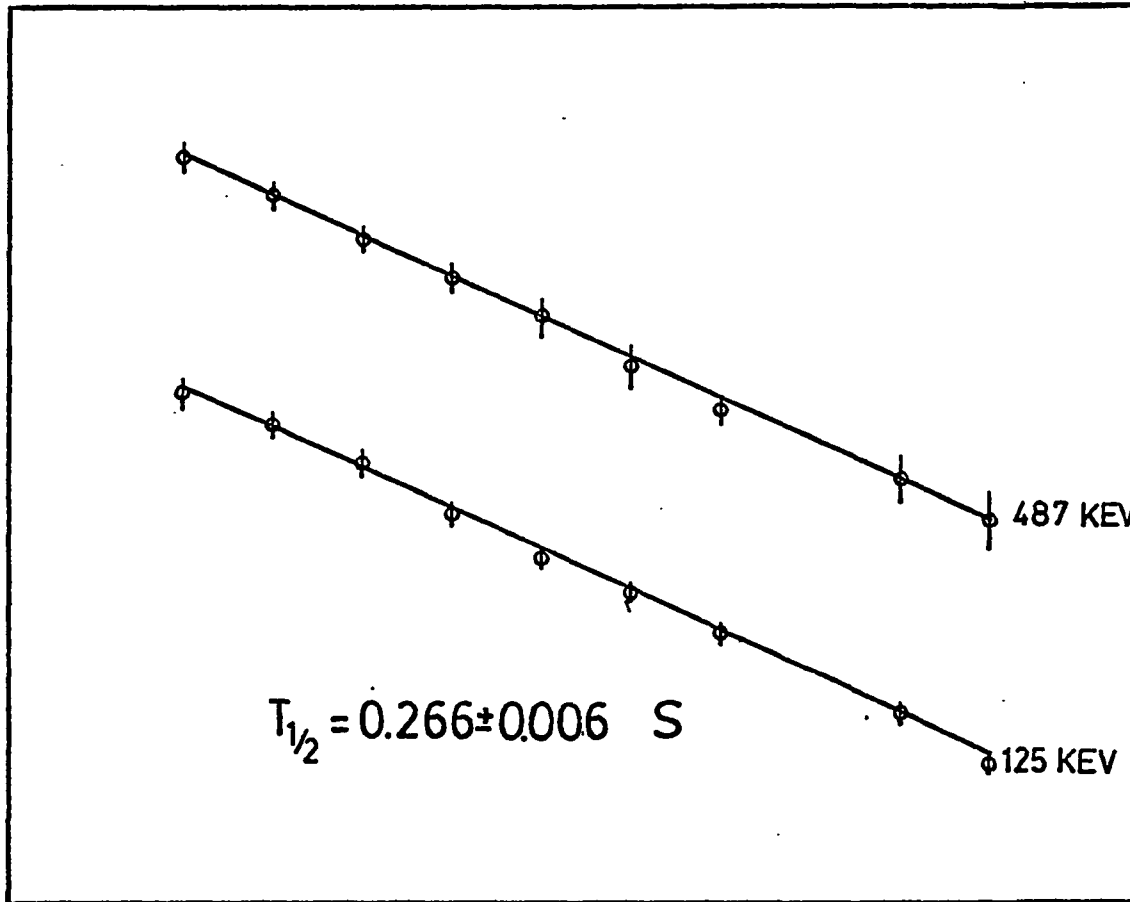
are used. Once branching ratios are known Logft values can be calculated provided the total decay energy (Q_β) is known. The Logft value for any level reflects the angular momentum selection rule for beta decay to that level. The rules associating Logft values with angular momentum changes are not strict, and Logft values can not usually be used by themselves to determine levels spins and parities. They can however support assignment made in other ways. Care must be taken in computing Logft values because a considerable amount of beta strength may go to high-energy levels whose gamma-ray de-excitation may be missed due to low detector efficiency for high-energy gamma-rays. The spins and parities assigned in this study were based on the indirect way explained above, because conversion electron and gamma-gamma angular correlation measurements were not possible.

CHAPTER V

EXPERIMENTAL RESULTS

5.1. ^{90}Sr

The beta-decay half-life of ^{90}Sr was obtained by following the decay of the 64-, 125-, 487-, 1198-, and 2239-keV strong gamma transitions in ^{90}Y . The decay curves for two of these transitions are shown in Figure 5.1. A half-life of $0.266 \pm .006$ sec was obtained from these lines. The half-life measured is in good agreement with the results of previous research which are 0.29 ± 0.04^{43} sec and $.25 \pm 0.04^{68}$ sec. The energies and relative intensities of gamma-rays associated with the decay of ^{90}Sr were determined from a beta-gated singles spectrum obtained from the GMS total sum. The singles spectrum is shown in Figures 5.2 a-f. Because the spectrum was beta-gated no background or contamination peaks were observed, and all the peaks in the spectrum were identified. The energies, relative intensities and placements of the observed gamma-transitions are given in Table 5.1. The relative intensities of these transitions were normalized to 100 for the 125-keV transition. For the most part the assignment of the gamma-ray transitions to ^{90}Sr decay was based on half-life. It was not possible to



5.1. Decay Curve of ^{99}Sr Transitions

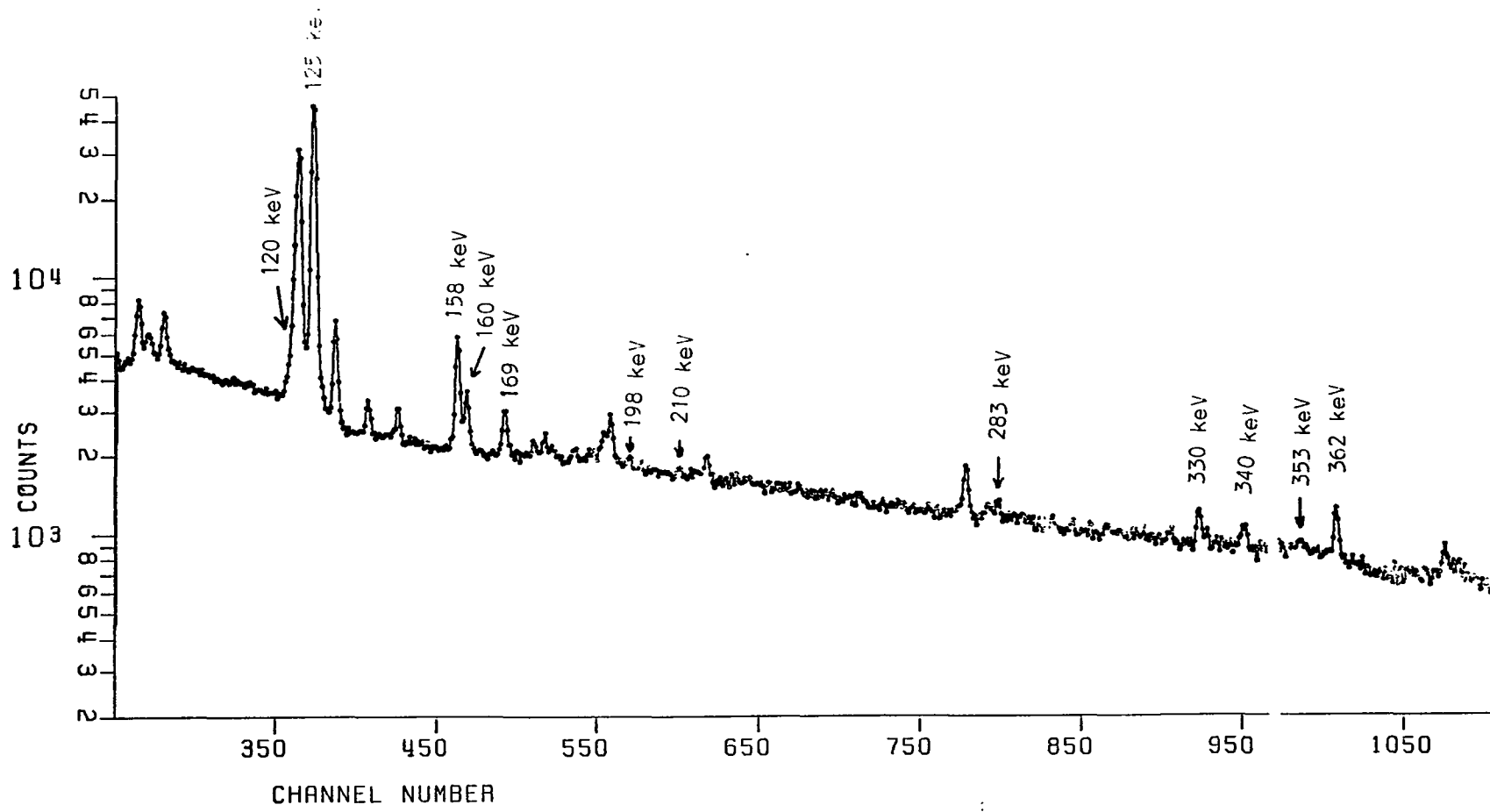


Figure 5.2a. Gamma Spectrum from ^{90}Sr Decay

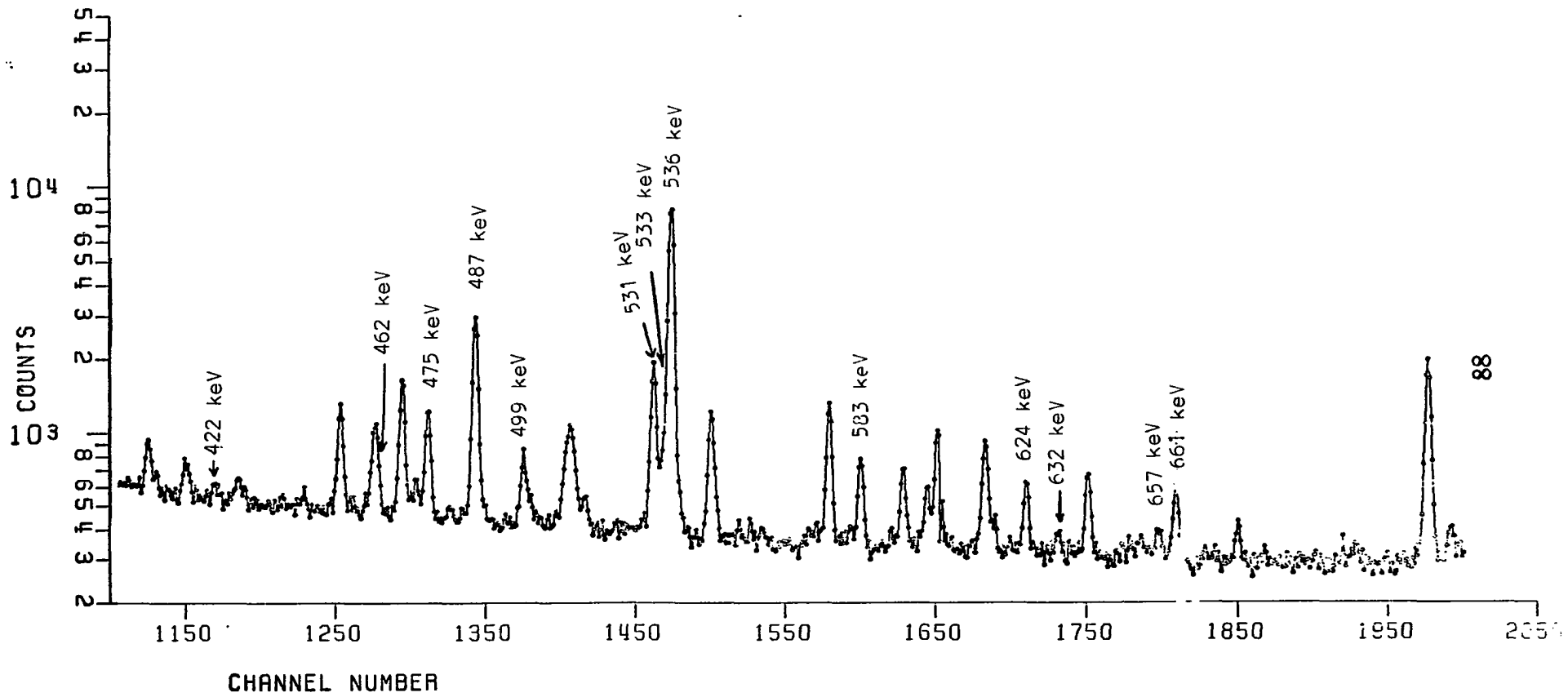


Figure 5.2b. Gamma Spectrum from ^{90}Sr Decay

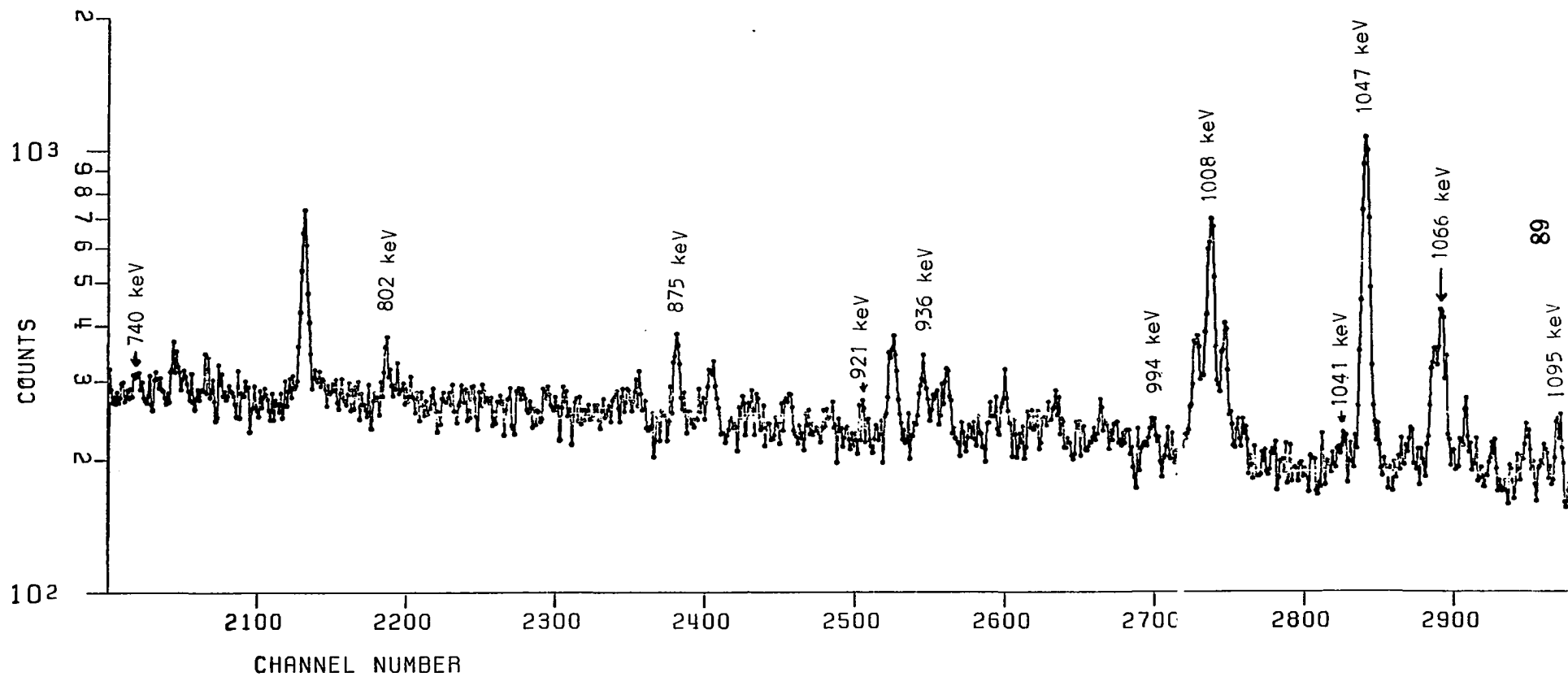


Figure 5.2c. Gamma Spectrum from ^{90}Sr Decay

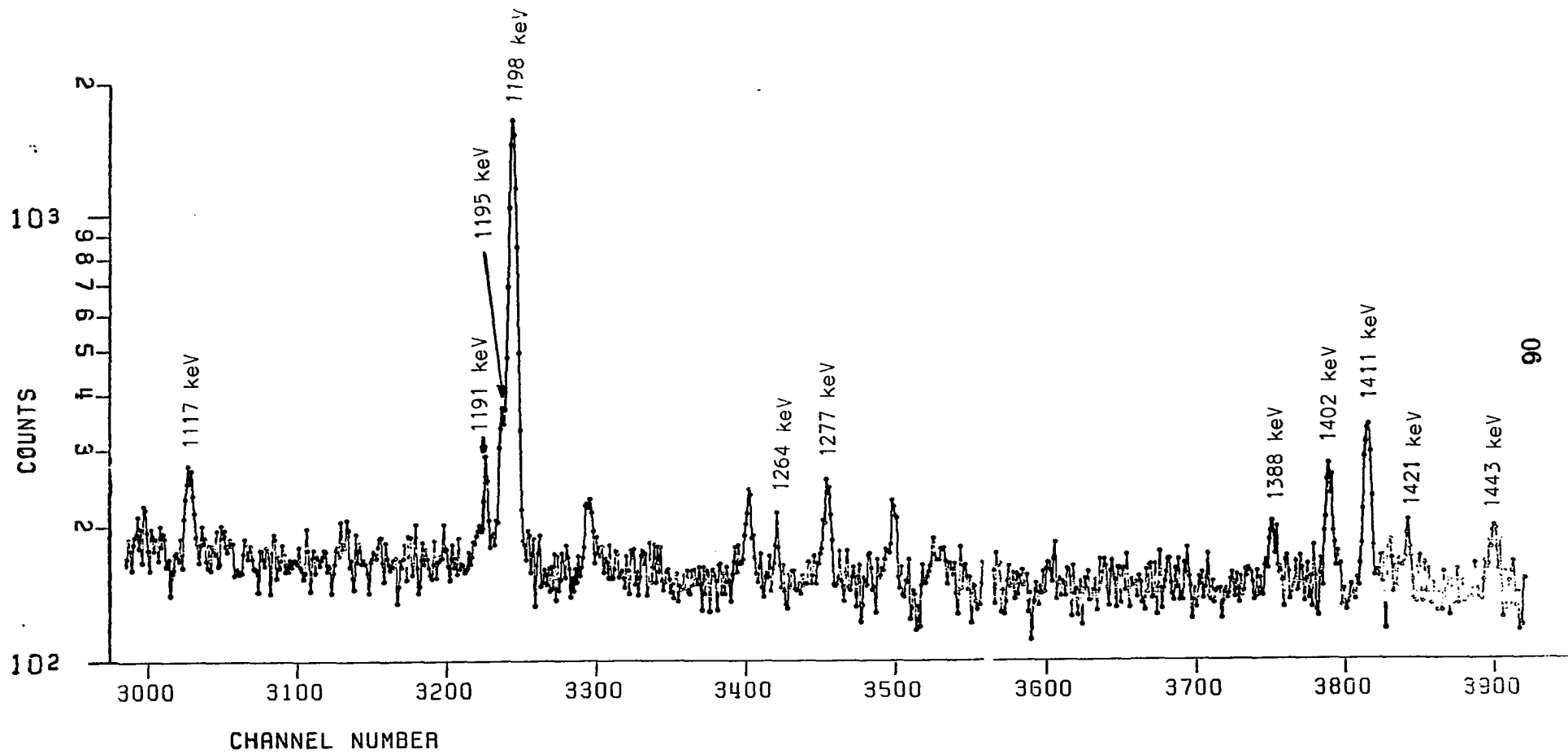


Figure 5.2d. Gamma Spectrum from ^{90}Sr Decay

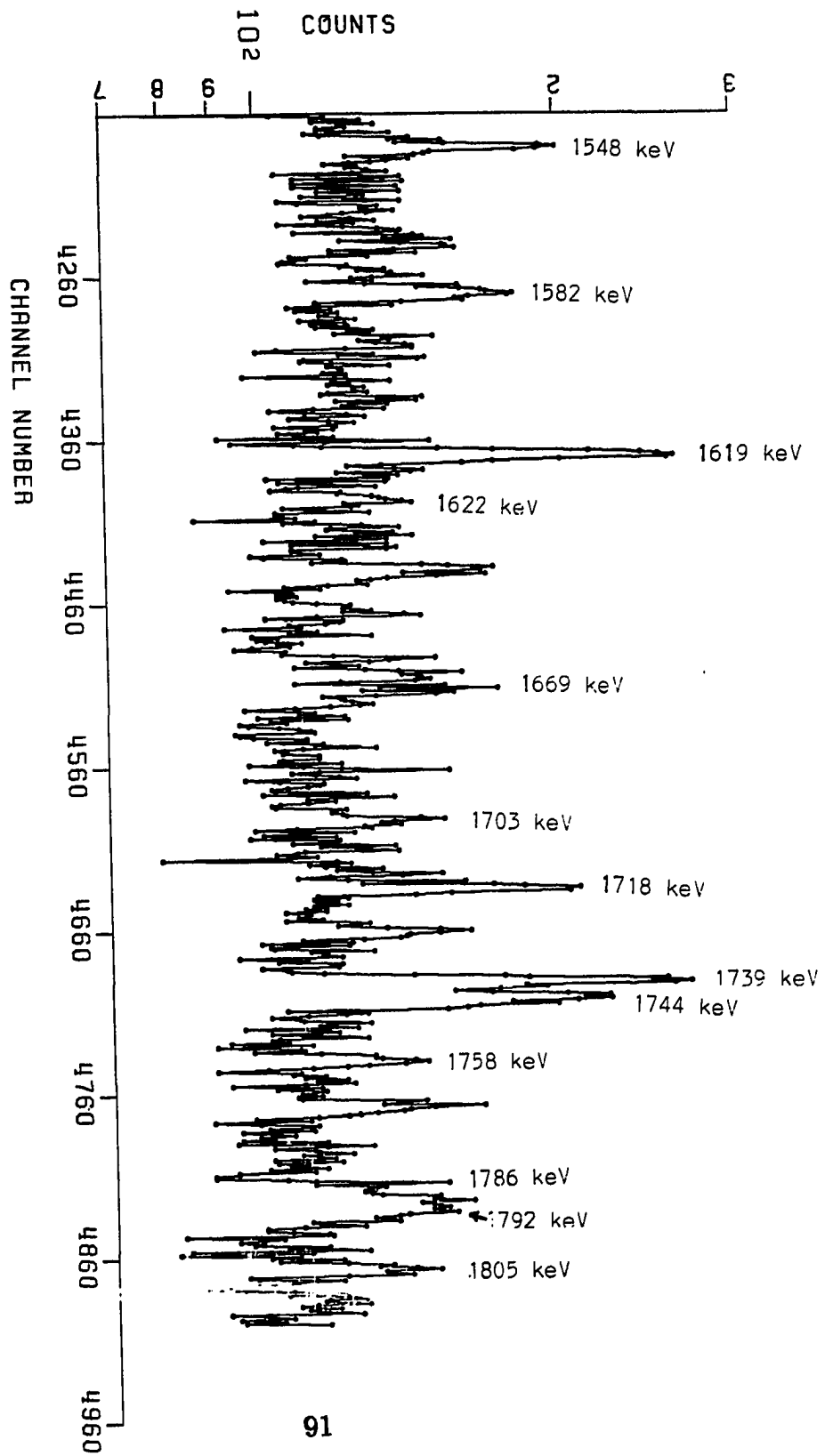


Figure 5.2e. Gamma Spectrum from ^{99}Sr Decay

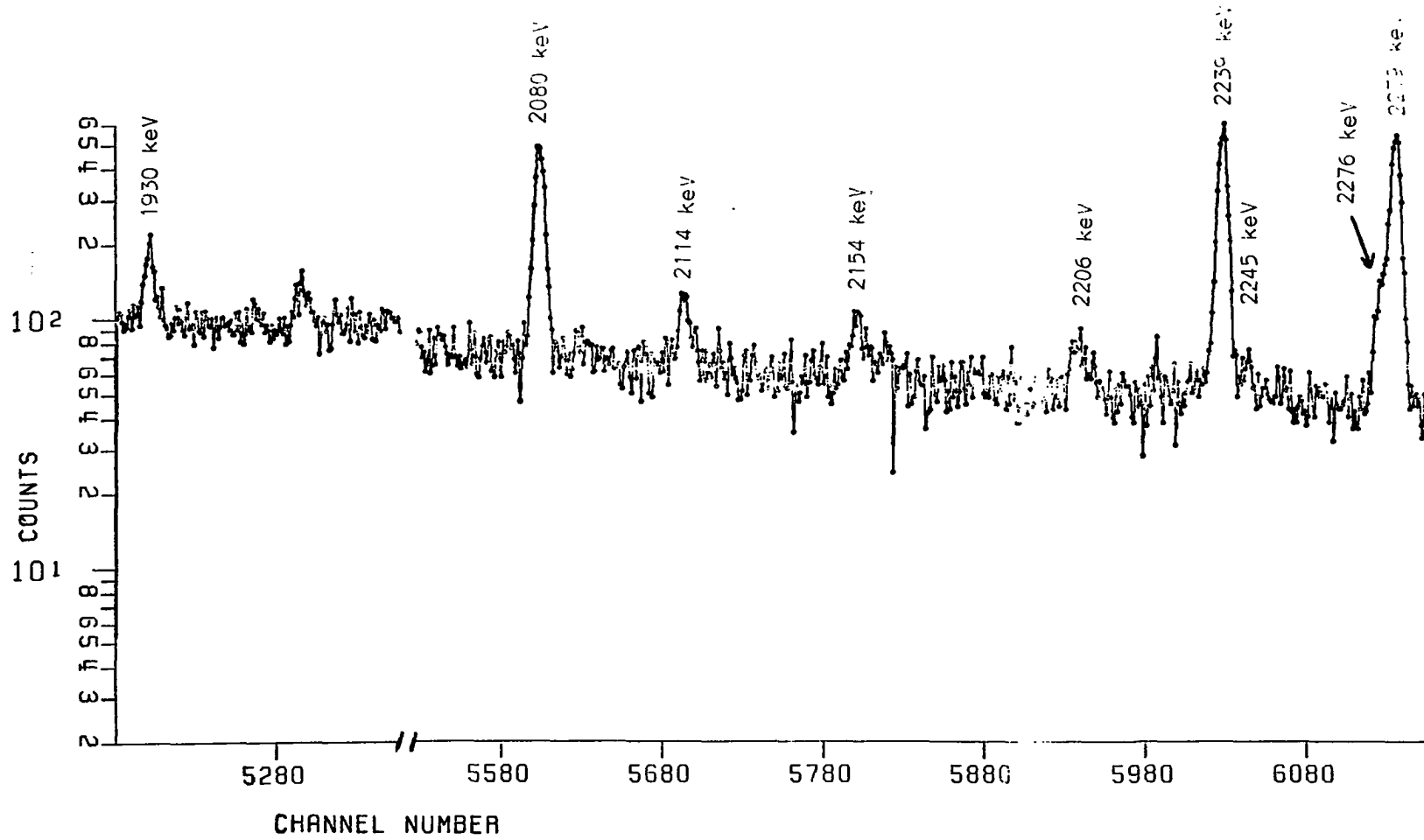


Figure 5.2f. Gamma Spectrum from ^{90}Sr Decay

Table 5.1. The measured energy, intensities of the gamma-rays and their placement in the decay scheme. * indicates a gamma-ray assigned and placed for the first time in this work. † indicates a ^{90}Sr gamma-ray which has not been placed in the decay scheme.

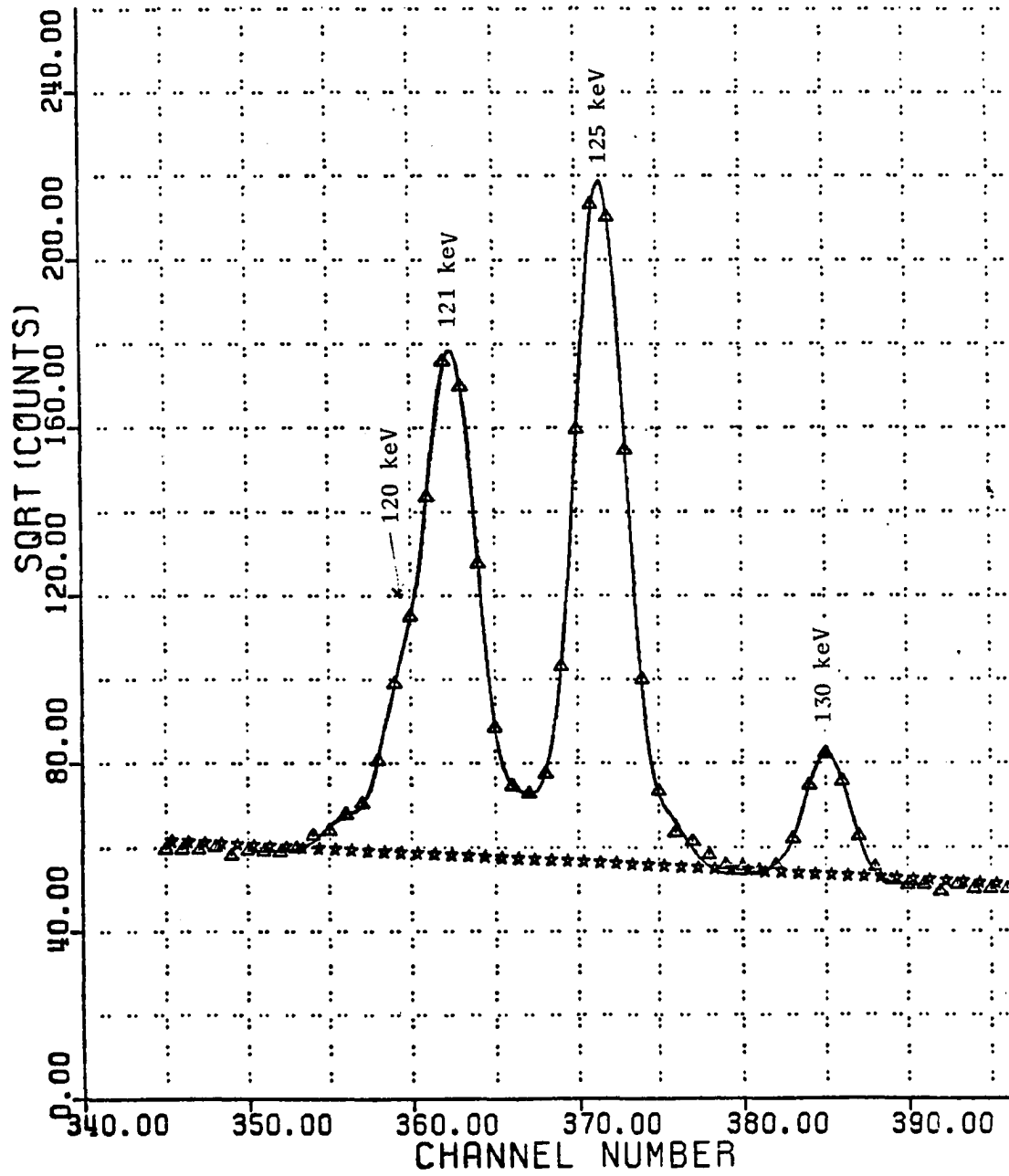
| Energy (KeV) | Intensity | Placement |
|---------------------|-----------------|-------------------------|
| *64.32 \pm 0.08 | 8.4 \pm 0.5 | 600 \rightarrow 536 |
| *120.86 \pm 0.30 | 9.8 \pm 4.1 | 656 \rightarrow 536 |
| 125.18 \pm 0.05 | 100.0 \pm 8.7 | 125 \rightarrow 0 |
| 158.67 \pm 0.06 | 10.3 \pm 0.7 | 283 \rightarrow 125 |
| *160.78 \pm 0.07 | 4.4 \pm 0.4 | 817 \rightarrow 656 |
| 169.62 \pm 0.09 | 3.1 \pm 0.4 | 656 \rightarrow 487 |
| *198.38 \pm 0.16 | 0.5 \pm 0.1 | 482 \rightarrow 283 |
| *210.13 \pm 0.19 | 0.8 \pm 0.2 | 1402 \rightarrow 1191 |
| 283.79 \pm 0.26 | 1.0 \pm 0.3 | 283 \rightarrow 0 |
| *330.43 \pm 0.13 | 2.3 \pm 0.5 | 817 \rightarrow 487 |
| *340.48 \pm 0.25 | 1.3 \pm 0.4 | 624 \rightarrow 283 |
| †353.27 \pm 0.20 | 1.0 \pm 0.2 | |
| 362.26 \pm 0.13 | 2.9 \pm 0.3 | 487 \rightarrow 125 |
| *375.20 \pm 1.0 | < 0.5 | 1119 \rightarrow 817 |
| †422.88 \pm 0.33 | 0.7 \pm 0.2 | |
| 462.72 \pm 0.10 | 5.6 \pm 0.8 | 1119 \rightarrow 656 |
| *475.57 \pm 0.05 | 8.3 \pm 0.7 | 1011 \rightarrow 536 |
| 487.28 \pm 0.05 | 28.1 \pm 2.0 | 487 \rightarrow 0 |
| 499.21 \pm 0.12 | 4.7 \pm 0.7 | 624 \rightarrow 125 |
| 531.68 \pm 0.09 | 18.5 \pm 2.1 | 656 \rightarrow 125 |
| *533.81 \pm 0.53 | 4.3 \pm 2.8 | 817 \rightarrow 283 |
| *536.05 \pm 0.05 | 87.9 \pm 7.0 | 536 \rightarrow 0 |
| *583.41 \pm 0.07 | 6.0 \pm 0.8 | 1119 \rightarrow 536 |
| 624.31 \pm 0.09 | 4.6 \pm 0.6 | 624 \rightarrow 0 |
| *632.16 \pm 0.62 | 1.3 \pm 0.7 | 1119 \rightarrow 487 |
| 657.16 \pm 0.22 | 2.0 \pm 0.4 | 656 \rightarrow 0 |
| *661.57 \pm 0.11 | 5.5 \pm 0.6 | 1198 \rightarrow 536 |
| *732.30 \pm 0.30 | 1.5 \pm 0.5 | 1930 \rightarrow 1198 |
| *740.15 \pm 0.72 | 0.9 \pm 0.4 | 1930 \rightarrow 1191 |
| *802.66 \pm 0.26 | 1.2 \pm 0.4 | 1402 \rightarrow 600 |
| *875.44 \pm 0.22 | 3.4 \pm 0.8 | 1411 \rightarrow 536 |
| †921.90 \pm 0.28 | 0.8 \pm 0.3 | |
| *936.93 \pm 0.19 | 2.9 \pm 0.5 | 1220 \rightarrow 283 |
| *994.21 \pm 0.38 | 3.3 \pm 0.6 | 1119 \rightarrow 125 |
| *1008.77 \pm 0.11 | 17.0 \pm 1.4 | 2205 \rightarrow 1198 |
| *1041.63 \pm 0.71 | 1.1 \pm 0.7 | 2239 \rightarrow 1198 |
| 1047.32 \pm 0.09 | 27.3 \pm 2.2 | 2245 \rightarrow 1198 |

Table 5.1, continued

| Energy (KeV) | Intensity | Placement |
|-------------------------------|------------|-----------|
| 1066.46 ± 0.16 | 8.8 ± 1.3 | 1191→125 |
| *1095.52 ± 0.27 | 3.9 ± 0.8 | 1220→125 |
| *1117.10 ± 0.22 | 4.8 ± 0.7 | 2315→1198 |
| *1191.51 ± 0.34 | 3.8 ± 1.0 | 1191→0 |
| *1195.51 ± 0.36 | 6.4 ± 2.6 | 2315→1119 |
| 1198.34 ± 0.18 | 60.2 ± 4.1 | 1198→0 |
| *1264.80 ± 0.46 | 2.0 ± 0.7 | 2276→1011 |
| *1277.13 ± 0.32 | 4.8 ± 0.8 | 1402→125 |
| *1388.51 ± 0.55 | 3.8 ± 1.2 | 2205→817 |
| *1402.21 ± 0.42 | 7.5 ± 1.4 | 1402→0 * |
| *1411.78 ± 0.39 | 10.7 ± 1.3 | 1411→0 |
| *1421.58 ± 0.48 | 3.1 ± 0.9 | 2239→817 |
| *1443.45 ± 0.29 | 4.6 ± 1.0 | 1930→487 |
| *1548.77 ± 0.57 | 5.5 ± 1.3 | 2205→656 |
| * ^a 1582.33 ± 0.58 | 6.0 ± 0.9 | 2205→624 |
| | | 2239→656 |
| 1619.00 ± 0.57 | 10.5 ± 1.4 | 2276→656 |
| *1622.76 ± 0.80 | 2.2 ± 0.8 | 2279→656 |
| *1669.65 ± 0.79 | 3.1 ± 1.3 | 2205→536 |
| *1703.12 ± 0.56 | 3.7 ± 0.7 | 2239→536 |
| *1718.68 ± 0.51 | 5.9 ± 1.2 | 2205→487 |
| *1739.96 ± 0.48 | 13.1 ± 3.1 | 2276→536 |
| 1744.06 ± 0.50 | 10.7 ± 1.7 | 2279→536 |
| *1758.00 ± 0.50 | 4.9 ± 0.8 | 2245→487 |
| †1786.24 ± 0.17 | 2.4 ± 0.6 | |
| *1792.95 ± 0.70 | 4.7 ± 1.7 | 2279→487 |
| *1805.60 ± 0.57 | 7.0 ± 1.4 | 1930→125 |
| *1930.63 ± 0.35 | 9.9 ± 1.4 | 1930→0 |
| *2080.43 ± 0.18 | 37.2 ± 3.2 | 2205→125 |
| *2114.48 ± 0.35 | 6.8 ± 1.2 | 2239→125 |
| *2154.69 ± 0.59 | 6.2 ± 1.9 | 2279→125 |
| *2206.21 ± 0.48 | 4.5 ± 1.1 | 2205→0 |
| *2239.47 ± 0.11 | 47.4 ± 3.3 | 2239→0 |
| *2245.46 ± 0.47 | 2.3 ± 0.8 | 2245→0 |
| *2276.23 ± 0.32 | 7.6 ± 3.1 | 2276→0 |
| *2279.65 ± 0.10 | 48.7 ± 3.5 | 2279→0 |

^aPlaced twice in decay scheme

determine the half-life of some of the transitions from multiscale measurements because of low statistics, and in these cases assignments were made from the coincidence relations. The 120-keV transition was clearly resolved from the 121-keV line (the strongest γ -ray transition from ^{90}Y decay) only in the first three multiscale spectra, and its growth was similar to other γ -transitions from ^{90}Sr decay. It is one of the complex gamma-transitions for which a half-life measurement was impossible to perform, and only the coincidence relationships give a definite identification for this line. The relative intensity of this gamma-ray was determined by fitting the 121-keV transition as a doublet (see Figure 5.3). The 536-keV transition had been previously assigned as a gamma-ray transition from ^{90}Y beta decay to a level in ^{90}Zr .⁶⁹ The decay of this transition showed that this gamma-ray belongs to ^{90}Sr beta decay also. Because the relative intensity of this gamma-transition from ^{90}Y is known, by using this relative intensity and simply subtracting the intensity associated with decay of ^{90}Y from total intensity of this transition, the relative intensity of the 536-keV transition associated with beta decay of ^{90}Sr was determined. The correction was made for the 536-keV line in all sixteen GMS spectra to determine the area under this peak in each of the spectra due only to the beta decay of ^{90}Sr . This correction was used to determine the half-life of the 536-keV line, which was in good agreement with other γ -transitions from ^{90}Sr beta decay. Figure 4.3 shows the decay of the 536-keV transition with and without correction.



5.3. Peak Fitting to 120-130 keV Region in Gamma Spectrum of ^{90}Sr

Comparisons of the relative intensities obtained in this work with values reported in a previous beta decay study⁵⁷ is given in Table 5.2.

The level scheme for ^{90}Y populated from ^{90}Sr beta decay is given in Figure 5.4. More than one million coincidence events were used to establish this level scheme, and coincidence spectra were obtained by setting gates on more than 200 transitions. Table 5.3 presents the coincidence information. Figures 5.5a-c show the coincidence spectrum of the 125-keV gate as an example.

A rather complete level scheme for ^{90}Y is proposed in this work with 24 energy levels and 65 transitions. A preliminary decay scheme was presented by Pfeiffer *et al.*⁵⁷ at the Fourth International Conference on Nuclei Far from Stability while the analysis of this data was still in progress. They reported eleven energy levels with 17 gamma-transitions. Three of the levels suggested in their work, 588, 1047 and 1743 keV, could not be confirmed in the present work and they will be discussed later on in this section. In the following, each level will be discussed individually.

Ground State: Using an absolute intensity for the 546-keV gamma transition in ^{90}Zr obtained from reference 68, the ground state beta feeding of ^{90}Y was calculated to be 30%. The $\text{Log}ft \simeq 5$ of this beta branch implies that this beta transition is allowed. There has no direct spin measurement for either the ^{90}Sr or ^{90}Y ground states, but based on indirect arguments an assignment of $3/2^+$ or $5/2^+$ has been made for the ^{90}Y ground state and

Table 5.2. The comparison of the intensity of present work with previous work.

| Energy (KeV) | Intensity (Ref. 13) | Intensity (This work) |
|-------------------------|--------------------------------|----------------------------------|
| 125.1 | 100 | 100.0 |
| 158.6 | 10 | 10.3 |
| 169.8 | 4 | 3.1 |
| 283.7 | 2 | 1.0 |
| 361.9 | 5 | 2.9 |
| 463.0 | 6 | 5.6 |
| 487.0 | 18 | 28.1 |
| 499.5 | 8 | 4.7 |
| 531.5 | 12 | 18.5 |
| 624.5 | 4 | 4.6 |
| 656.8 | 7 | 2.0 |
| 1047.7 | 18 | 27.3 |
| 1065.5 | 10 | 8.8 |
| 1072.5 | 10 | --- |
| 1198.0 | 15 | 60.2 |
| 1618.6 | 6 | 10.5 |
| 1744.0 | 6 | 10.7 |

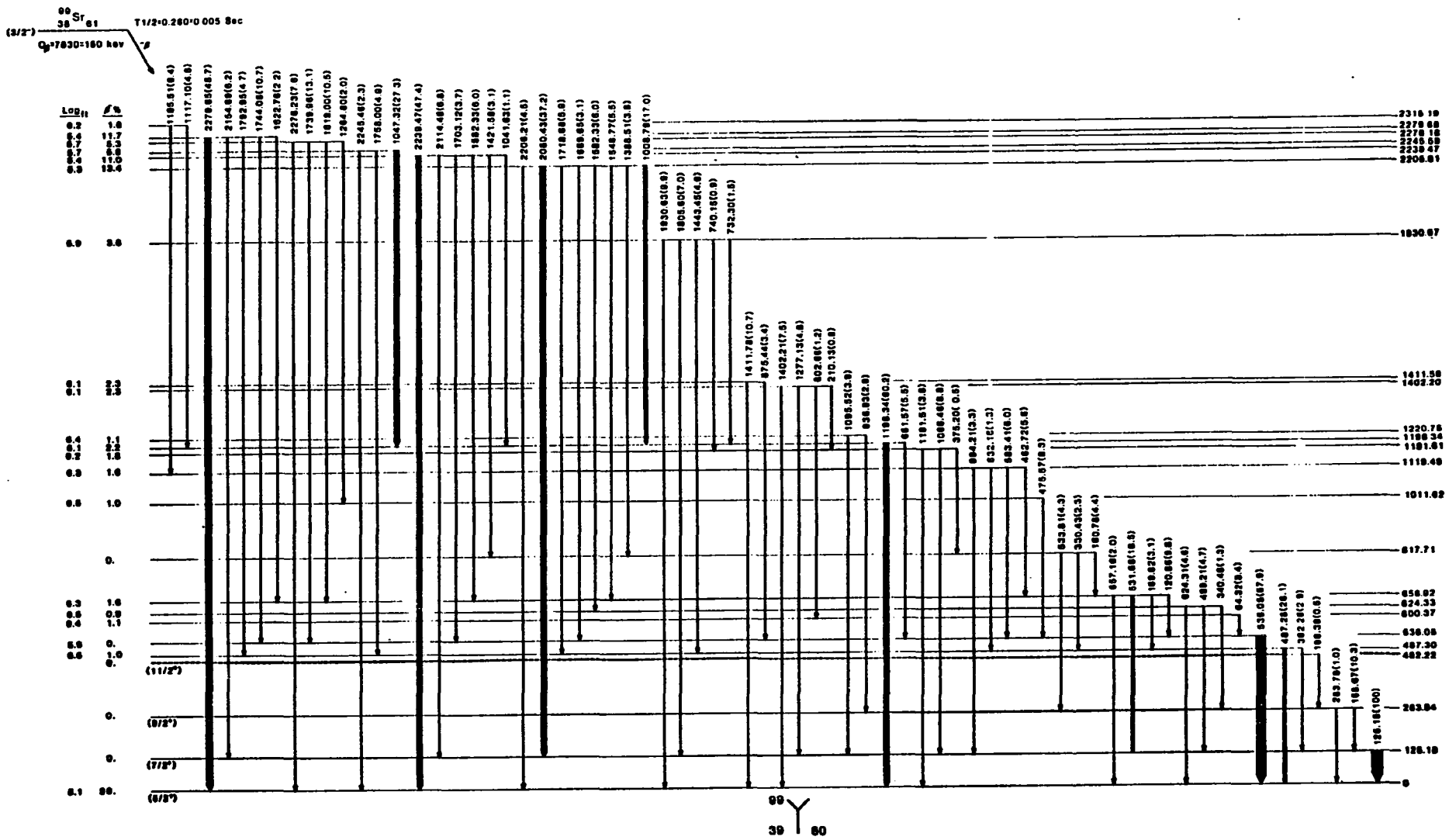


Figure 5.4. Decay Scheme of ^{90}Sr

Table 5.3. The coincidence relationships of the gamma-rays studied in decay of ^{90}Sr . [] indicates possible coincidence.

| Coincidence Gate (KeV) | Coincidence (KeV) |
|------------------------|--|
| 64.32 | 536, |
| 120.86 | 160, 536, 1195, 1421, 1619, |
| 125.18 | 158, 160, 198, 340, 362, [375], 462, 499, 531, 534, 936, 1066, 1095, 1195, 1277, 1388, [1421], 1548, 1619, 1805, 2080, 2114, [2154], |
| 158.67 | 125, 340, 534, 936, |
| 160.78 | 120, 125, 169, 373, 531, 536, 1388, 1421, |
| 169.62 | 125, 160, 487, |
| 198.38 | 125, 158, 160, |
| 210.13 | 125, 1066, [1191], |
| 283.78 | |
| 330.43 | 362, [373], 487, |
| 340.48 | 125, 158, [283], |
| 353.27 | |
| 362.26 | 125, 330, |
| 375.20 | |
| 422.88 | |
| 462.72 | 120, 125, 169, 531, 536, [487], 1195 |
| 475.57 | 536, 1264, |
| 487.28 | 169, 330, [632], [462], 1943, 1718, 1792 |
| 499.21 | 125, 1582, |
| 531.68 | 125, 160, 462, [1421], 1619, 1195 |
| 533.81 | 125, 158, |
| 536.05 | 64, 120, 160, [462], 475, 583, 661, 802, 875, 1047, 1195, 1264, 1619, [1623], 1669, 1703, 1739, 1744, |
| 583.41 | 536, 1195 |

Table 5.3, continued

| Coincidence Gate (KeV) | Coincidence (KeV) |
|------------------------|-------------------------------|
| 624.31 | 1582, |
| 632.16 | [487], |
| 657.16 | |
| 661.57 | 536, [1047], |
| 732.30 | |
| 740.15 | 1191, |
| 802.66 | 64, 536, |
| 875.44 | 536, |
| 921.90 | 125, |
| 936.93 | 125, 158, |
| 994.21 | [125] |
| 1008.77 | 1198, |
| 1041.63 | |
| 1047.32 | 536, 661, 1198, |
| 1066.46 | 125, 210, |
| 1095.52 | 125, |
| 1117.10 | 1198, |
| 1191.51 | [210], |
| 1195.51 | 120, 125, 462, 531, 536, 583, |
| 1198.34 | 1008, [1041], 1047, 1117, |
| 1264.80 | 536, |
| 1277.13 | 125, |
| 1388.51 | [120], [125], 160, [531], |
| 1402.21 | |
| 1411.78 | |
| 1421.58 | 125, [160], 160, 536 |

Table 5.3, continued

| Coincidence Gate (KeV) | Coincidence (KeV) |
|------------------------|---------------------|
| 1443.45 | [125], 487, |
| 1548.77 | [120], 125, |
| 1582.33 | [125] |
| 1619.00 | 120, 125, 531, 536, |
| 1622.00 | 536, |
| 1669.65 | 536, |
| 1703.12 | 536, |
| 1718.68 | [125], 487 |
| 1739.96 | 536, |
| 1744.06 | [536], |
| 1758.00 | 487, |
| 1786.24 | |
| 1792.95 | [487], |
| 1805.60 | 125, |
| 1930.63 | |
| 2080.43 | 125, |
| 2114.48 | 125, |
| 2154.69 | 125, |
| 2206.21 | |
| 2239.47 | |
| 2245.46 | |
| 2276.23 | |
| 2279.65 | |

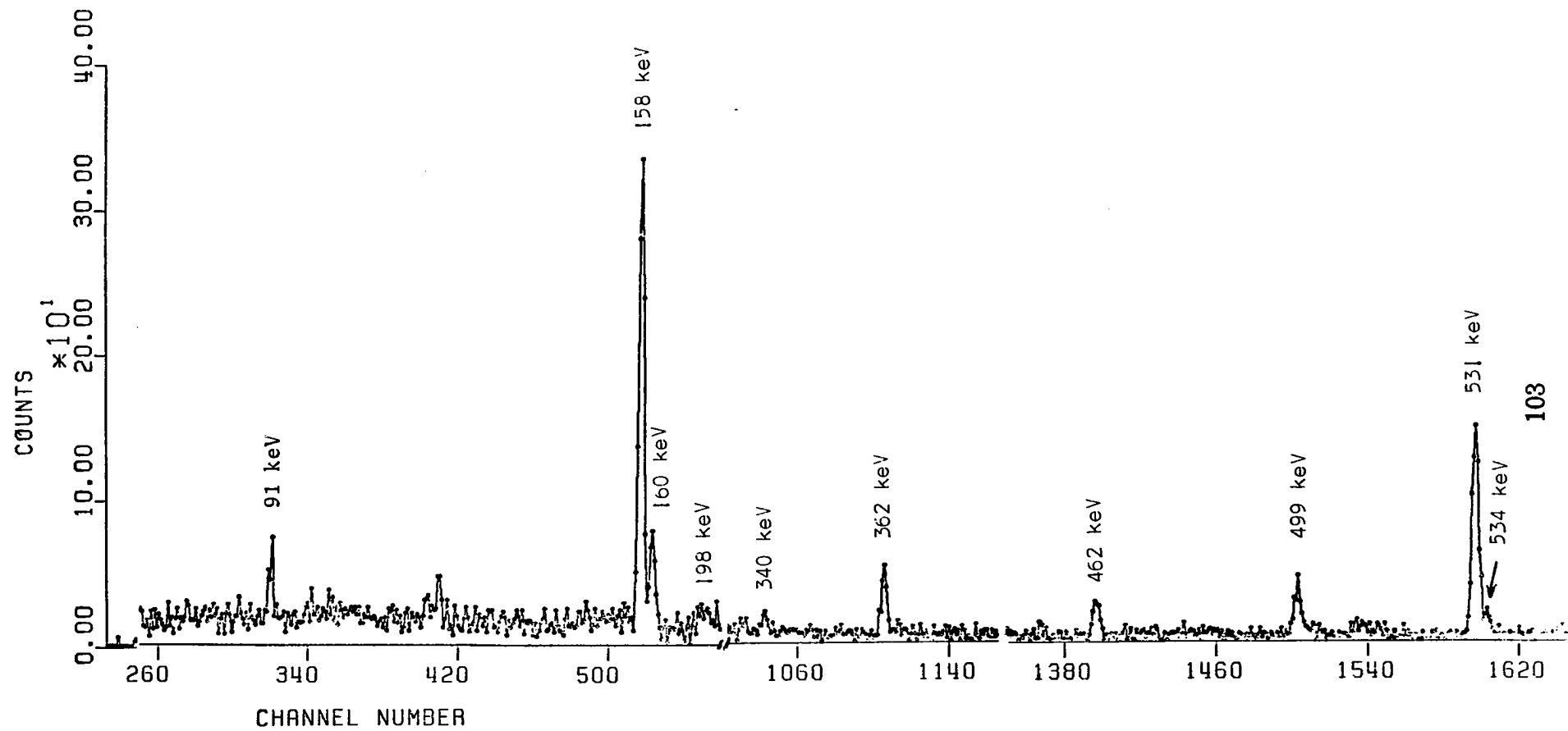


Figure 5.5a. Spectrum in Coincidence with the 125-keV Transition in ^{90}Sr

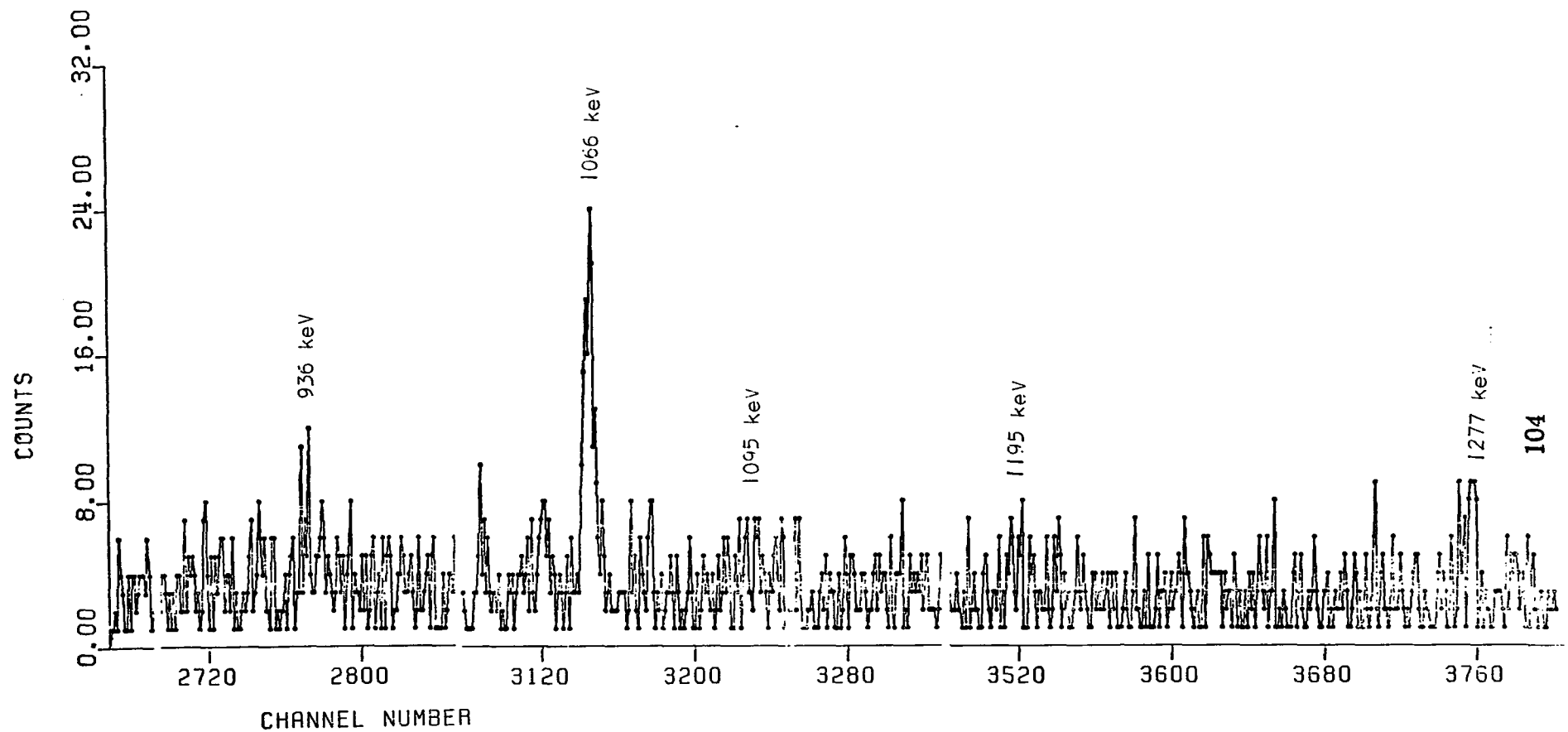


Figure 5.5b. Spectrum in Coincidence with the 125-keV Transition in ^{90}Sr

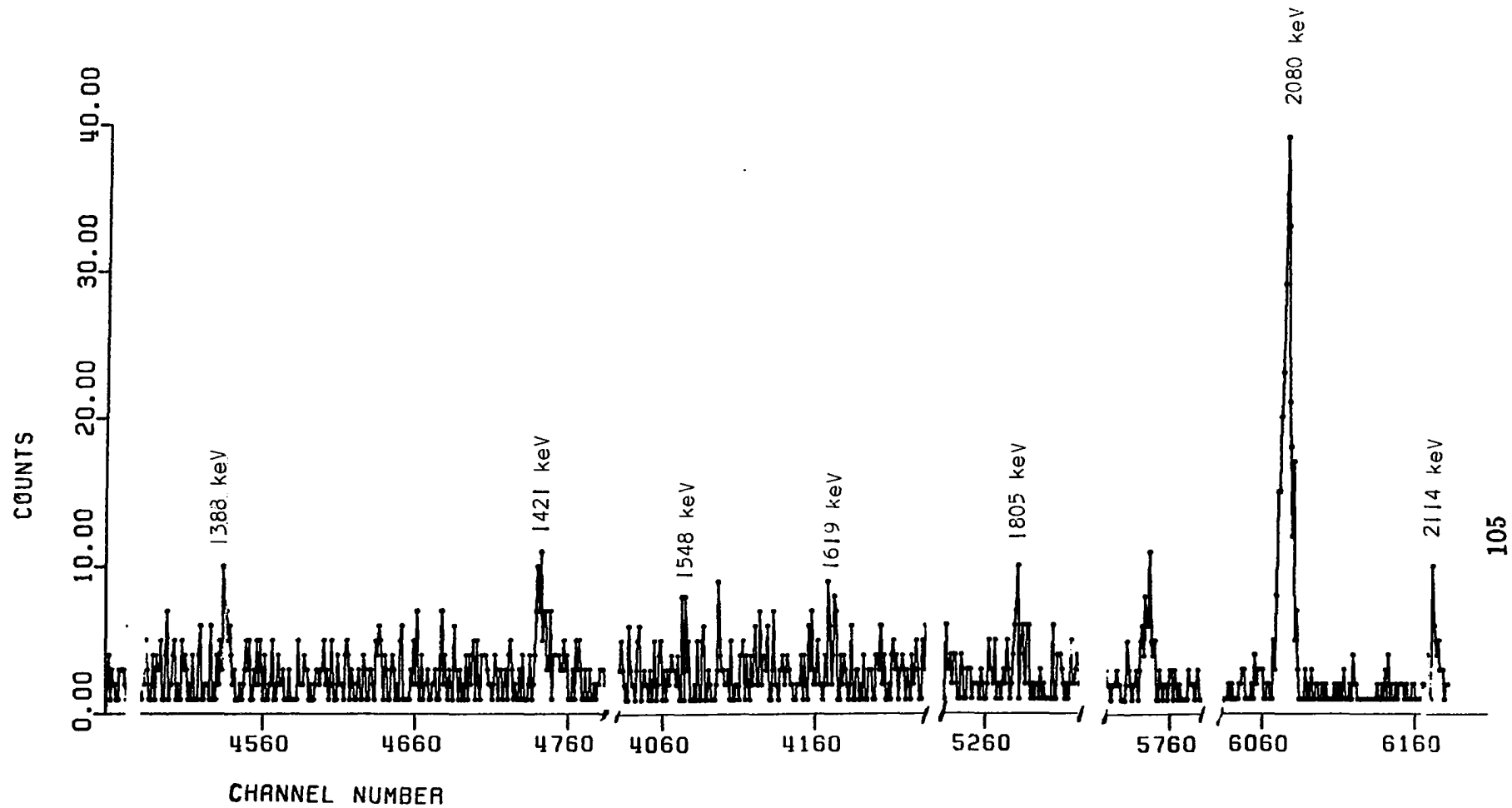


Figure 5.5c. Spectrum in Coincidence with the 125-keV
Transition in ^{90}Sr

either $3/2^+$ or $5/2^+$ for the ^{90}Sr ground state.⁶¹ The most recent published work lists $5/2^+$ for the ^{90}Y ground state.⁴⁹ The results in this work are consistent with any of these assignments. The discussion of the remainder of the levels is based on the assumption that the ground states of ^{90}Sr and ^{90}Y being $3/2^+$ and $5/2^+$ respectively.

125-keV level: This level is very well established by the coincidence relationships (see Figure 5.5). The gamma-ray intensity balance for this level suggests no beta feeding which implies either a negative parity or a spin differing from $3/2$ by 2 units. Based on the spin of the ground state, this level can have spin of $\frac{7}{2}^+$.

283-keV Level: This level is very well established by coincidence relationships in this work. There is no beta feeding to this level which would indicate an assignment of $7/2^+$ or greater or negative parity.

482-keV Level: The 198-keV transition is very weak but it has been observed in the 125-keV gate (see Figure 5.5). This level is based on coincidence relationships in this work.

487-keV Level: This level is very well confirmed by coincidence relationships. The beta feeding to this level is very small and a $\text{Logft} \simeq 6.4$ suggests a first forbidden non-unique beta transition, which indicates a change in parity. This level might be another intrinsic state. The most likely negative parity intrinsic state is a $5/2^-$ Nilsson state. This would be consistent with the gamma branching of this level.

536-keV Level: The level at 536 keV has a strong transition to the ground state and no feeding to any other levels below it, and the Logft tends to favor a first forbidden beta transition. The fact that there are no transitions to lower excited states suggests that the level at 536 keV might be another intrinsic state with different parity. An $I^\pi = 3/2^-$ assignment for this level is consistent with a transition only to ground state.

600-keV Level: The establishment of this level is based on the 64-keV gamma-ray transition to the 536-keV level. It is very well confirmed by coincidence relationships (see Figure 5.6). The beta feeding to this level is small and Logft $\simeq 6.42$ suggest a change in parity. An assignment of $I^\pi = 1/2^-$ is consistent with the fact that this level has a gamma branch only to the 536-keV level.

624-keV Level: It is very well established by the coincidence relationship of the three gamma-rays depopulating the level. A negligible beta feeding has been observed to this level. The deduced Logft is the same as that for the 487-keV level, which suggests a change in parity. An $I^\pi = 7/2^-$ seems to be a reasonable choice for this level.

656-keV Level: This is very well established level based on coincidence relationships (see Figures 5.5 and 5.6). The beta feeding to this level is small. The Logft of 6.3 indicates a first forbidden beta transition, but could also be consistent with an allowed decay. From the gamma

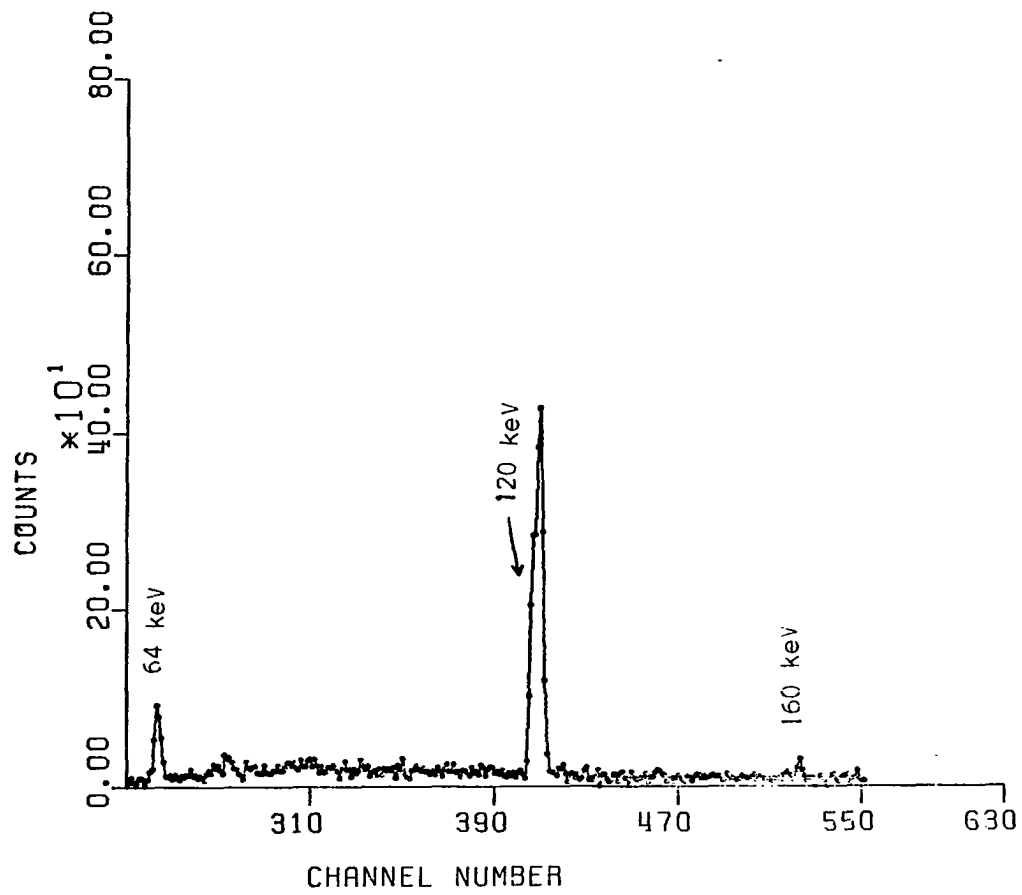


Figure 5.6a. Spectrum in Coincidence with the 536-keV Transition in ^{99}Sr

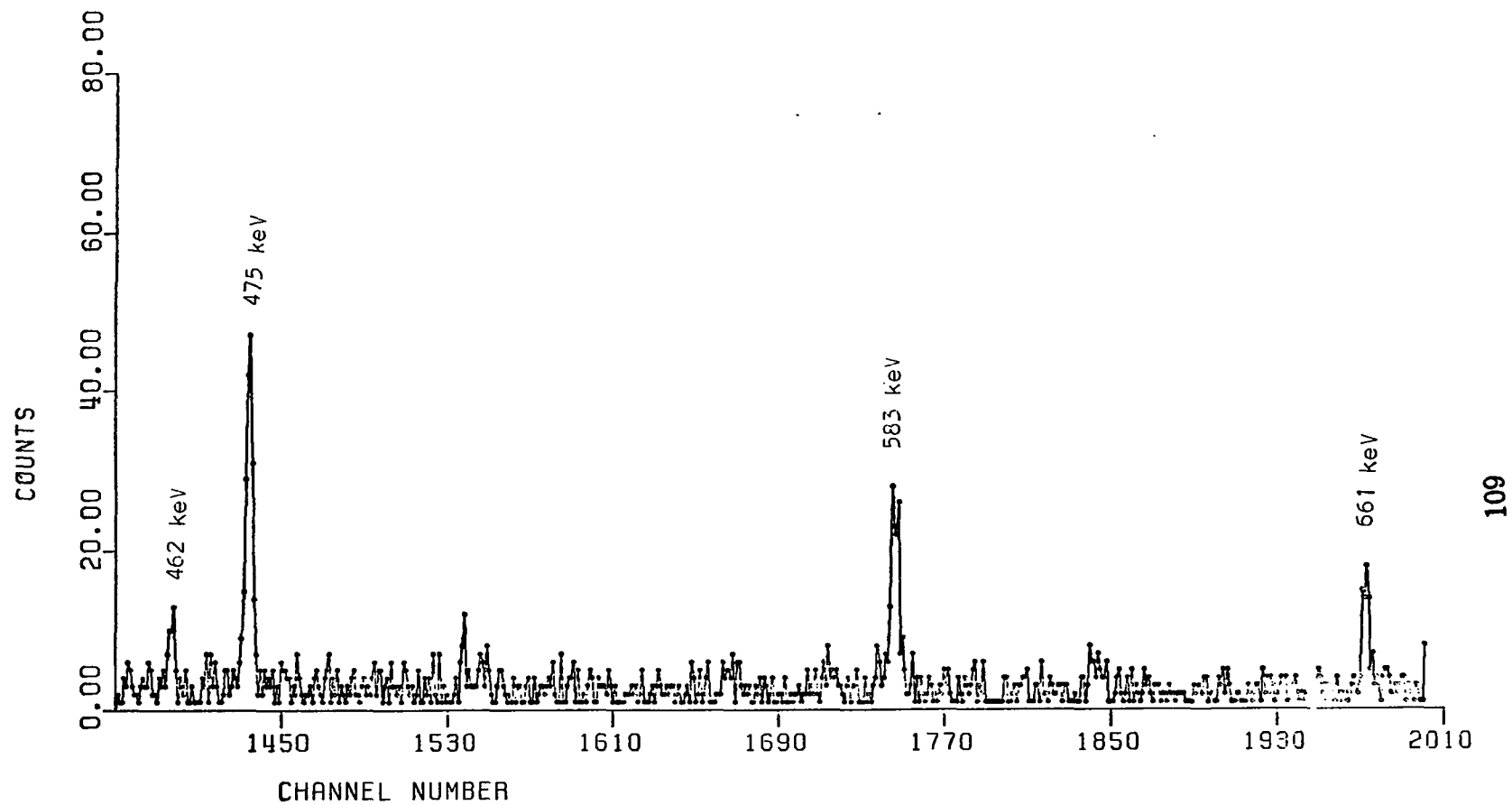


Figure 5.6b. Spectrum in Coincidence with the 536-keV
Transition in ^{90}Sr

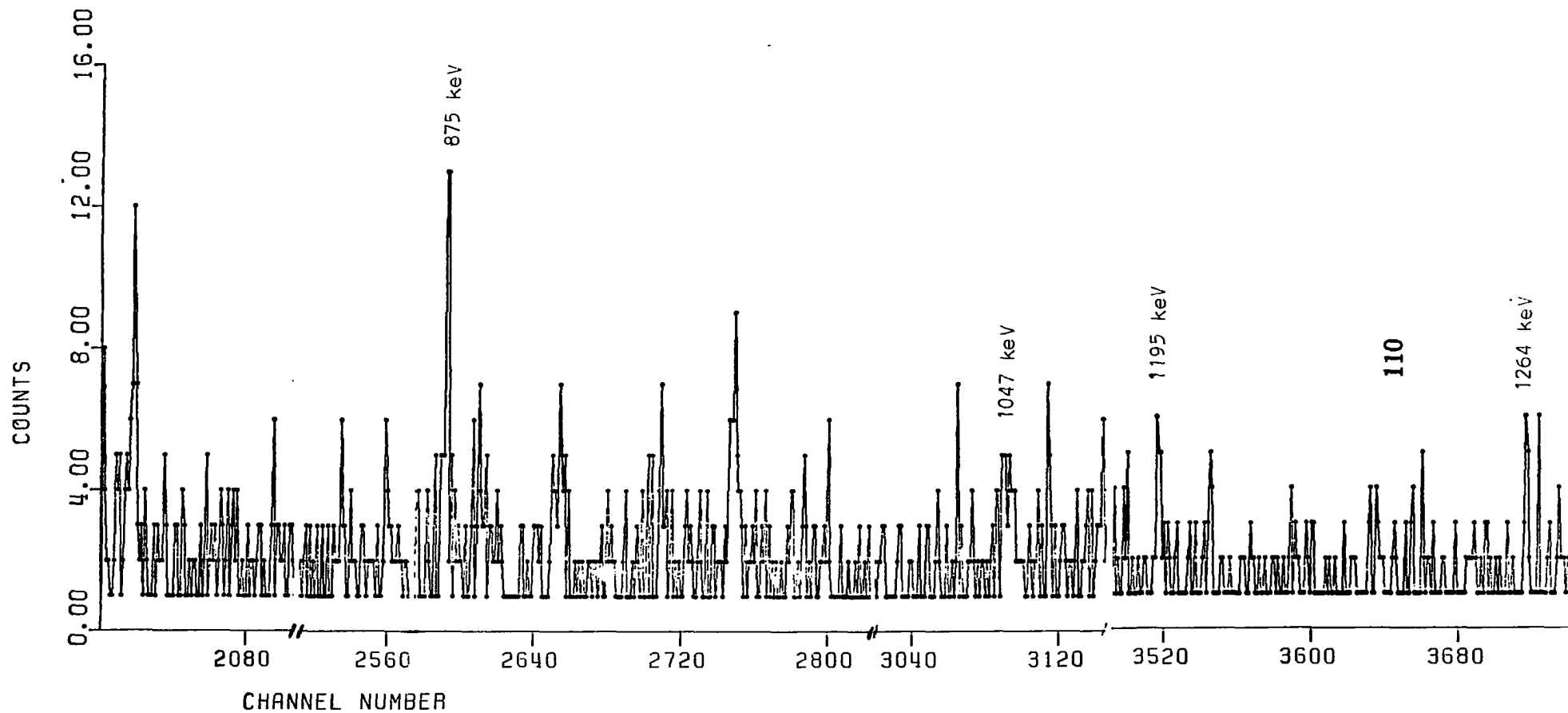


Figure 5.6c. Spectrum in Coincidence with the 536-keV Transition in ^{90}Sr

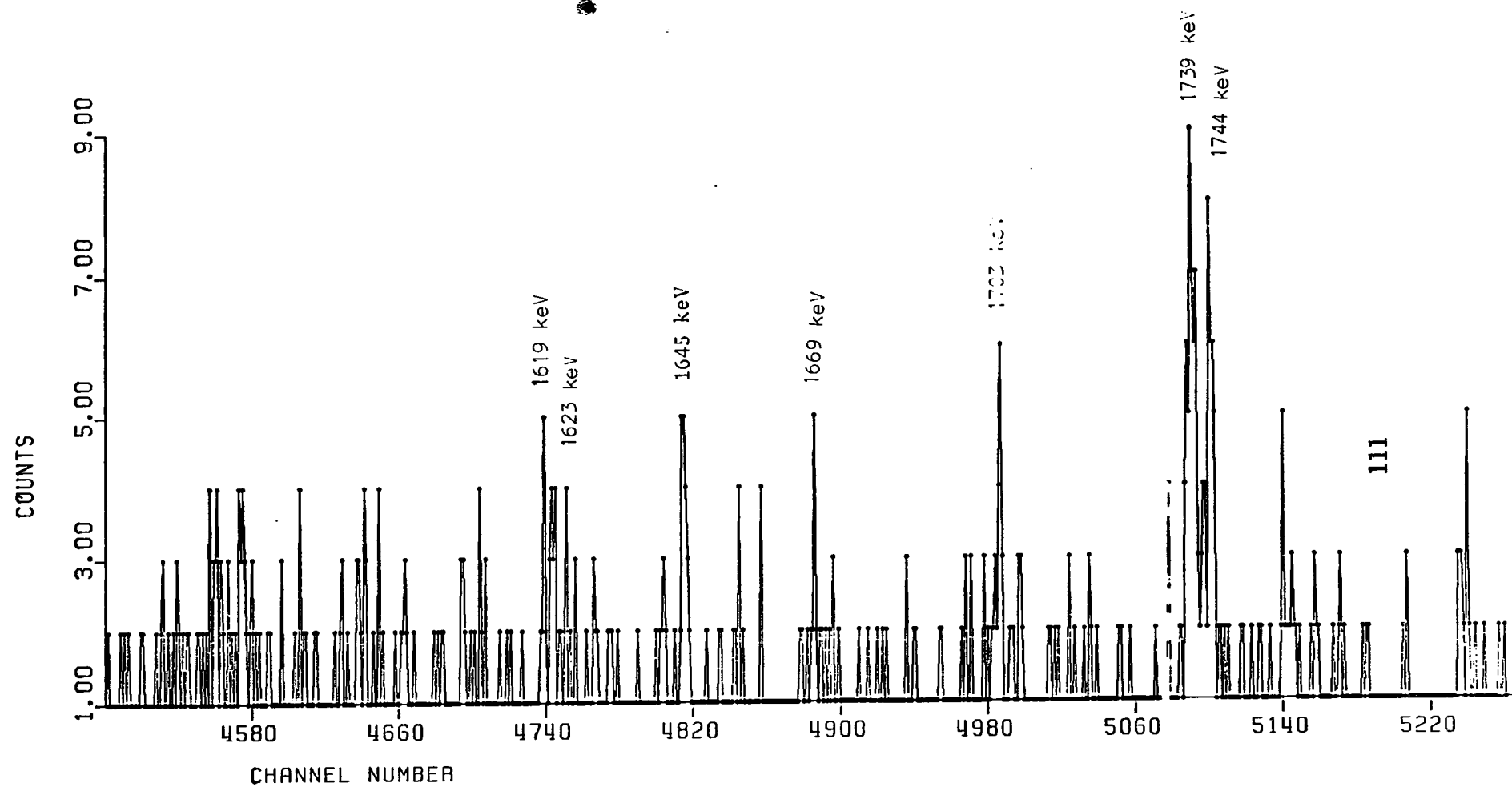


Figure 5.6d. Spectrum in Coincidence with the 536-keV Transition in ^{99}Sr

branching of this state to the lower excited state a spin of $5/2$ seems most likely.

818-keV Level: This level is very well confirmed from the coincidence relationships. The absence of beta feeding to this level indicates the negative parity level or spin difference from $3/2$ of at least 2 units.

1012-keV Level: The establishment of this level is based on coincidence relation of the 475-keV transition. The beta feeding to this level is small, and the deduced $\text{Log}ft$ for this level is similar to that for the 487-keV level. Because there is only a single gamma branch from this level, no inference about the I^π can be made.

1119-keV Level: A level at 588-keV which has been observed in previous beta decay work⁵⁷ was based on a 462-keV transition to the first excited state. This level is not supported by present work because the 462-keV transition is in coincidence with the 125-keV and 531-keV transitions (see Figure 5.7). This leads to the establishment of a new level at 1119-keV which is supported by three other transitions with definite coincidence relationships. The beta feeding to this level is small, and no I^π assignment consistent with this and the gamma-branching can be inferred.

1192-keV Level: This level is well established by coincidence relationships. The beta decay work, beta feeding to this level is small, and the gamma branching to only the ground and first excited state would seem to indicate a spin of $3/2$ or $5/2$ for this level.

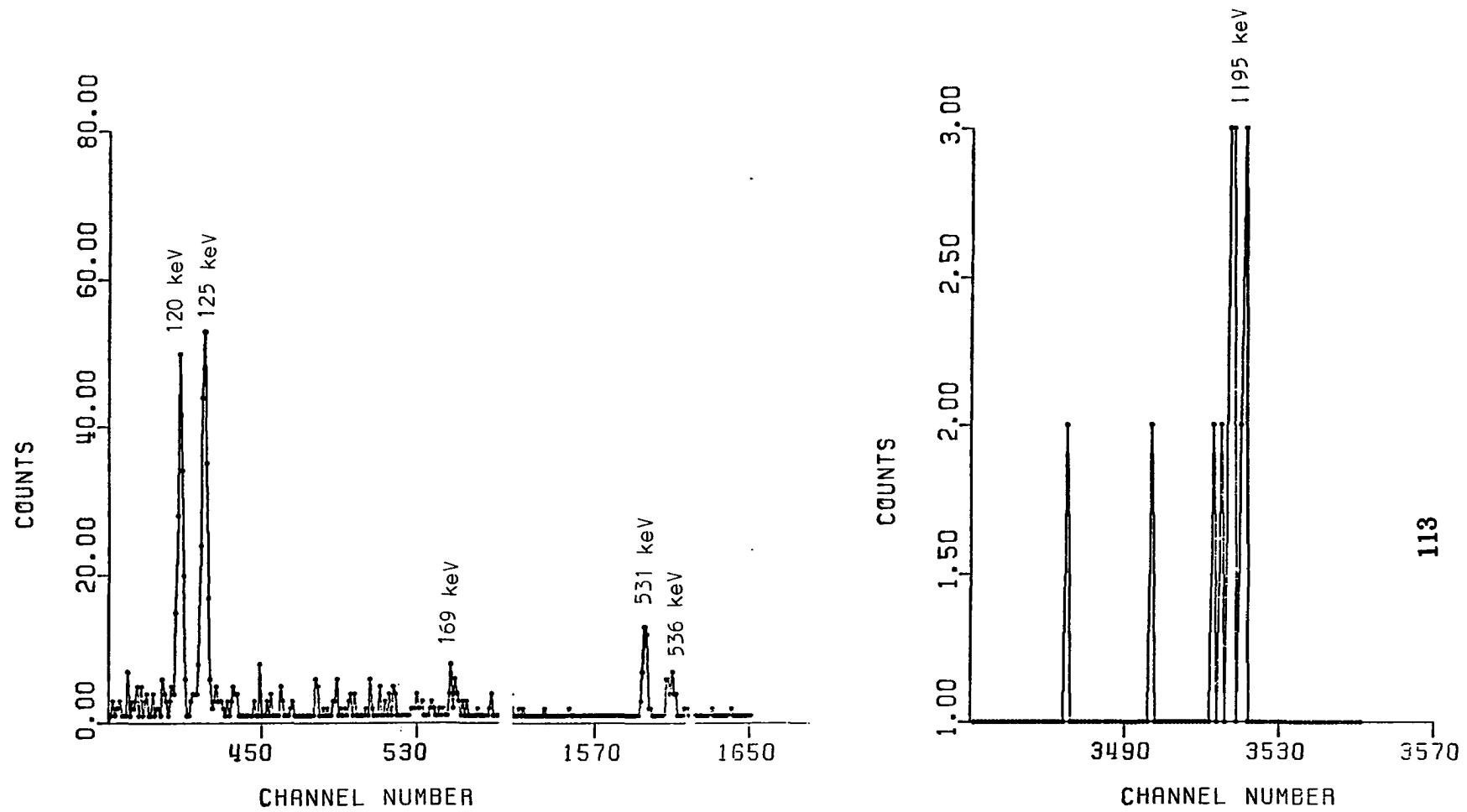


Figure 5.7. Spectrum in Coincidence with the 462-keV Transition in ^{89}Sr

1198-keV Level: This is a very well established level by coincidence relationships. The beta feeding to this level is small. The Logft of 6.1 indicates an allowed or first forbidden transition. An $I^\pi = \frac{1}{2}$ or $\frac{3}{2}$ is consistent with the gamma branching from this level.

1220-keV Level: This level is depopulated by two gamma-ray transitions, which are in coincidence with 125-keV (see Figure 5.5) and 158-keV transitions respectively. The beta feeding to this level is small. It has a similar Logft value as the 487-keV level. A spin of 9/2 or 11/2 for this level is consistent with gamma-ray branching.

1402-keV Level: This level has been very well established by coincidence relationships. The beta feeding is small, and a spin of 3/2 or 5/2 is consistent with gamma branching from the level.

1412-keV Level. The establishment of this level is based on two transitions with definite coincidence relationships. The beta feeding to this level is small. A spin of 1/2 is consistent with the gamma branching from this level.

1930-keV Level: Five gamma-ray transitions which depopulate this level establish it very well.

2206-keV Level: This level, which is depopulated by eight γ -ray transitions, is one of the best established levels with a large beta feeding. A Logft of 5.3 indicates an allowed transition, and this fact plus the γ branching to lower states suggests an $I^\pi = \frac{5}{2}^+$ for this level.

2239-keV Level: This level is another well established level, and has similar beta feeding and gamma branching characteristics to the 2206-keV level. Therefore a $5/2^+$ assignment is also appropriate for this level.

2245-keV Level: The dashed level at 1047 keV in previous work⁵⁷ can not be supported in the present work because the 1047-keV transition is in coincidence with 1198-keV transition (see Figure 5.8). This fact leads to the construction of a new level at 2245 keV. This level is also supported by a ground state transition and by the coincidence relationship between the 1758-keV and 487-keV transitions. Beta feeding to this level is small, and no I^π assignment consistent with this and the gamma branching can be inferred.

2275-and 2279-keV Levels: The level at 1743-keV proposed in previous work⁴ can not be supported by the present work, because the 1619-keV transition is not only in coincidence with the 125-keV transition but also with 531-keV transition (see Figure 5.9). The 1744-keV transition is in coincidence with the 536-keV transition as is shown in Figure 5.10. These two relations lead to establishment of two new levels at 2275 keV and 2279 keV respectively. Each level is supported by several other transitions as well. The beta feeding to the 2275-keV level is small and the Logft and gamma branching do not allow a spin assignment to be inferred. The beta

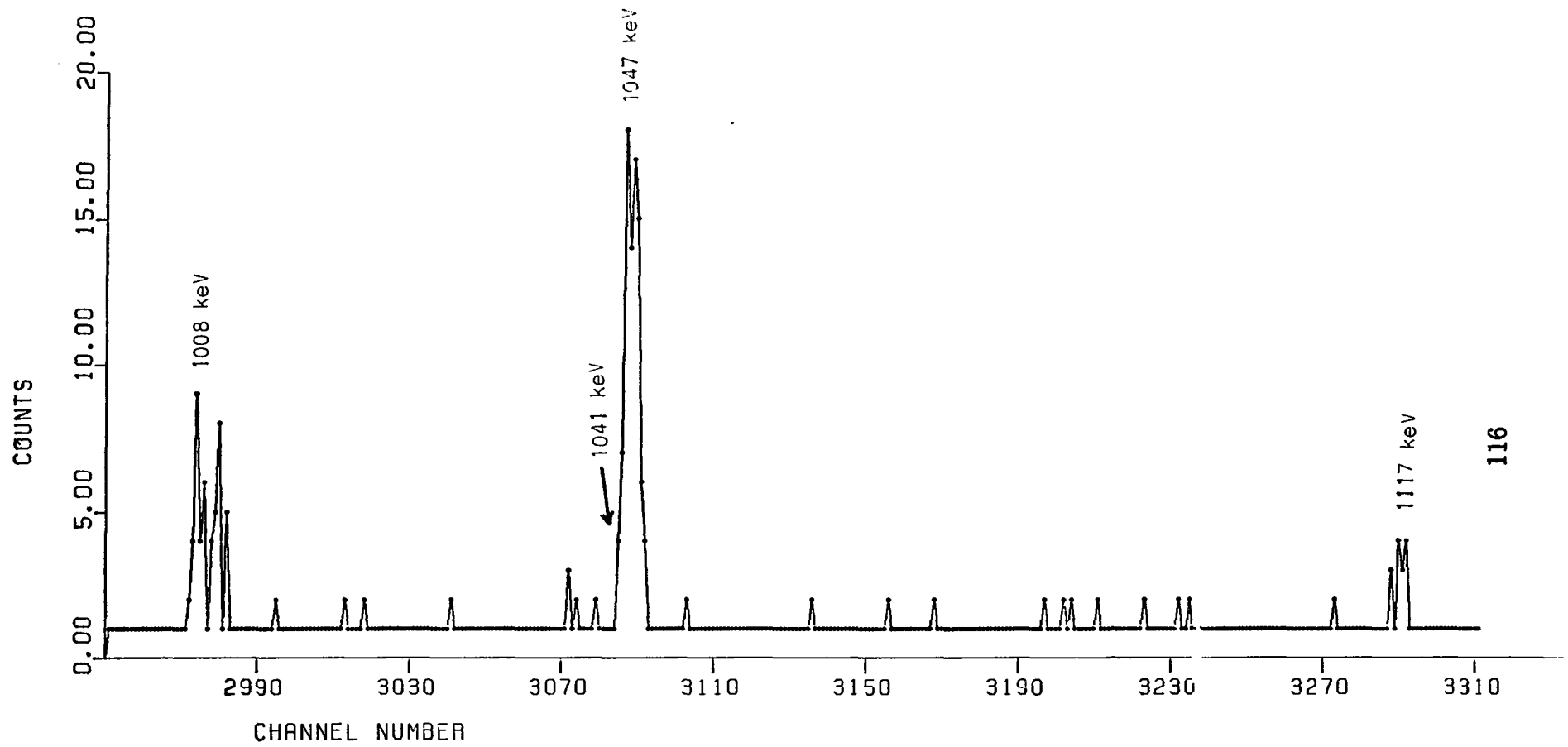


Figure 5.8. Spectrum in Coincidence with the 1198-keV Transition in ^{90}Sr

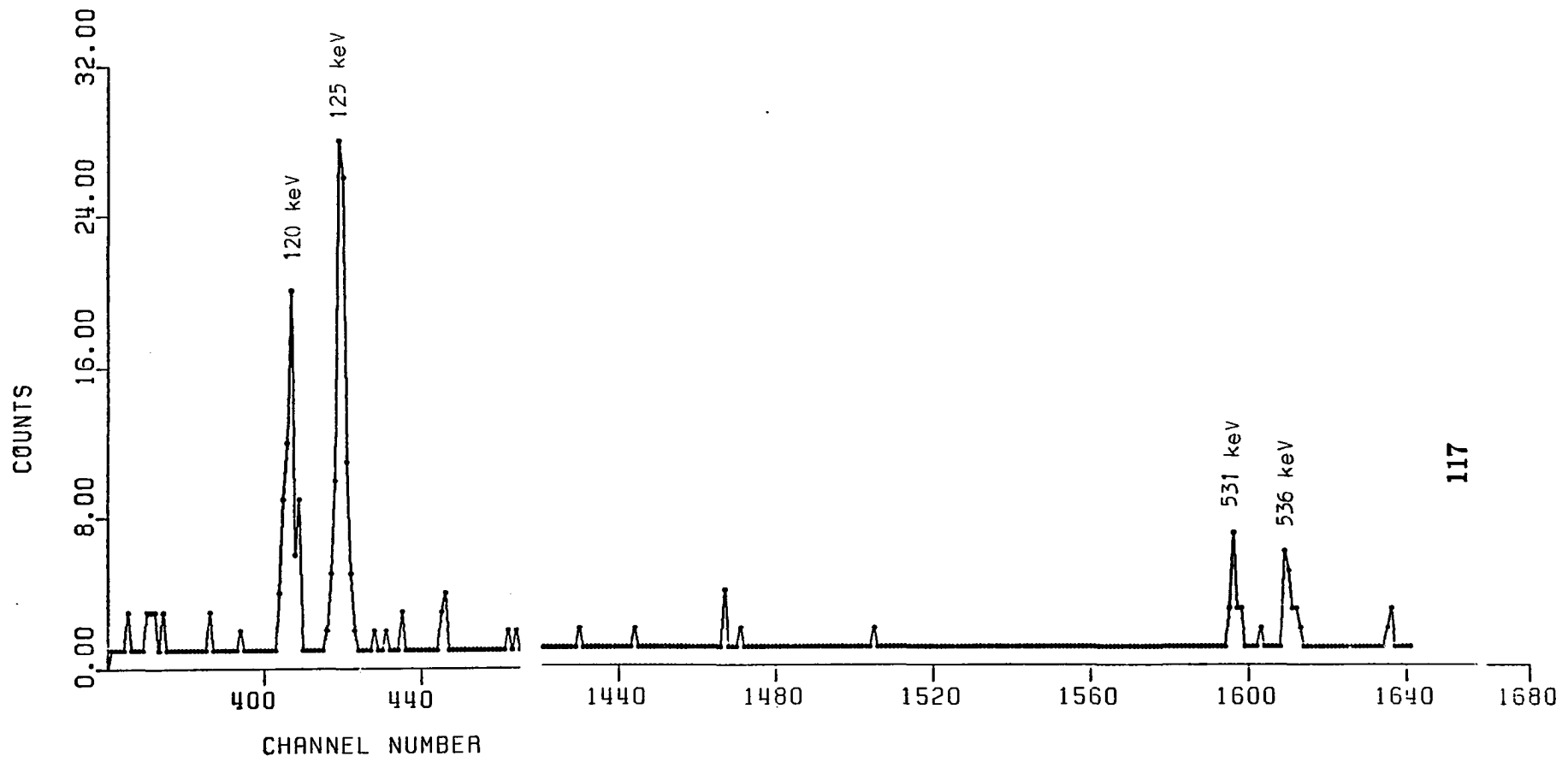
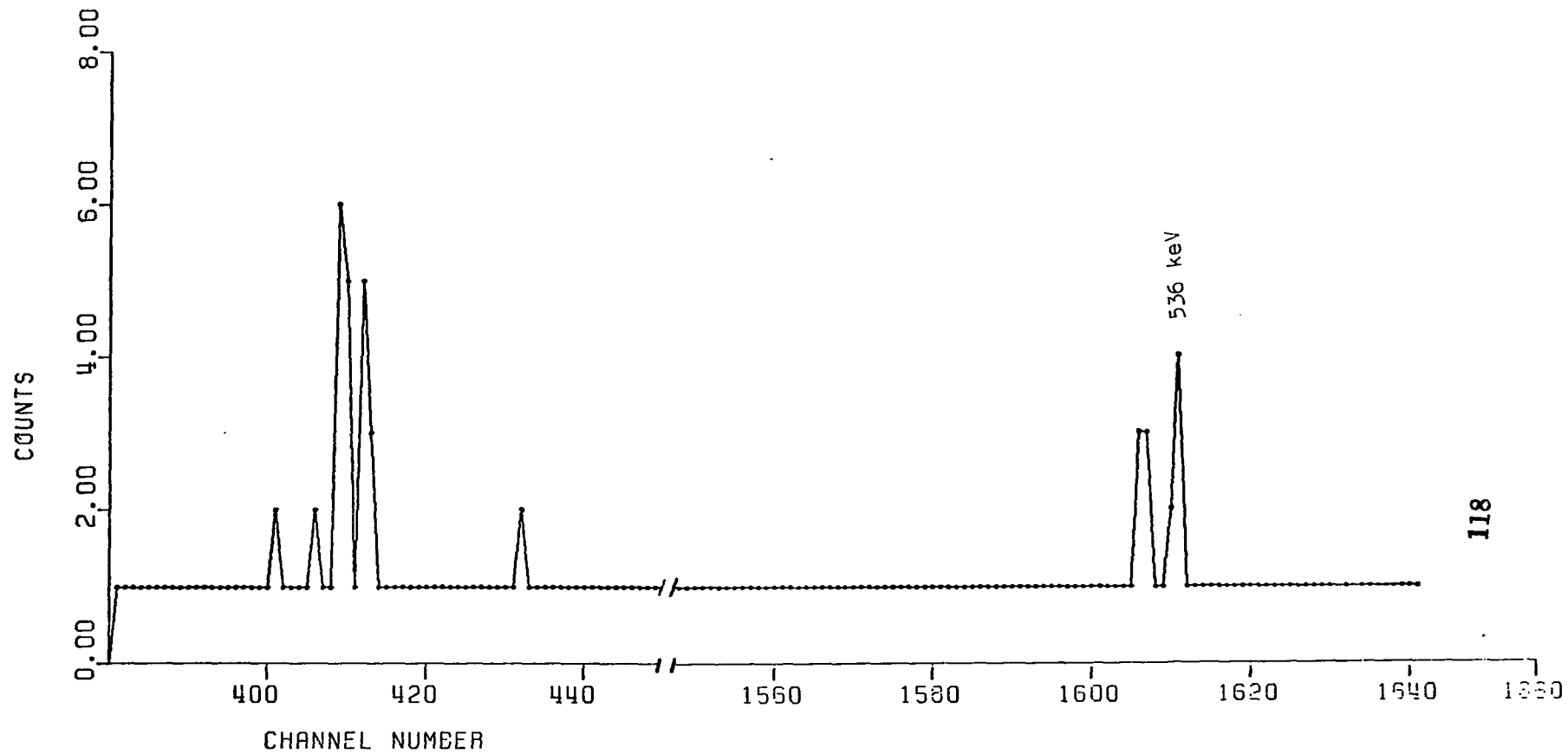


Figure 5.9. Spectrum in Coincidence with the 1619-keV Transition in ^{90}Sr



**Figure 5.10. Spectrum in Coincidence with the 1744-keV
Transition in ^{90}Sr**

branching to 2279-keV level is large with Logft of 5.4. This fact plus the gamma branching from this level indicate an $I^\pi = 5/2^+$.

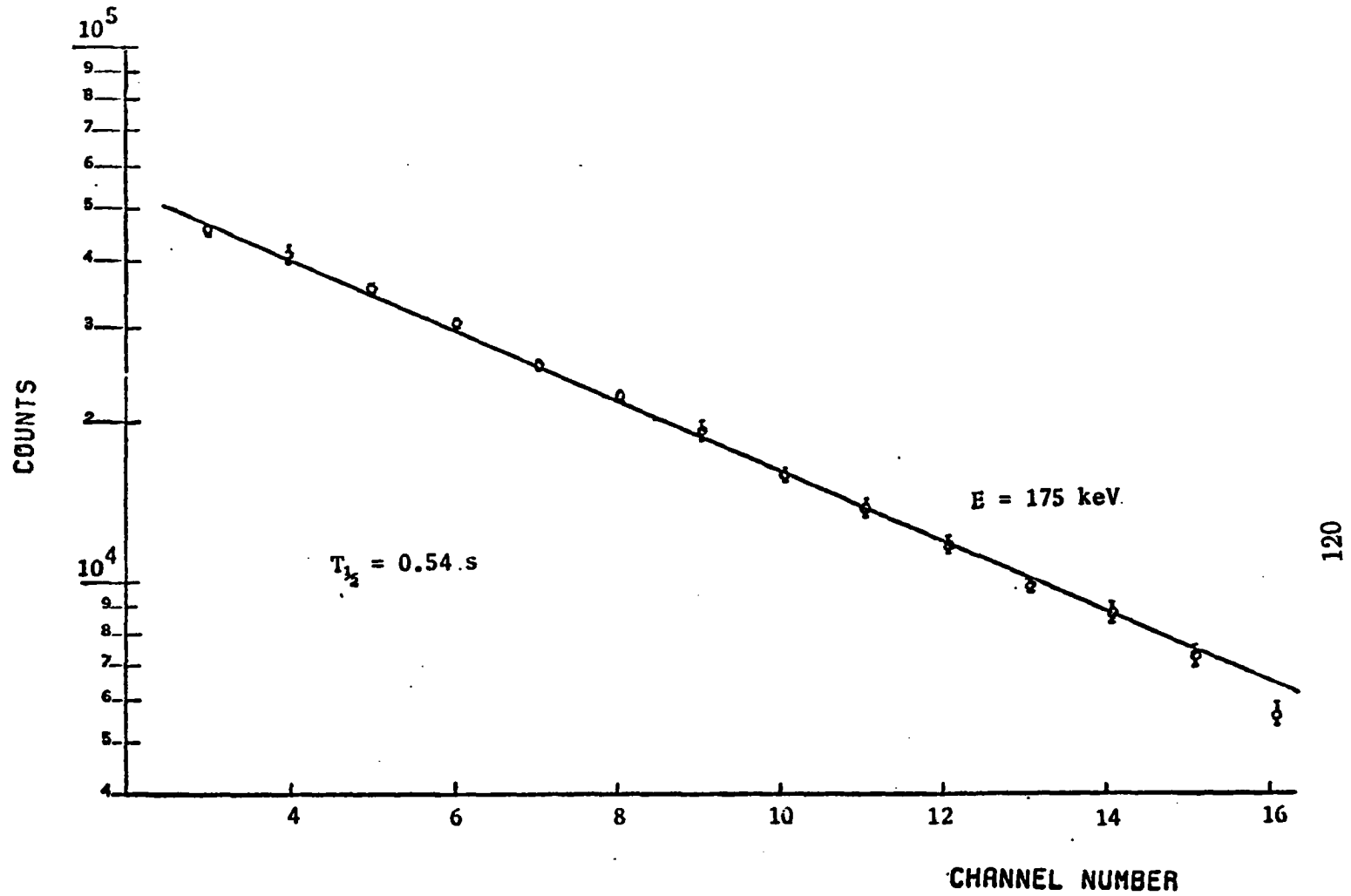
2314-keV Level: The establishment of this level is based on two transitions with definite coincidence relationships. The beta feeding to this level is small, and there is insufficient data to infer an I^π assignment.

5.2 ^{145}Cs

This is the first attempt to construct a level scheme of ^{145}Ba from beta decay of ^{145}Cs ; very little data on the levels in ^{145}Ba exist in the literature. Only the energies of three gamma-ray transitions and a half-life^{27,28,81} have been reported.⁸²

The beta decay half-life of ^{145}Cs in this work was obtained by following the decay of the 175-keV gamma transition. The decay curve for this transition is shown in Figure 5.11. A half-life of 0.54 ± 0.02 second was obtained from this curve which is in good agreement with the results of previous work^{27,28,81} which are 0.59 ± 0.02 , 0.61 and 0.563 ± 0.027 second respectively.

The energies and relative intensities of gamma-rays were determined from a gamma-singles spectrum, which is shown in Figures 5.12a-f. Because of the performance of the ion source, as mentioned in section 3.2.1, the gamma-ray transitions of ^{145}Ba beta decay were much stronger than those from ^{145}Cs beta decay (see Figure 5.12), and the spectrum was extremely complex. Many ^{145}Cs lines were distorted by nearby ^{145}Ba



5.11. Decay Curve of ^{145}Cs Transition

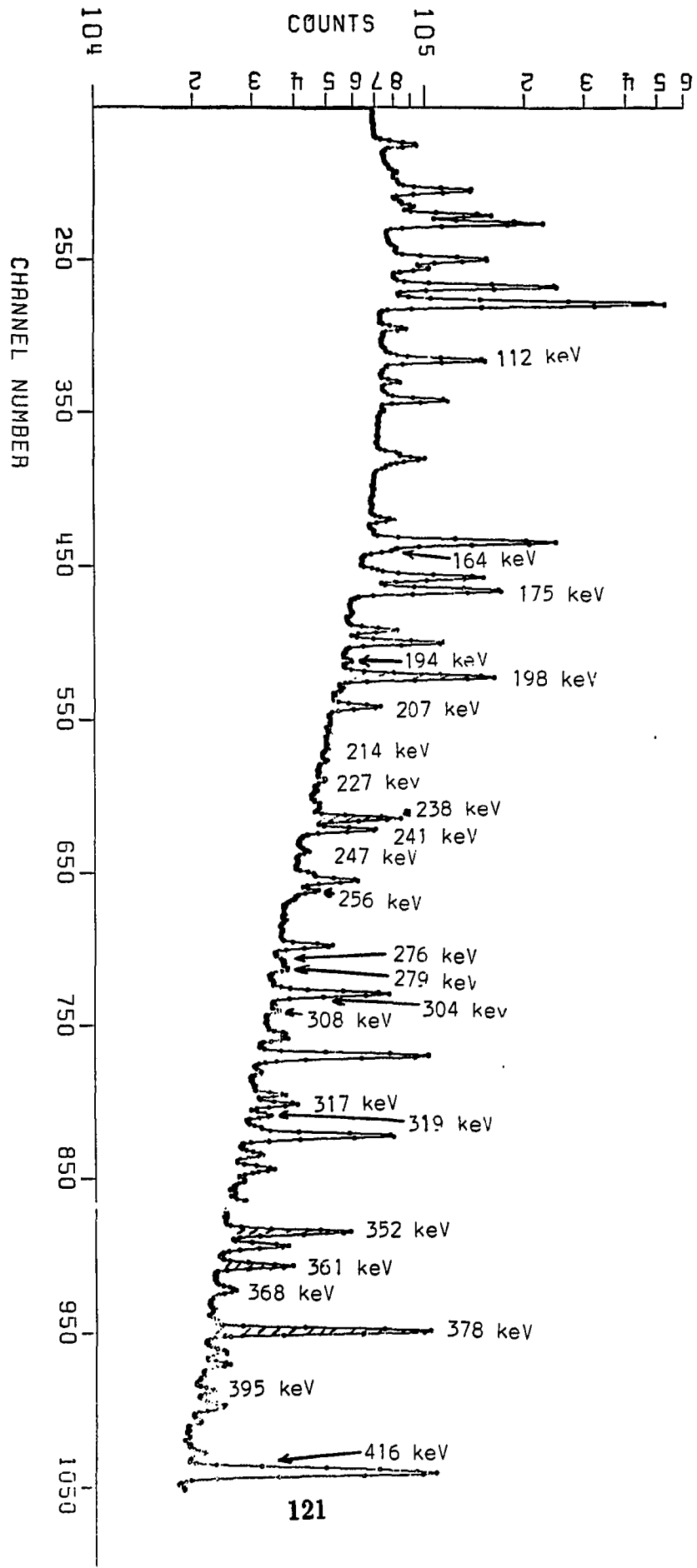


Figure 5.12a. Gamma Spectrum from ^{145}Cs Decay

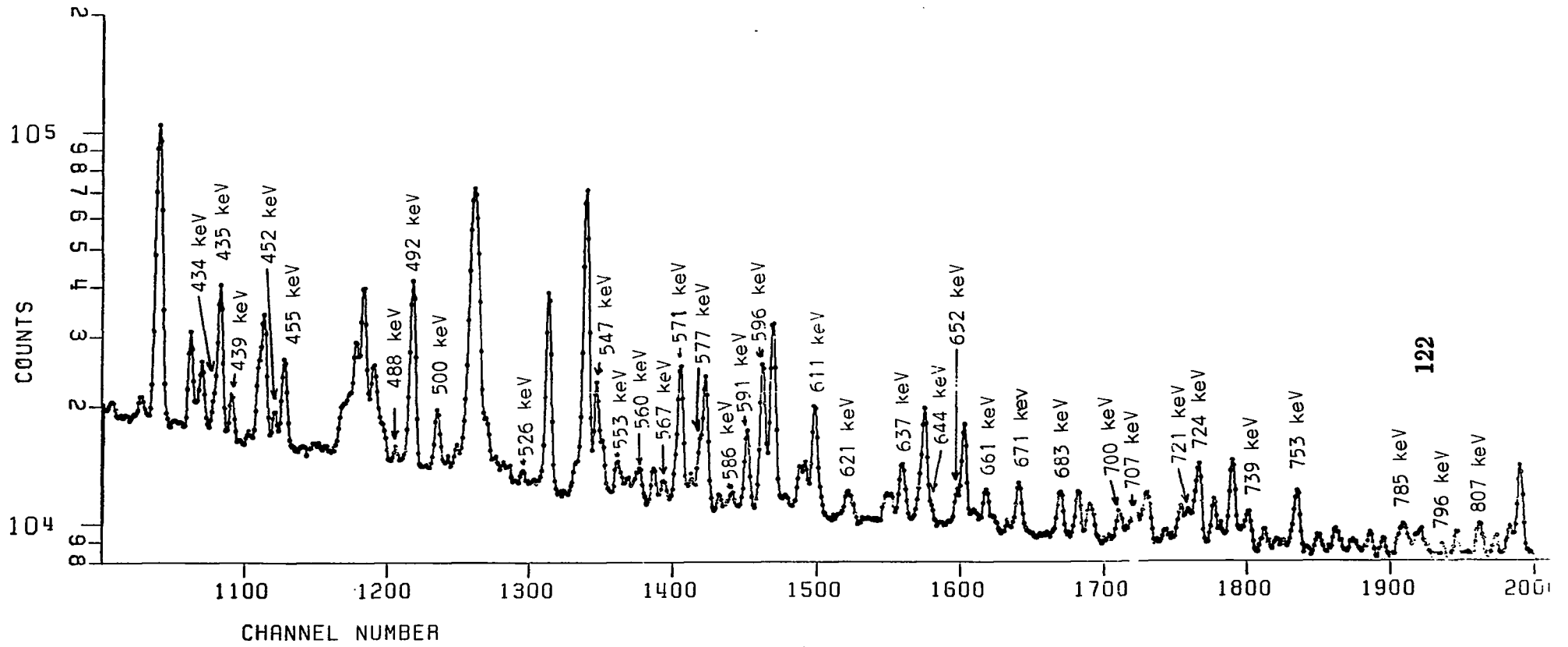


Figure 5.12b. Gamma Spectrum from ^{145}Cs Decay

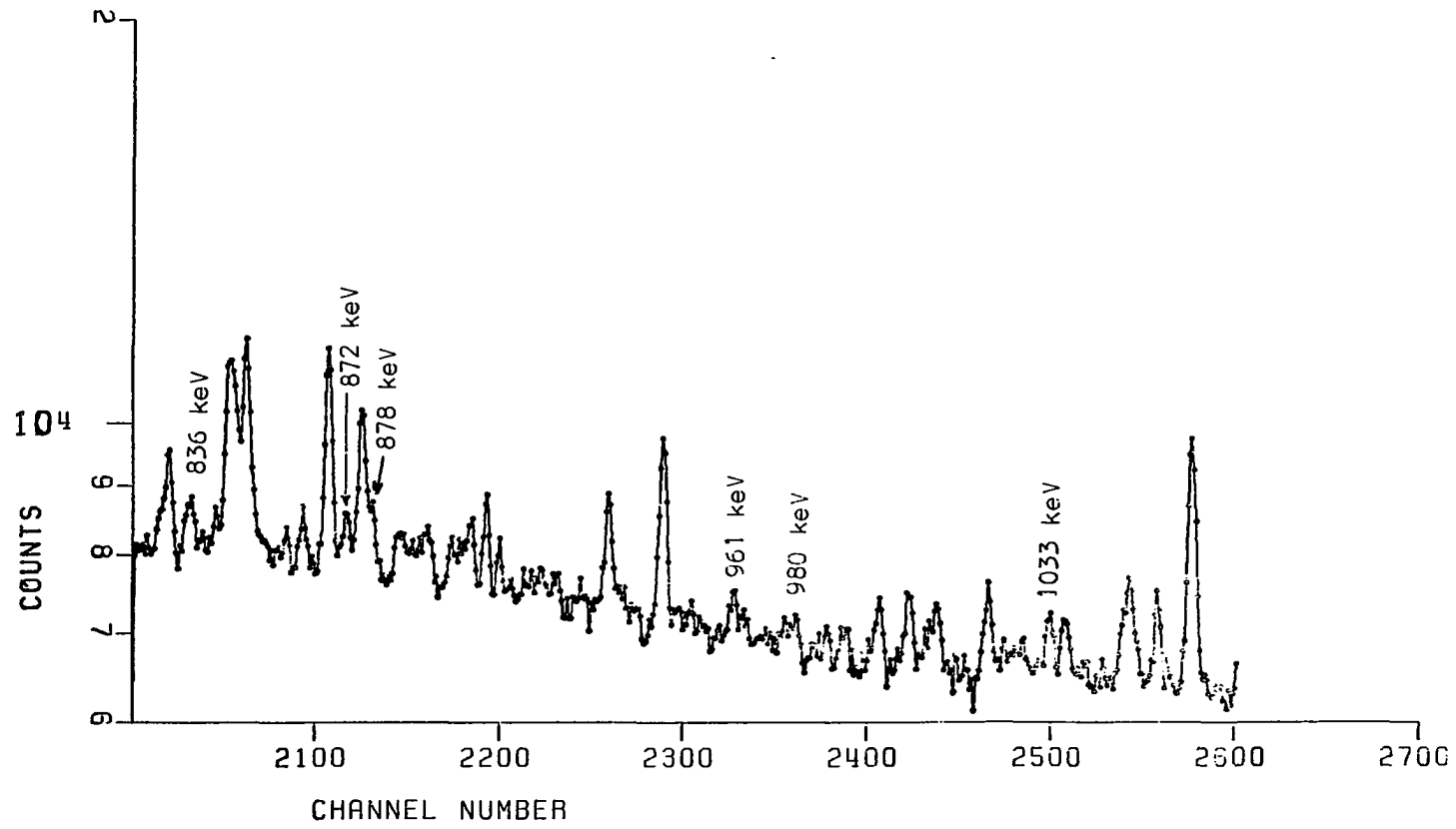


Figure 5.12c. Gamma Spectrum from ^{145}Cs Decay

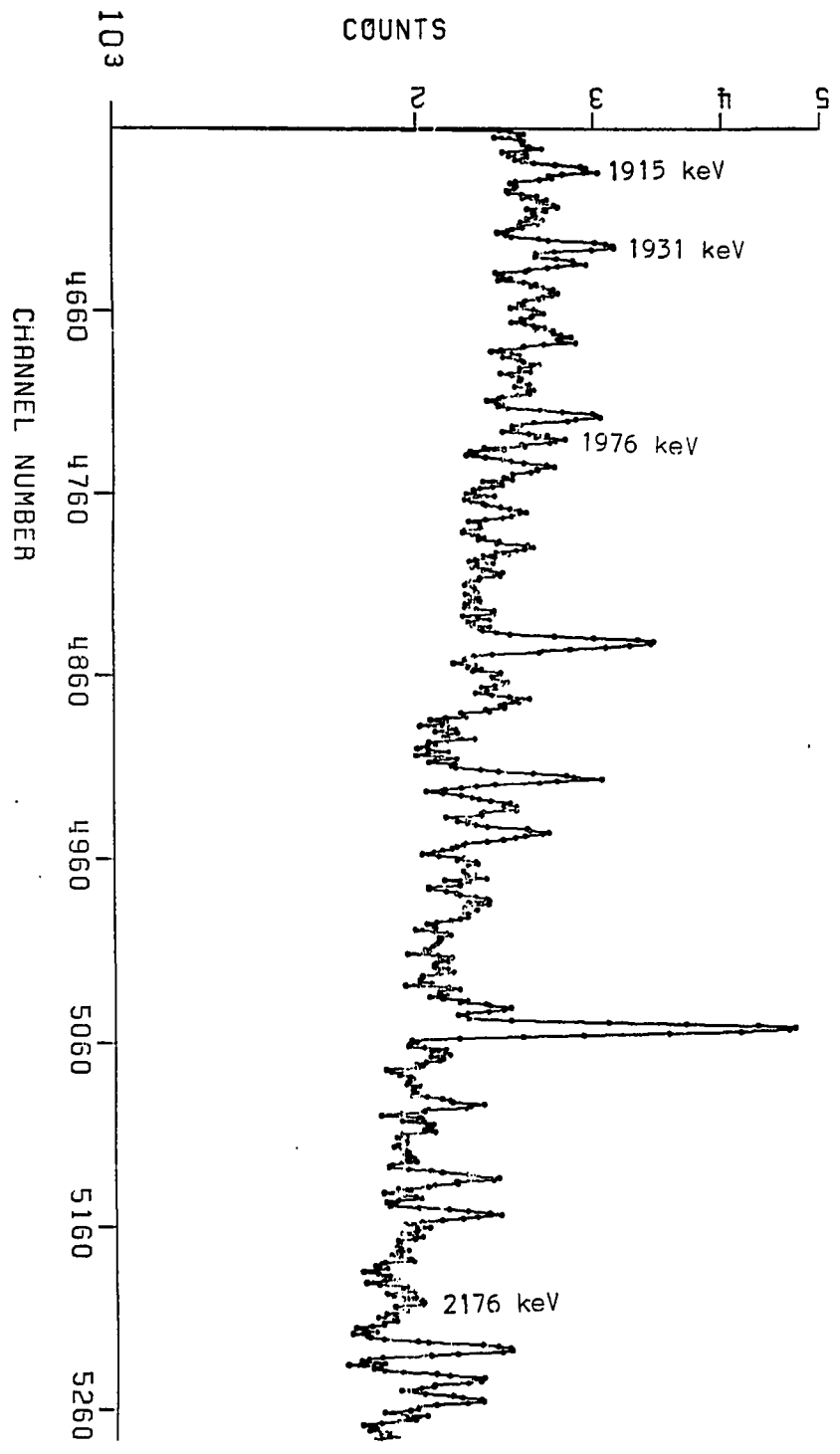


Figure 5.12d. Gamma Spectrum from ^{145}Cs Decay

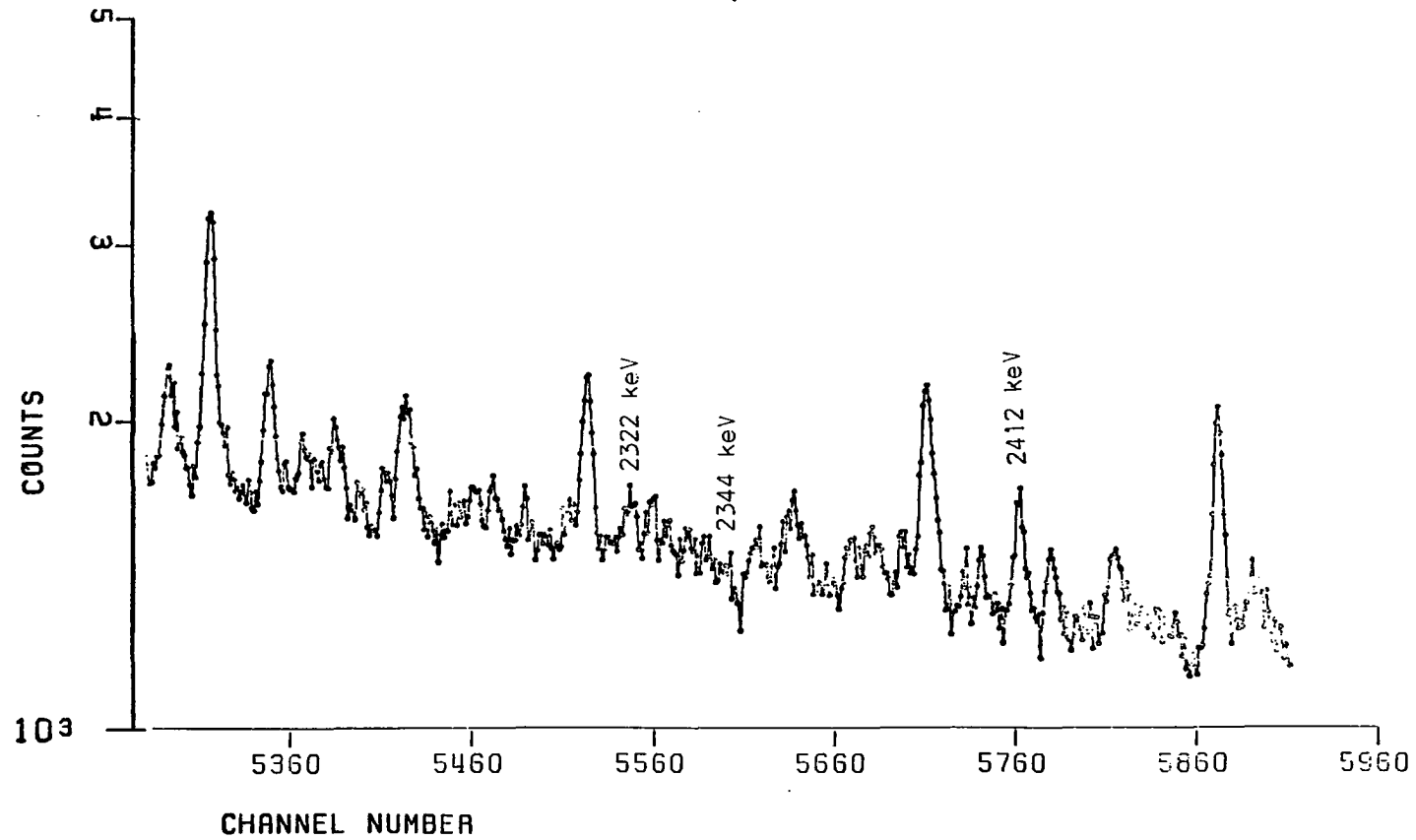


Figure 5.12e. Gamma Spectrum from ¹⁴⁵Cs Decay

lines, and several were entirely hidden under strong ^{145}Ba lines. This made precise energy determinations difficult and some of the relative intensity determinations unreliable. With these qualifications, the energies, relative intensities and placements of the observed gamma-transitions are given in Table 5.4. The relative intensities of these transitions were normalized to 100 for the 175-keV transition. The assignment of the gamma-transitions to ^{145}Cs beta decay was primarily based on their decay. For some transitions the determination of half-lives was impossible because of the contamination from other members of isobaric chain. The coincidence relationships made the identification of these lines possible.

The level scheme of ^{145}Ba from the beta decay of ^{145}Cs is shown in Figure 5.13a,b. The level scheme consists of 30 energy levels and 88 gamma transitions. More than 80 percent of gamma transitions have been placed in the decay scheme. The coincidence information was extracted from almost 6 million coincidence events by setting gates on more than 200 transitions. These coincidence data are highly selective and have permitted the construction of a level scheme with good confidence, even though the poor relative intensity values for some of the transitions make the determination of reliable beta feedings impossible. Table 5.5 presents the coincidence information. The coincidence spectrum of the 112-keV gate is shown in Figures 5.14a-c as an example.

Table 5.4. The energies and intensities of the gamma-rays and their placement in the decay scheme of ^{145}Cs . * indicates a gamma-ray assigned or placed for the first time in this work. † assigned for the first time but not been placed in decay scheme. ^a placed twice in decay scheme.

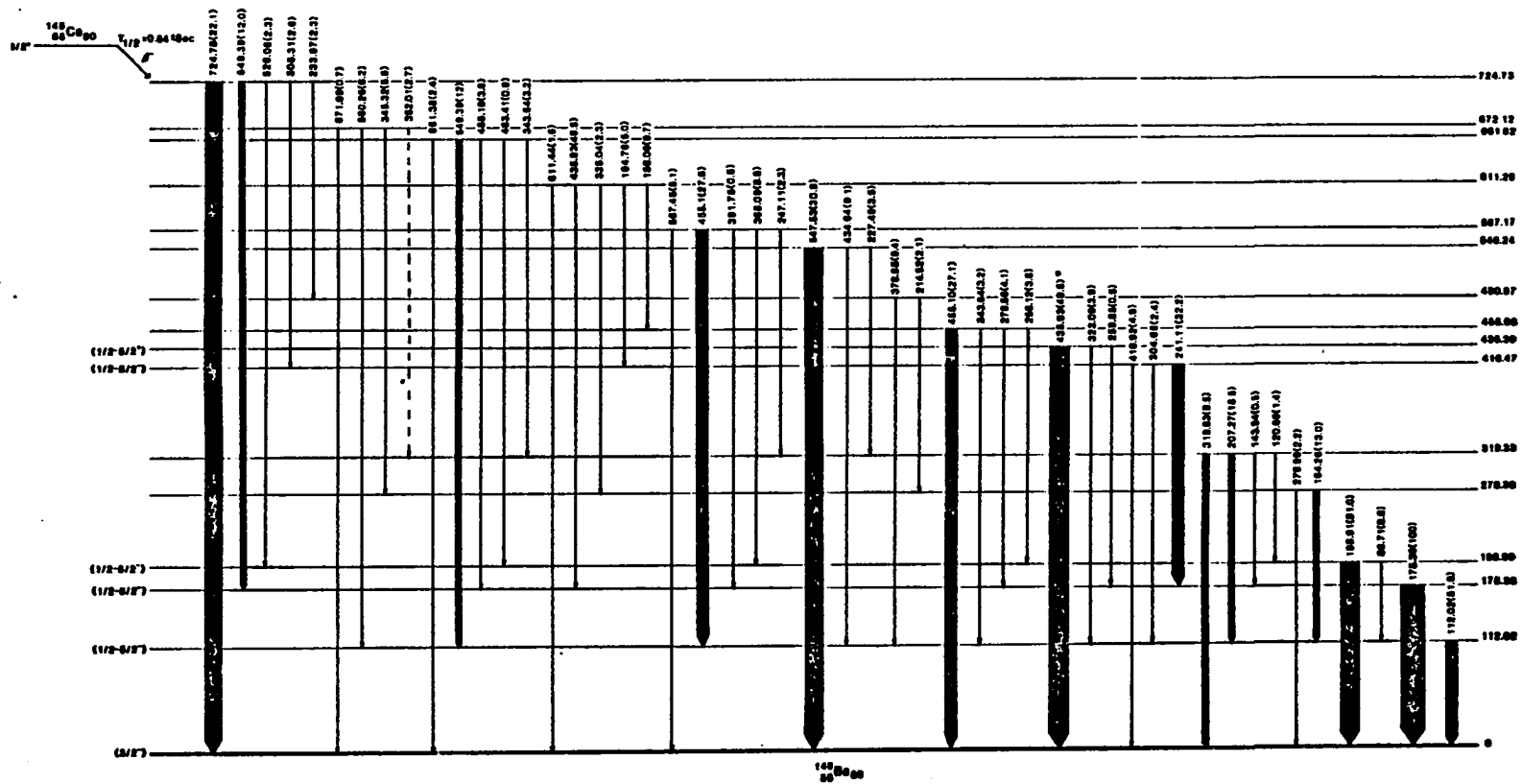
| Energy (KeV) | Intensity | Placement |
|----------------|-------------|-----------|
| †22.13 ± 0.12 | | |
| †66.04 ± 0.11 | 1.1 ± 0.3 | |
| 86.71 ± 0.10 | 8.8 ± 0.8 | 198→112 |
| 112.02 ± 0.02 | 51.8 ± 2.8 | 112→0 |
| *120.66 ± 0.31 | 1.4 ± 0.6 | 319→198 |
| *143.94 ± 0.31 | 0.5 ± 0.3 | 319→175 |
| *156.06 ± 0.10 | 9.7 ± 1.3 | 611→455 |
| *164.26 ± 0.09 | 13.0 ± 1.5 | 276→112 |
| †171.73 ± 0.03 | 6.5 ± 0.7 | |
| 175.36 ± 0.03 | 100.0 ± 1.8 | 175→0 |
| 194.76 ± 0.14 | 3.4 ± 0.5 | 611→416 |
| 198.91 ± 0.03 | 91.1 ± 4.8 | 198→0 |
| 207.27 ± 0.02 | 18.6 ± 1.0 | 319→112 |
| *214.52 ± 0.22 | 2.1 ± 0.9 | 490→276 |
| 227.49 ± 0.11 | 3.5 ± 0.5 | 546→319 |
| *233.97 ± 0.16 | 2.3 ± 0.5 | 724→491 |
| 238.04 ± 0.03 | 11.1 ± 0.8 | 784→546 |
| 241.11 ± 0.04 | 30.4 ± 2.3 | 416→175 |
| 247.11 ± 0.14 | 4.2 ± 0.6 | 567→319 |
| *249.74 ± 0.14 | 5.7 ± 0.5 | 796→546 |
| *256.12 ± 0.16 | 3.8 ± 0.4 | 455→198 |
| *259.85 ± 0.51 | 0.5 ± 0.3 | 435→175 |
| *276.99 ± 0.25 | 2.2 ± 0.7 | 276→0 |
| 279.56 ± 0.11 | 4.1 ± 0.7 | 455→175 |
| *289.46 ± 0.28 | 1.2 ± 0.4 | 836→546 |
| *304.65 ± 0.29 | 2.4 ± 0.4 | 416→112 |
| *308.31 ± 0.29 | 2.6 ± 0.3 | 724→416 |
| 317.66 ± 0.30 | 3.6 ± 0.4 | 753→435 |
| 319.83 ± 0.10 | 8.3 ± 0.6 | 319→0 |
| 323.09 ± 0.27 | 3.9 ± 0.4 | 435→112 |
| *325.48 ± 0.04 | 1.7 ± 0.4 | 871→546 |
| *335.04 ± 0.98 | 2.3 ± 0.8 | 611→276 |
| †338.01 ± 0.20 | 4.4 ± 0.9 | |
| *341.23 ± 0.46 | 1.8 ± 0.9 | 1137→796 |
| 343.64 ± 0.16 | 3.2 ± 0.6 | 661→319 |
| *352.01 ± 0.42 | 2.7 ± 0.6 | 671→319 |

Table 5.4, continued

| Energy (KeV) | Intensity | Placement |
|----------------------------|------------|--------------------|
| *361.12 ± 0.04 | 3.2 ± 0.7 | 796→435 |
| 368.09 ± 0.18 | 4.7 ± 1.3 | 784→416 |
| 378.95 ± 0.04 | 9.4 ± 0.7 | 419→112 |
| *391.75 ± 0.10 | < 0.5 | 567→175 |
| *395.32 ± 0.11 | 5.9 ± 0.7 | 672→276 |
| 416.92 ± 0.06 | 4.9 ± 0.5 | 416→0 |
| †431.50 ± 0.21 | 2.9 ± 0.6 | |
| *434.19 ± 0.11 | 9.1 ± 1.1 | 546→112 |
| ^a 435.93 ± 0.03 | 49.5 ± 2.8 | 611→416 435→0 |
| †439.43 ± 0.04 | 3.1 ± 0.5 | |
| †444.36 ± 0.15 | 3.7 ± 1.2 | |
| †452.13 ± 0.08 | 8.7 ± 0.8 | |
| ^a 455.10 ± 0.04 | 27.1 ± 1.6 | 455→0 567→112 |
| *463.41 ± 0.25 | 0.9 ± 0.3 | 661→198 |
| *474.46 ± 0.17 | 2.1 ± 0.6 | 1138→661 |
| *477.03 ± 0.15 | 3.1 ± 0.5 | 796→319 |
| *481.55 ± 0.13 | 2.7 ± 0.5 | 1353→871 |
| *488.18 ± 0.17 | 3.6 ± 0.8 | 661→175 |
| †492.62 ± 0.10 | 12.9 ± 0.9 | |
| 500.43 ± 0.05 | 5.1 ± 1.3 | 819→319 |
| †503.40 ± 0.22 | 2.3 ± 0.6 | |
| *517.84 ± 0.13 | 4.8 ± 0.7 | 1353→836 |
| *526.06 ± 0.21 | 2.3 ± 0.6 | 724→198 |
| 547.53 ± 0.05 | 30.3 ± 2.1 | 547→0 |
| ^a 549.39 ± 0.09 | 12.0 ± 1.4 | 661→112 724→175 |
| †551.96 ± 0.25 | 1.7 ± 0.4 | |
| 553.91 ± 0.11 | 8.3 ± 1.2 | 753→198 |
| *560.26 ± 0.20 | 6.2 ± 1.4 | 672→112 |
| 567.45 ± 0.09 | 5.2 ± 0.9 | 567→0 |
| *571.00 ± 0.14 | 5.1 ± 0.5 | 1138→567 |
| *574.24 ± 0.46 | 2.4 ± 1.0 | 851→276 |
| 577.92 ± 0.07 | 5.3 ± 0.5 | 753→175 |
| *586.10 ± 0.47 | 1.5 ± 0.7 | 784→198 |
| †591.52 ± 0.38 | 0.7 ± 0.3 | |
| *596.62 ± 0.25 | 1.3 ± 0.3 | 796→198 |

Table 5.4, continued

| Energy (KeV) | Intensity | Placement |
|----------------------------|------------|--------------------|
| *611.44 ± 0.20 | 1.6 ± 0.3 | 611→0 |
| ^a 621.15 ± 0.15 | 6.0 ± 1.2 | 796→175 819→198 |
| *637.33 ± 0.12 | 5.8 ± 0.7 | 836→198 |
| 644.08 ± 0.18 | 1.3 ± 0.3 | 819→175 |
| 652.85 ± 0.20 | 1.1 ± 0.4 | 851→198 |
| ^a 661.38 ± 0.16 | 2.4 ± 0.4 | 661→0 836→175 |
| *671.99 ± 0.46 | 0.7 ± 0.3 | 672→0 |
| *683.95 ± 0.09 | 7.3 ± 0.5 | 796→112 |
| *700.92 ± 0.53 | 5.2 ± 0.5 | 1155→454 |
| *707.17 ± 0.13 | 2.5 ± 0.3 | 819→112 |
| *721.31 ± 0.13 | 4.9 ± 0.5 | 1138→416 |
| *724.78 ± 0.08 | 22.1 ± 1.9 | 724→0 |
| *739.35 ± 0.10 | 10.2 ± 1.1 | 1155→416 |
| *753.54 ± 0.08 | 13.8 ± 0.9 | 753→0 |
| *759.70 ± 0.35 | 2.6 ± 0.4 | 871→112 |
| *784.14 ± 0.28 | 4.8 ± 0.9 | 784→0 |
| 785.62 ± 0.29 | 3.8 ± 0.5 | 1353→567 |
| *796.43 ± 0.14 | 3.6 ± 0.7 | 796→0 |
| *807.02 ± 0.18 | 2.9 ± 0.5 | 1353→546 |
| *836.25 ± 0.78 | 1.0 ± 0.5 | 836→0 |
| *872.34 ± 0.16 | 4.5 ± 0.7 | 871→0 |
| †875.94 ± 0.07 | 1.9 ± 0.4 | |
| †878.27 ± 0.16 | 5.2 ± 0.8 | |
| †961.14 ± 0.18 | 4.9 ± 0.8 | |
| *980.38 ± 0.56 | 2.6 ± 0.9 | 1155→175 |
| *1033.88 ± 0.19 | 6.3 ± 0.8 | 1353→319 |
| †1242.27 ± 0.37 | 2.4 ± 1.1 | |
| *1736.98 ± 0.28 | 4.2 ± 0.9 | 2461→724 |
| *1915.13 ± 0.41 | 6.8 ± 1.3 | 2461→546 |
| †1931.87 ± 0.15 | 10.8 ± 1.2 | |
| †1935.82 ± 0.19 | 6.6 ± 0.9 | |
| *1976.80 ± 0.25 | 7.3 ± 0.9 | 2588→611 |
| *2176.07 ± 0.40 | 4.1 ± 1.4 | 2787→611 |
| *2322.24 ± 0.55 | 4.8 ± 2.0 | 2434→112 |
| †2344.22 ± 0.66 | 1.9 ± 0.6 | |
| *2412.79 ± 0.19 | 7.9 ± 0.8 | 2588→175 |
| †2466.99 ± 0.35 | 5.1 ± 0.9 | |



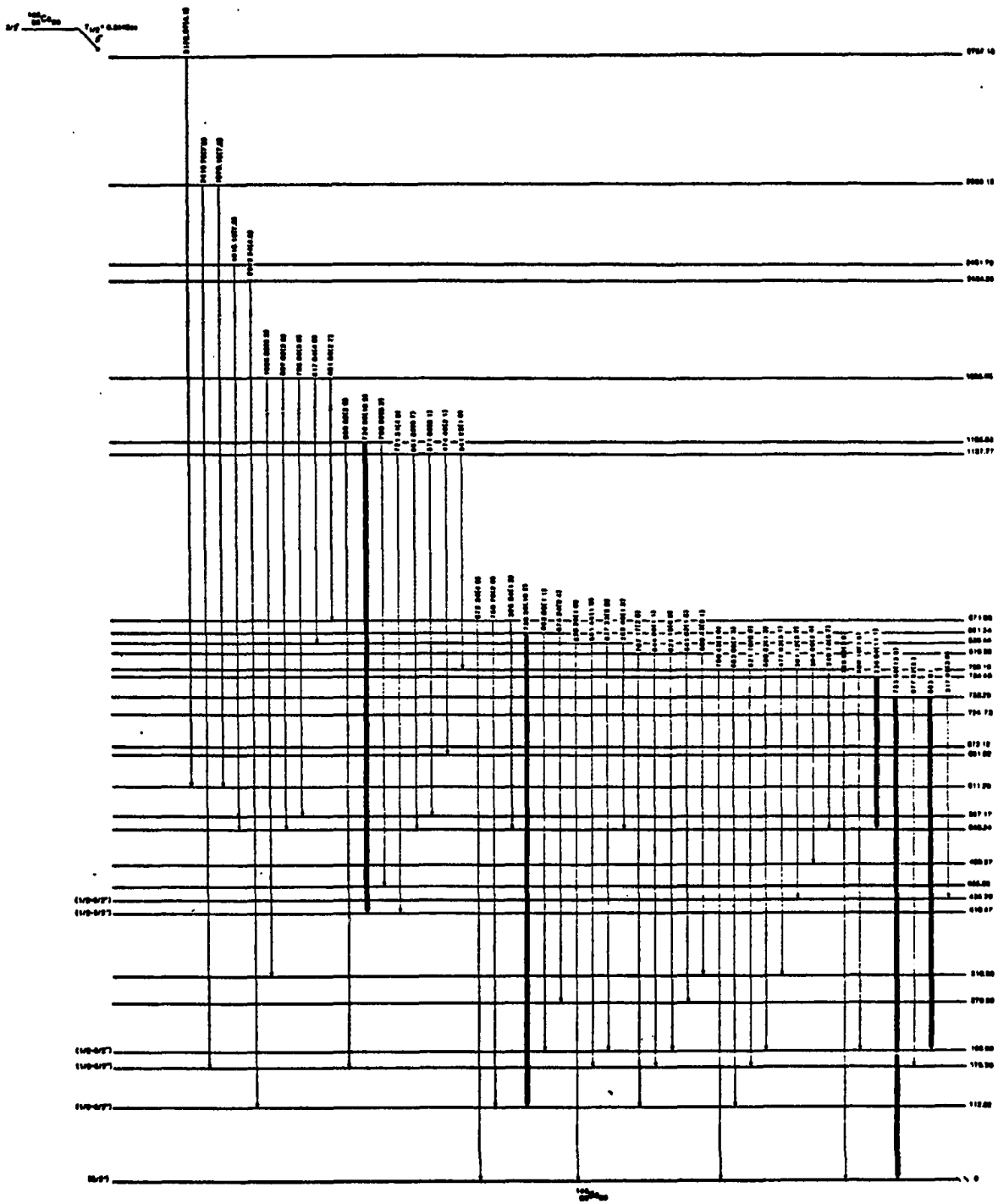


Figure 5.13b. Decay Scheme of ^{145}Cs

Table 5.5. The coincidence relationships of the gamma-rays studied in decay of ^{145}Cs .
 [] indicates possible coincidence. X no coincidence relation is available.

| Coincidence Gate (KeV) | Coincidence (KeV) |
|------------------------|---|
| 22. | |
| 66.04 | 171, 189, 286, 448, 478, 525, 533 |
| 86.71 | 112, 256, 298, 368, 435, 525, 554, 637, [652] |
| 112.02 | 85, 164, 207, 214, 227, 234, 238, 247, 256, 304, 317, 323, 338, 343, 368, 378, 395, 434, 444, 455, 476, 481, 501, 525, 550, 560, 571, 574, 621, 637, 644, 661, 683, 701, 707, 721, 739, 759, 1034 |
| 120.66 | [86], 112, 120, 199 |
| 143.94 | 175, 234 |
| 156.06 | 112, 175, 241, 256, 279, 430, 455 |
| 164.26 | 112, 214, 289, 395, 574 |
| 171.73 | 65, 175 |
| 175.36 | 143, 171, 194, 241, 259, 279, 308, 368, 391, 435, 439, 452, 488, 549, 577, 621, 644, 661, 700, 721, 739, 980, [1976], [2412] |
| 194.76 | 175, 241, [304], 416 |
| 198.90 | 256, 368, 429, 463, 474, 517, 526, 554, 559, 571, 586, 596, 621, 637, 652, 1101, 1564 |
| 207.24 | 112, 227, 238, 247, [289], 343, [352], 378, 477, 500, [807], 1034 |
| 214.52 | 112, 164, [233], 276, 304 |
| 227.49 | 112, 207, 238, [289], 319, [807] |
| 233.97 | 112, [214], 308, 378, 435, 491 |
| 238.04 | 112, 207, 227, 256, 319, 335, 352, 361, 434, 435, 437, 455, 547 |
| 241.11 | 175, 194, 308, 721, 739 |
| 247.11 | 112, 207, 319, [571], [785] |
| 249.74 | X |
| 256.12 | 85, 112, 156, 198, [721] |
| 259.85 | 175, [317], [361] |
| 276.99 | 214, [335], 395, 574 |
| 279.56 | 156, 175, 700 |
| 289.46 | [112], [207], [227], [319], [434], [517], 547 |
| 304. | 112, 352, 378, 492 |
| 308.31 | 175, 241, 416 |
| 317.66 | 112, 175, [259], 323, 338, 416, 435 |
| 319.83 | 227, 238, 247, 343, 477, 500, 1034 |
| 323.09 | 112, 317, [361] |
| 325.48 | X |
| 335.04 | X |
| 338.01 | 112, 164, 175, 256, 500 |

Table 5.5, continued

| Coincidence Gate (KeV) | Coincidence (KeV) |
|------------------------|--|
| 341.23 | 112, 207, [319], [477], 683 |
| 343.64 | 112, 207, 319, 395, 474 |
| 352.01 | |
| 361.12 | 171, 238, 435 |
| 368.09 | 86, 112, 198, 571, [785] |
| 378.95 | 112, 355, 578, 671, 701 |
| 391.75 | 175 |
| 395.32 | 112, 164, 227, [276], 343, 444 |
| 416.92 | 194, 607, 721, 739 |
| 431.50 | 175 |
| 434.19 | 112, 238 |
| 435.93 | 175, 238, 317, 334, 352, 361, 438, 491, [525], 982 |
| 439.43 | |
| 444. | 112, 395, 503 |
| 452.13 | 175 |
| 455.10 | 112, 156, 171, 238, 571, 700, 784 |
| 463.41 | [86], [112], 198, [477] |
| 474.46 | 112, 175, 207, 241, 343 |
| 477.03 | [112], 207, 319 |
| 482.34 | 112, 171, 241, 759, 872 |
| 488.18 | 175 |
| 492.62 | [86], 175, 198, 241, 304, 352, 378 |
| 500.43 | 112, 207, 319 |
| 503.40 | 112, 444, 547 |
| 517.84 | [86], 198, 289, 638 |
| 526.06 | 86, 112, 198 |
| 547.53 | 238, 289, 503 |
| 549.39 | 112, 175, 238 |
| 551.96 | × |
| 553.91 | 86, 112, 198 |
| 560.26 | 112, 198 |
| 567.45 | 571, [785] |
| 571.00 | [86], 112, 198, 247, 368, 455, 547, 567 |
| 574.24 | 112, 164, 276 |
| 577.92 | 175 |
| 586.10 | [86], [112], 198 |
| 591.52 | × |

Table 5.5, continued

| Coincidence Gate (KeV) | Coincidence (KeV) |
|------------------------|---------------------------|
| 596.62 | 198 |
| 611.44 | |
| 621.15 | [86], [112], 175, 198 |
| 637.33 | 86, 112, 198, 517 |
| 644.08 | [175] |
| 652.85 | [86], [112], 198 |
| 661.38 | 175 |
| 671.99 | 175, 378 |
| 683.95 | 112, 341 |
| 700.92 | 175, 241, 256, [416], 455 |
| 707.17 | 112 |
| 721.31 | 175, 241, 416 |
| 724.78 | — |
| 739.35 | 175, 241, 416 |
| 753.54 | — |
| 759.70 | 112 |
| 784.14 | — |
| 785.62 | 175, 256, 455 |
| 796.43 | — |
| 807.02 | 547 |
| 836.25 | — |
| 872.34 | 482 |
| 875.94 | × |
| 878.27 | × |
| 961.14 | 547 |
| 980.38 | 175 |
| 1033.88 | 112, 207, 319 |
| 1077.20 | — |
| 1242.27 | — |
| 1736.98 | — |
| 1915.13 | 434, 547 |
| 1931.87 | 361, 751 |
| 1935.82 | 112, 175, 343 |
| 1976.80 | 175, 435 |
| 2176.07 | 175, 435 |
| 2322.24 | 112 |
| 2412.79 | 175 |
| 2466.99 | 112 |

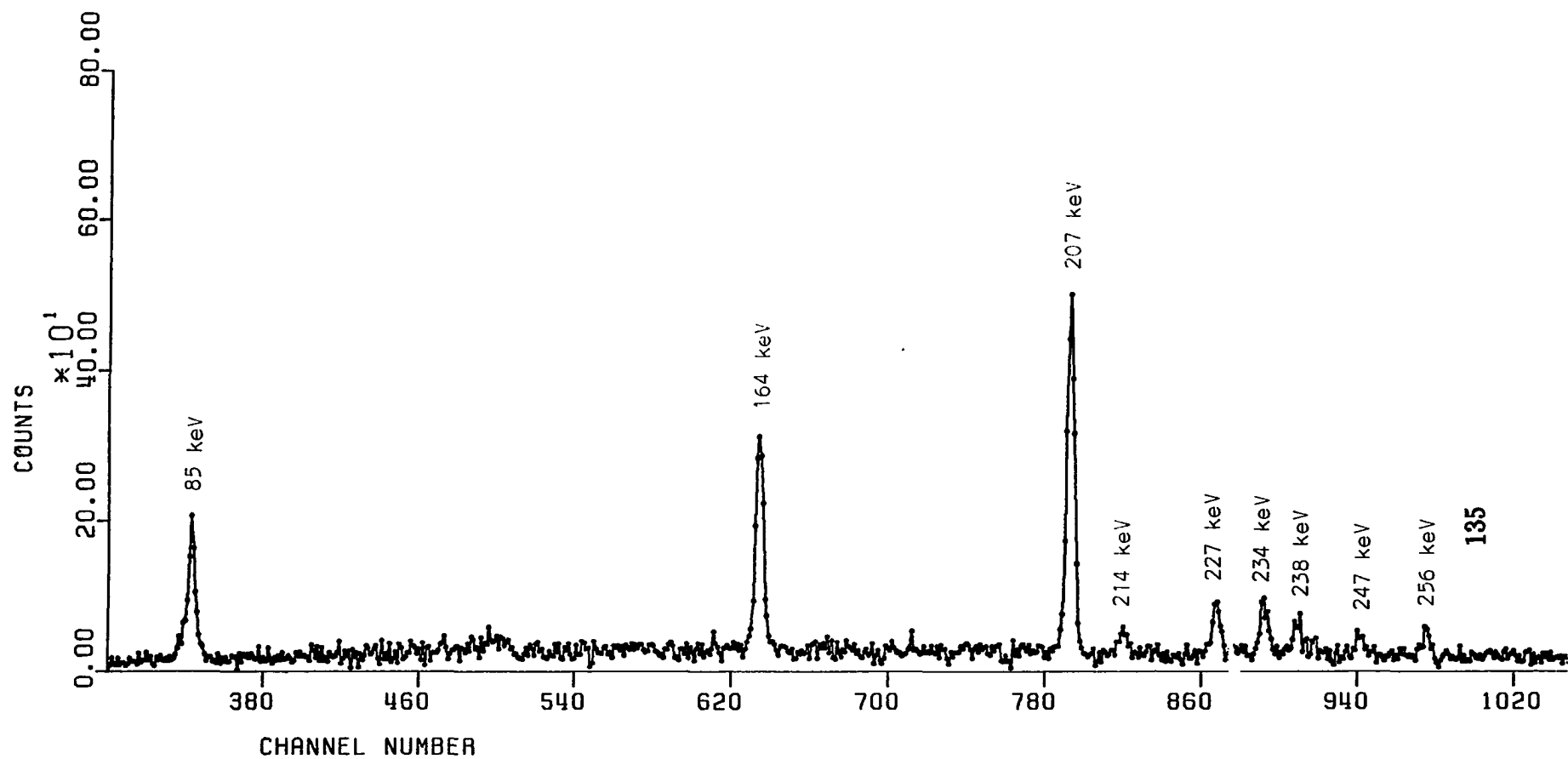


Figure 5.14a. Spectrum in Coincidence with the 112-keV Transition in ^{145}Cs

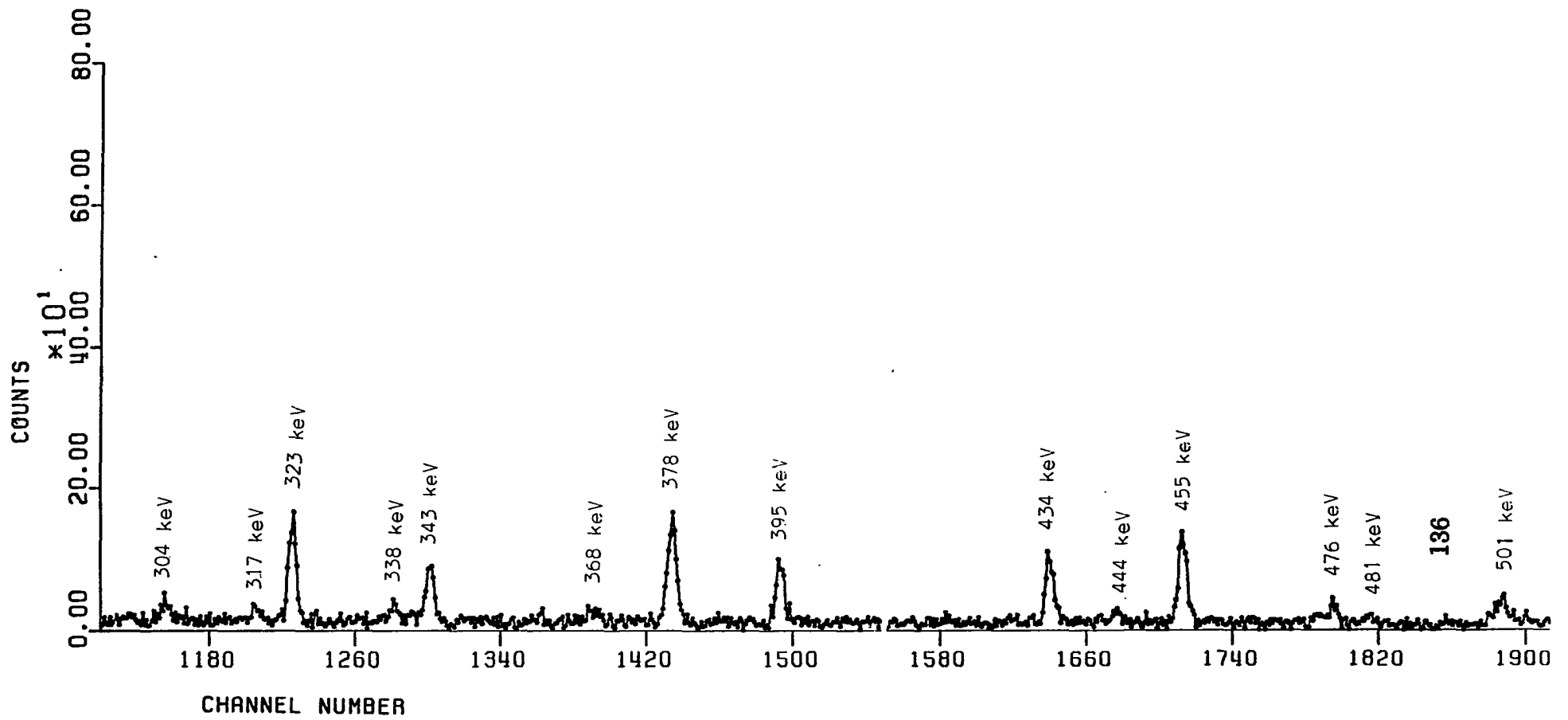


Figure 5.14b. Spectrum in Coincidence with the 112-keV Transition in ^{145}Cs

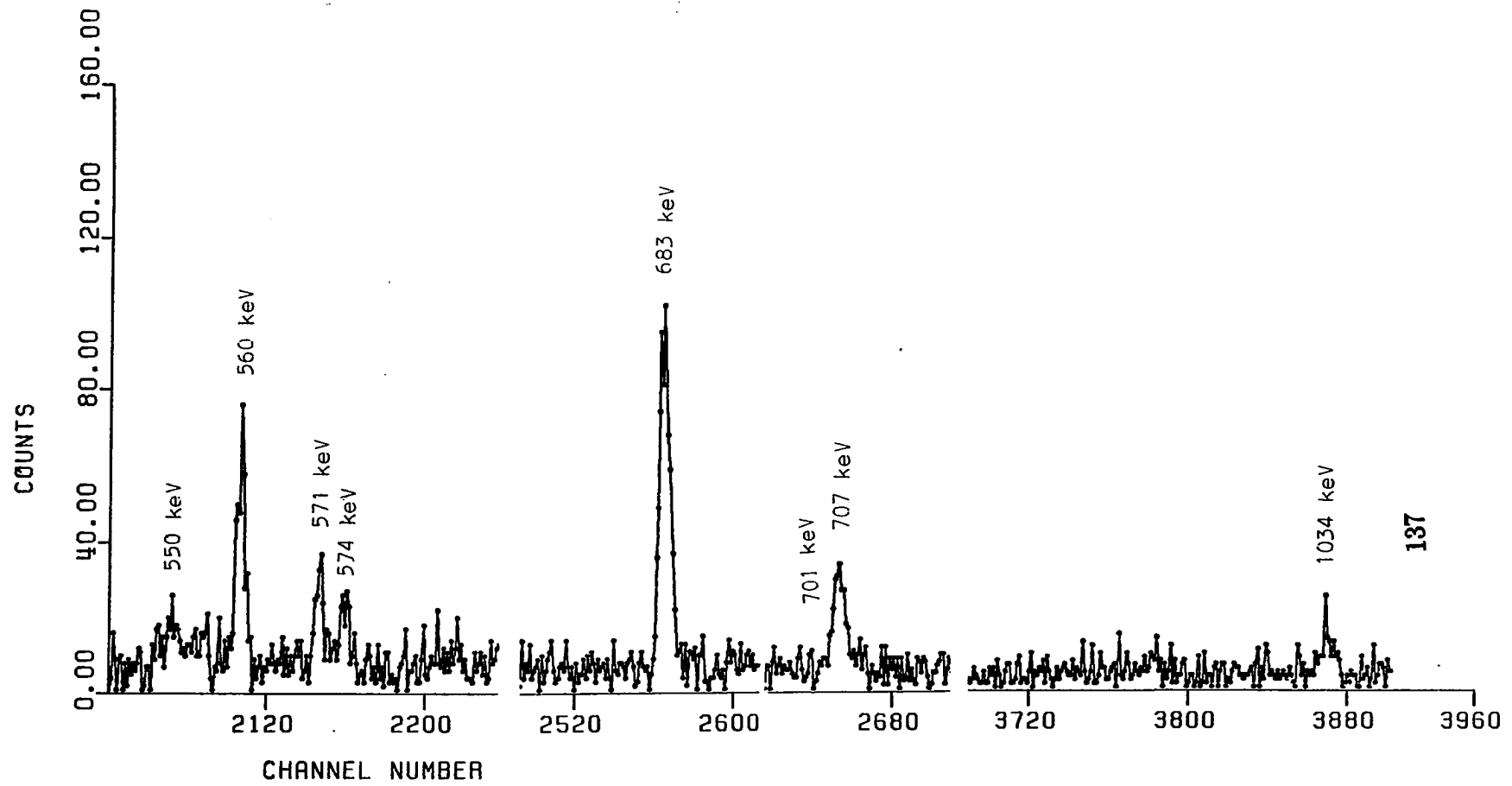


Figure 5.14c. Spectrum in Coincidence with the 112-keV Transition in ^{145}Cs

During the writing of this dissertation a report of ^{145}Cs beta decay was published by Rapaport *et al.*⁶⁰ The gamma singles spectrum and beta spectrum were investigated by them, and a preliminary decay scheme with 12 energy levels and 23 gamma transitions based only on sum and differences of the transitions was proposed.

In the following section the levels up to 491-keV will be discussed.

Ground State Level: The beta feeding to this level was determined using the absolute intensity of the 724-keV transition in ^{145}Ce decay. The ground state beta feeding of ^{145}B was calculated to be 35%. This value is probably overestimated due to an incomplete knowledge of the decay scheme and the difficulty with intensity measurements of the gamma transitions which have been placed twice in level scheme. The ground state spin of ^{145}Ba has been measured directly,⁵⁰ and a spin value of $3/2$ was obtained. The ground state spin of ^{145}Cs has also been measured directly and $\frac{3}{2}^+$ has been assigned²⁷. In later discussion a negative parity assignment will be suggested for this level. A ground state $I^\pi = 3/2^-$ assignment would imply a first forbidden non-unique beta transition. In the discussion to follow an $I^\pi = 3/2^-$ for the ground state will be assumed.

112-keV Level: The coincidence relationships made this level well established (see Figures 5.14a-c). If the K/L ratio from conversion electron experiments⁵⁵ is accepted this would be an M_1 transition. Based on ground

state $I^\pi = \frac{3}{2}^-$ and the assigned multipolarity, the possible I^π for this level can be $\frac{1}{2}^-$, $\frac{3}{2}^-$, $\frac{5}{2}^-$.

175-keV Level: This is a very well established level based on coincidence relationships (see Figure 5.15). It is a M_1 transition by its K/L ratio,⁵⁵ which makes the possible spin assignments $\frac{1}{2}^-$, $\frac{3}{2}^-$, $\frac{5}{2}^-$.

199-keV Level: This is another well established level by coincidence relationships (see Figures 5.16a-c). With an M_1 multipolarity assigned to the transitions depopulating this level,⁵⁵ the possible spin assignments can be $\frac{1}{2}^-$, $\frac{3}{2}^-$, $\frac{5}{2}^-$.

276-and 319-keV Levels: Both of these levels are established based on a ground state transition and a transition in coincidence with the 112-keV transition (see Figures 5.14a-c). The possible spin assignments for this level can be $\frac{3}{2}^-$, $\frac{5}{2}^-$, $\frac{7}{2}^-$ regarding the gamma branching to lower levels.

416-keV Level: The coincidence relationships make this level very well established (see Figures 5.14 and 5.15).

435-keV Level: Based on coincidence relationships this is a well established level (see Figures 5.14 and 5.15). If an E_1 assignment for the 435-keV transition is correct by reference 55, the possible spin assignment could be $\frac{1}{2}^+$, $\frac{3}{2}^+$, $\frac{5}{2}^+$.

455-keV Level: The coincidence relationships of four gamma transitions depopulating this level make it very well established. The

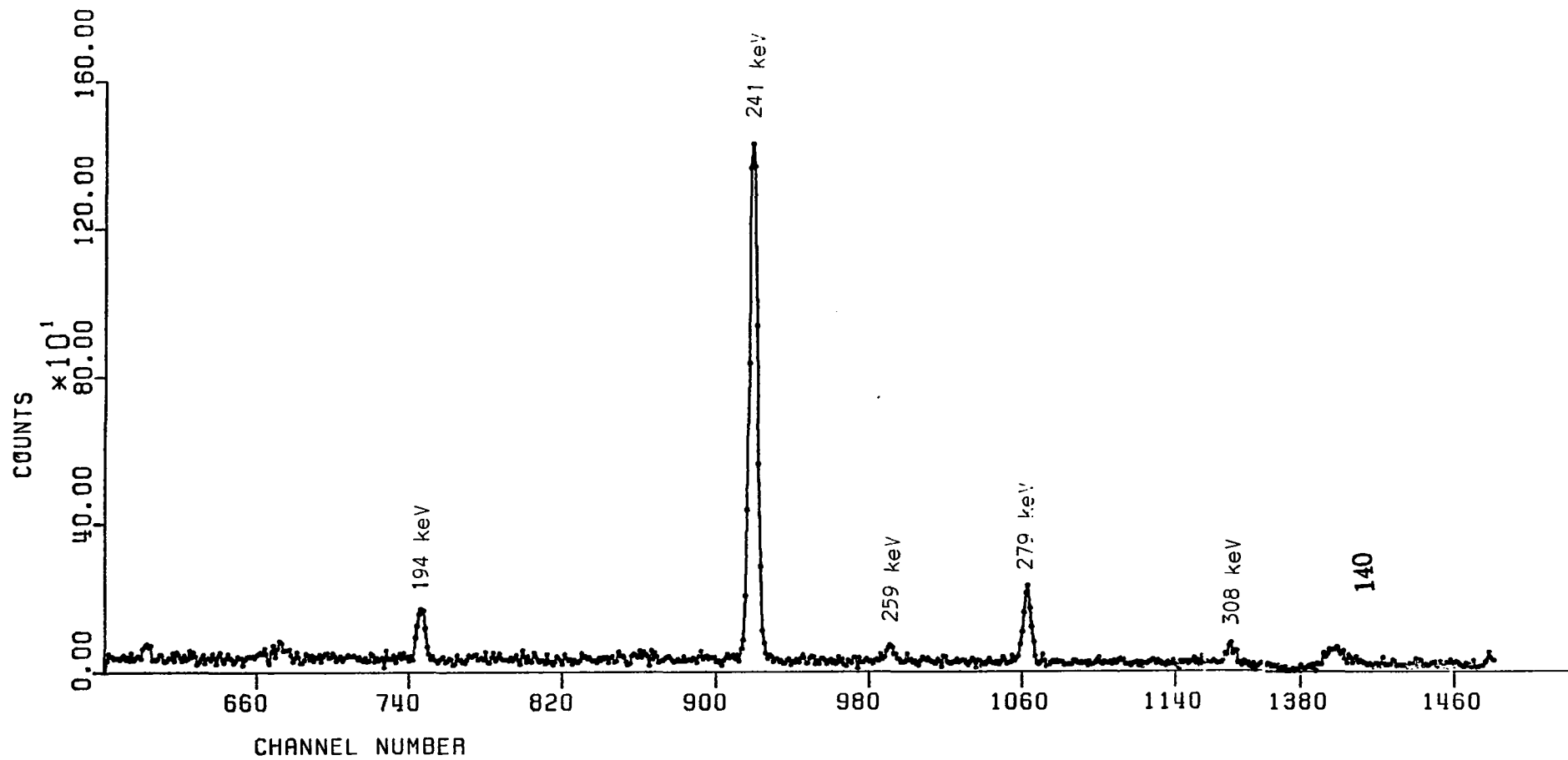


Figure 5.15a. Spectrum in Coincidence with the 175-keV Transition in ^{145}Cs

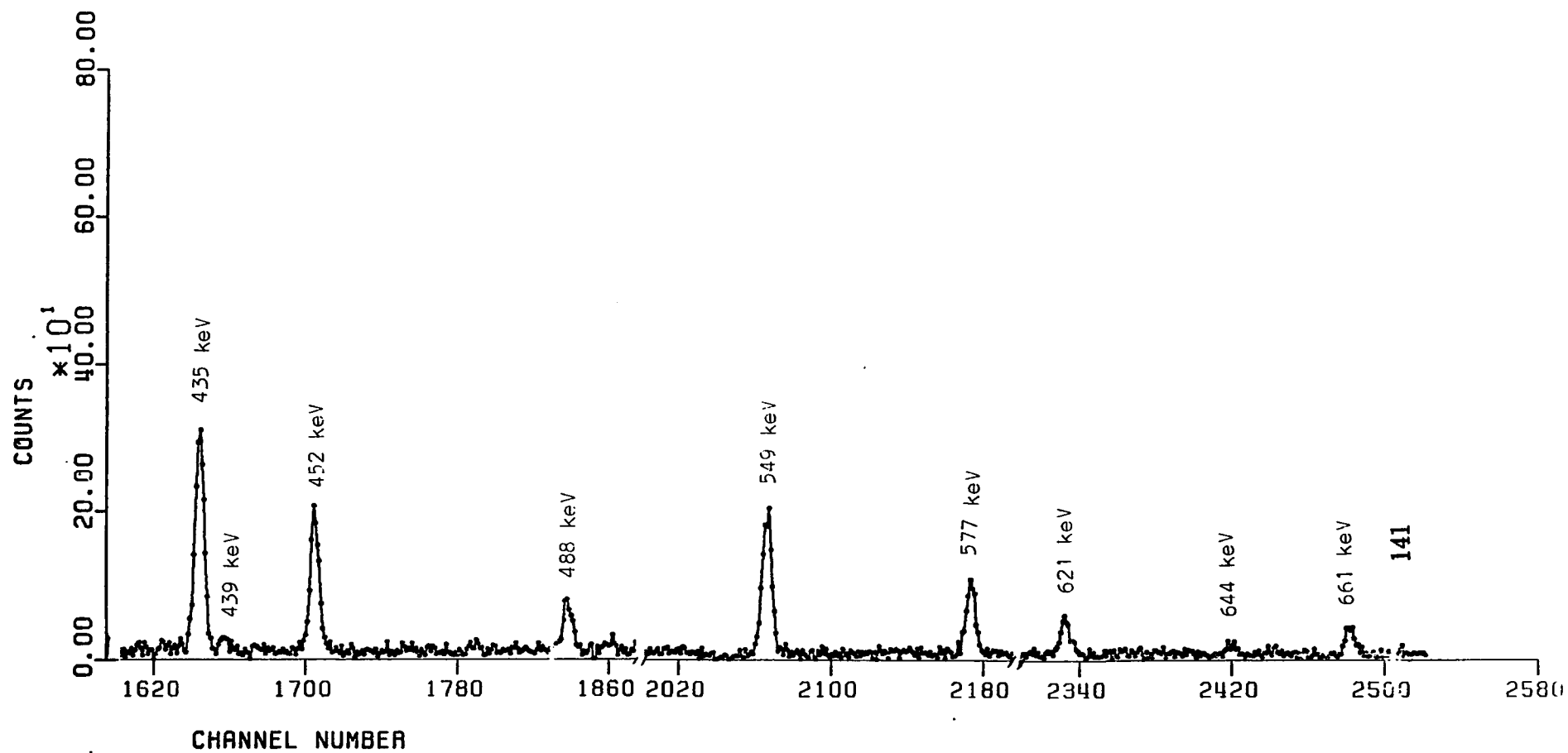


Figure 5.15b. Spectrum in Coincidence with the 175-keV Transition in ^{145}Cs

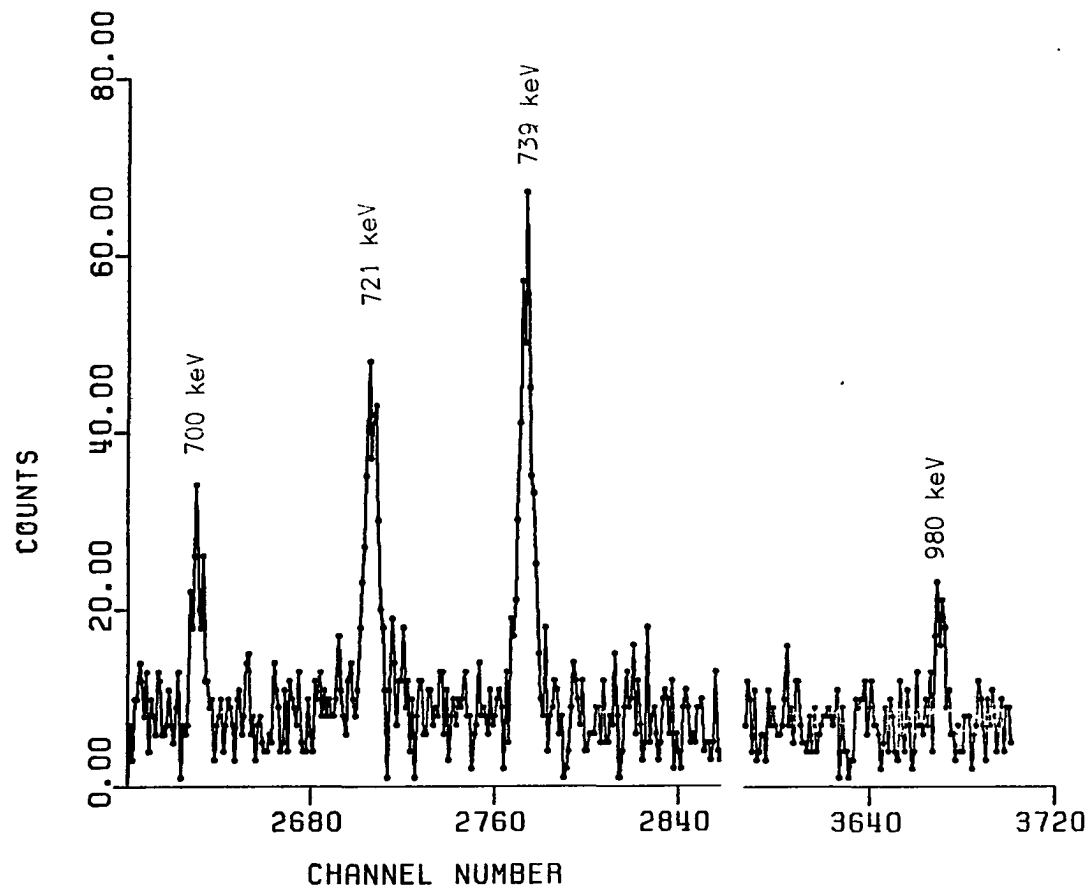


Figure 5.15c. Spectrum in Coincidence with the 175-keV Transition in ^{145}Cs

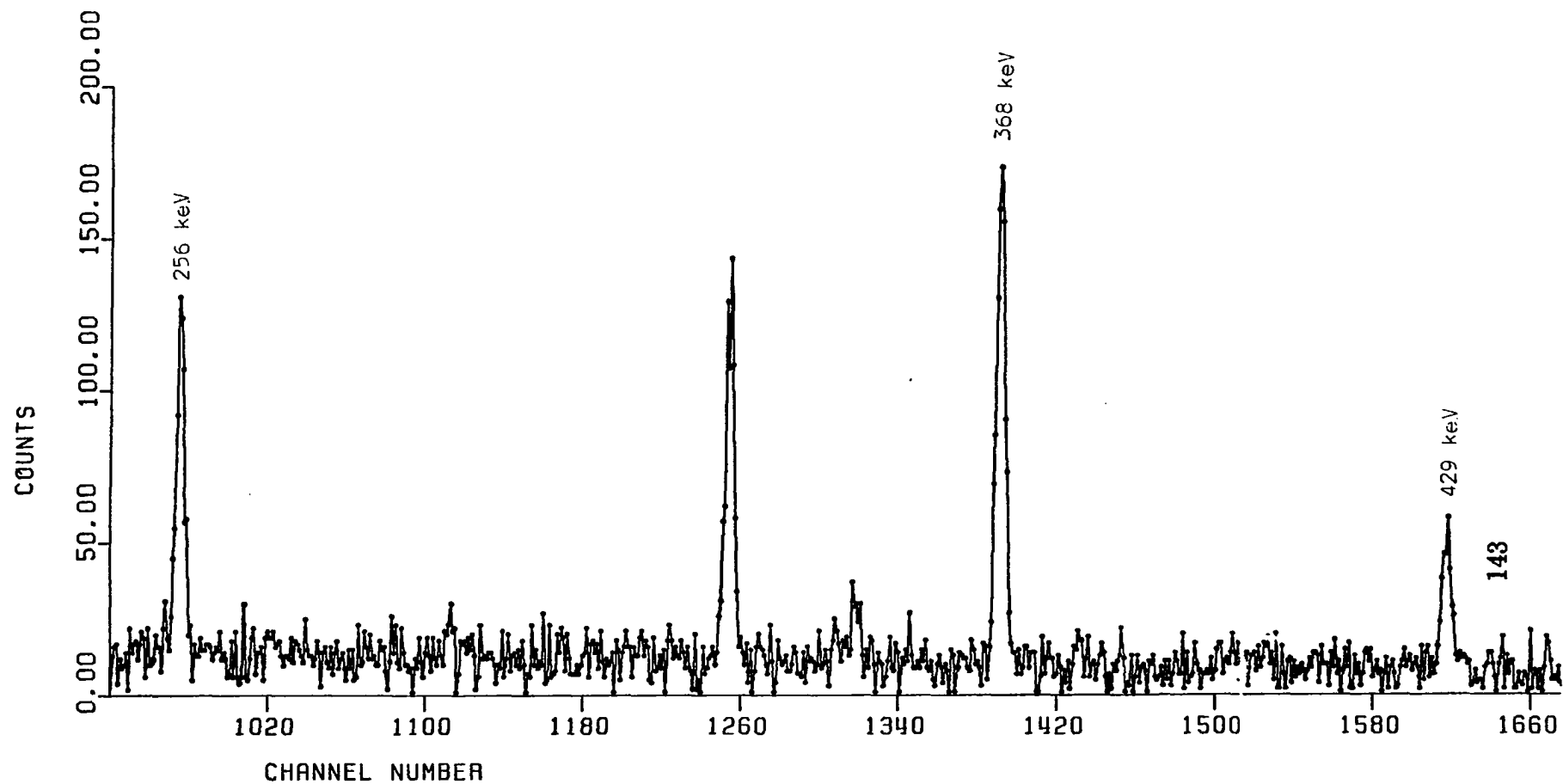


Figure 5.16a. Spectrum in Coincidence with the 199-keV Transition in ^{145}Cs

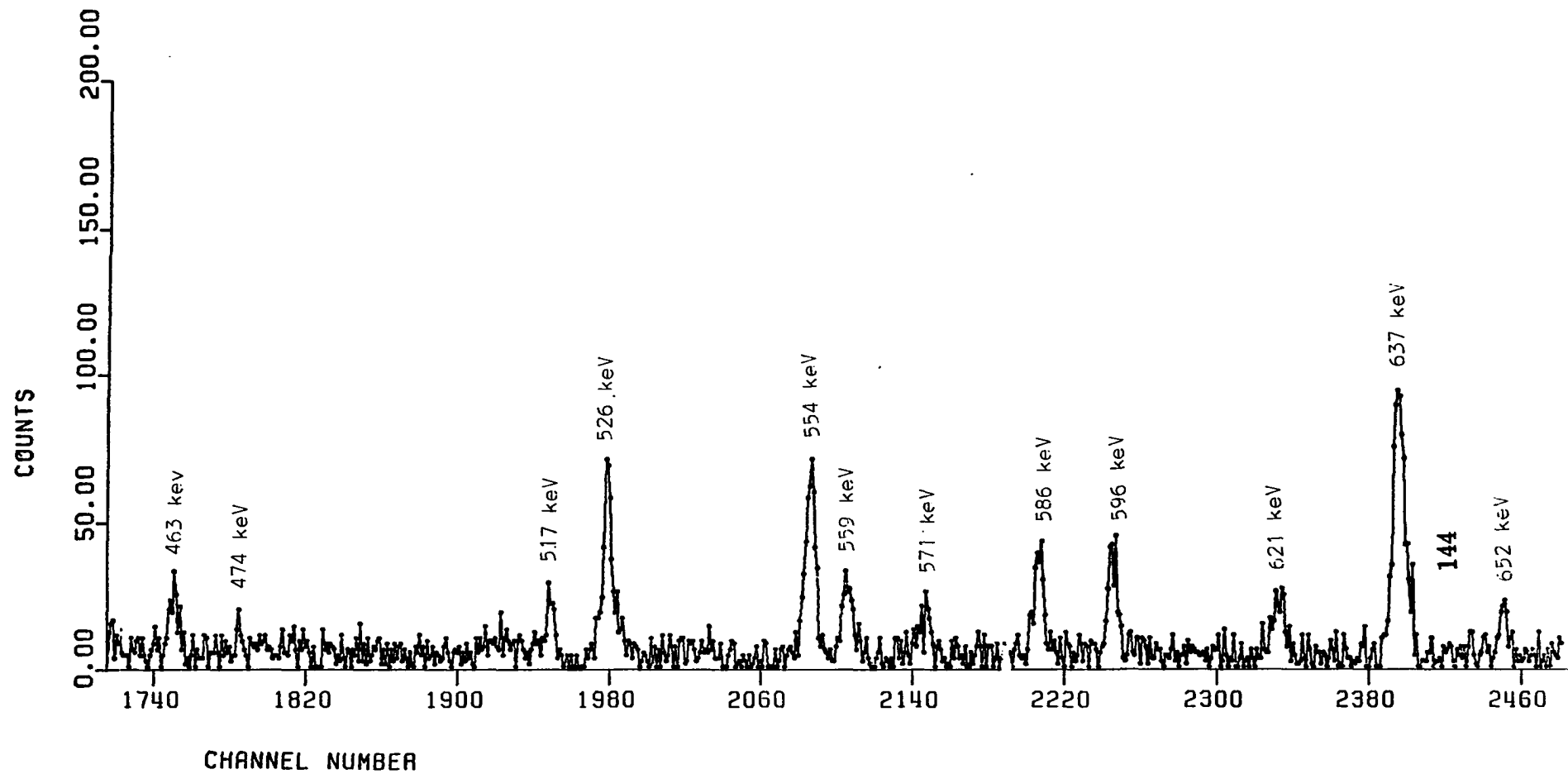


Figure 5.16b. Spectrum in Coincidence with the 199-keV Transition in ^{145}Cs

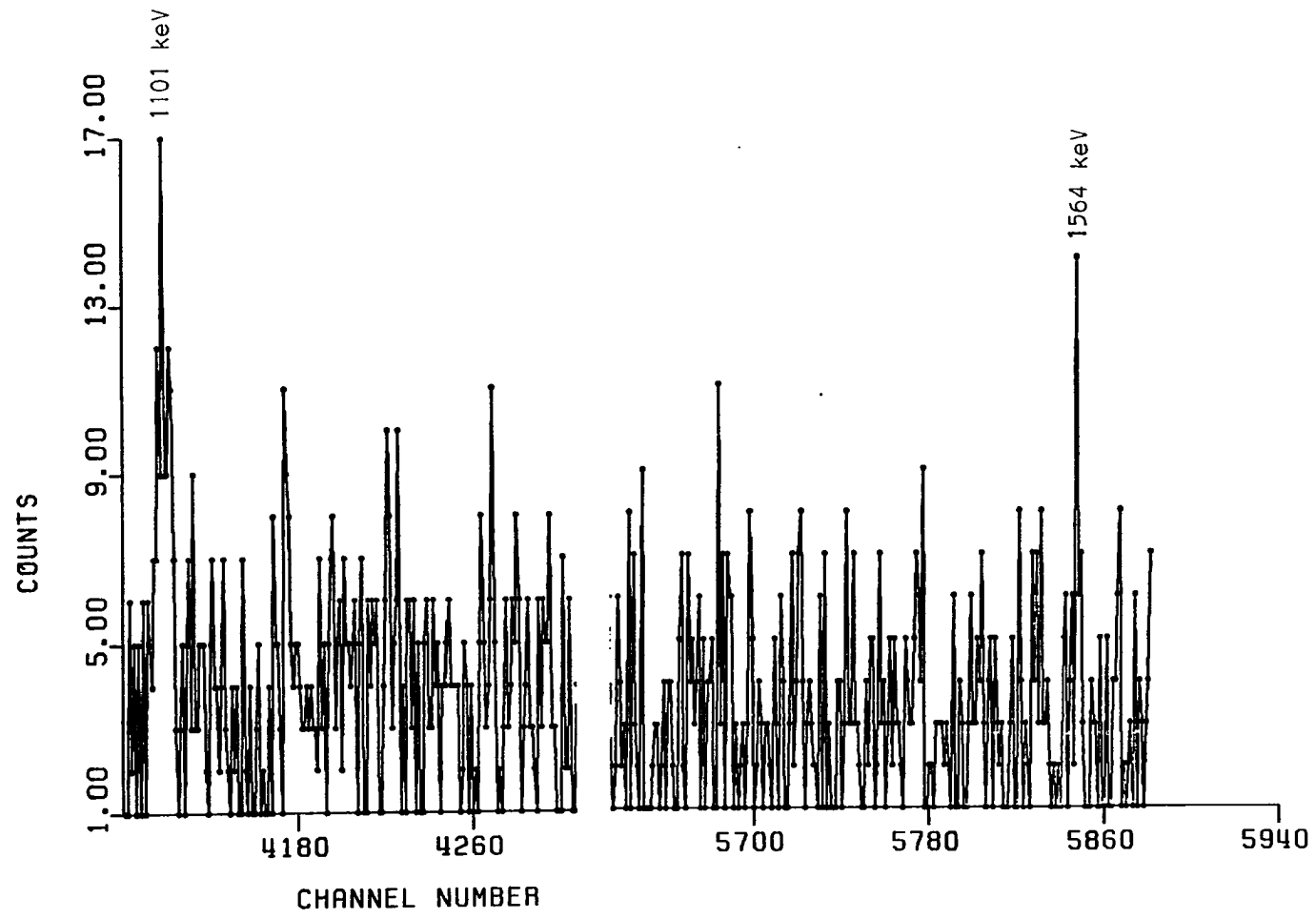


Figure 5.16c. Spectrum in Coincidence with the 199-keV Transition in ^{145}Cs

possible spin assignments can be $\frac{1}{2}$, $\frac{3}{2}$, $\frac{5}{2}$, $\frac{7}{2}$ based on gamma branching from this level.

490-keV Level: The establishment of this level is based on the 379-keV transition in coincidence with the 112-keV transition (see Figures 5.14a-c) and the 214-keV transition in coincidence with the 164-keV transition.

5.3 ^{147}La

The half-life and a decay scheme were published¹⁹ for this nuclide when we started the experiment. The determination of the half-life of ^{147}La was carried out by following the decay of the 117-, 186- and 235-keV strong gamma transitions in ^{147}La . The decay curves for the above transitions are shown in Figure 5.17. A mean half-life of 4.48 ± 0.08 second was obtained from the weighted average of above transitions and the 215-, 399-, 438- and 517-keV transitions following the beta decay of ^{147}La . The measured half-life is in good agreement with previous reported values which are 4.4 ± 0.2 ²⁸ sec and 4.0 ± 0.2 ¹⁰ sec.

The energies and relative intensities of gamma-transitions were determined from gamma singles spectra. The gamma singles spectrum is shown in Figures 5.18. The energies, relative intensities and placements of the observed gamma transitions are given in Table 5.6. The relative intensities of these transitions were normalized to 100 for the 117-keV transition. The assignments of the gamma-ray transitions were based on

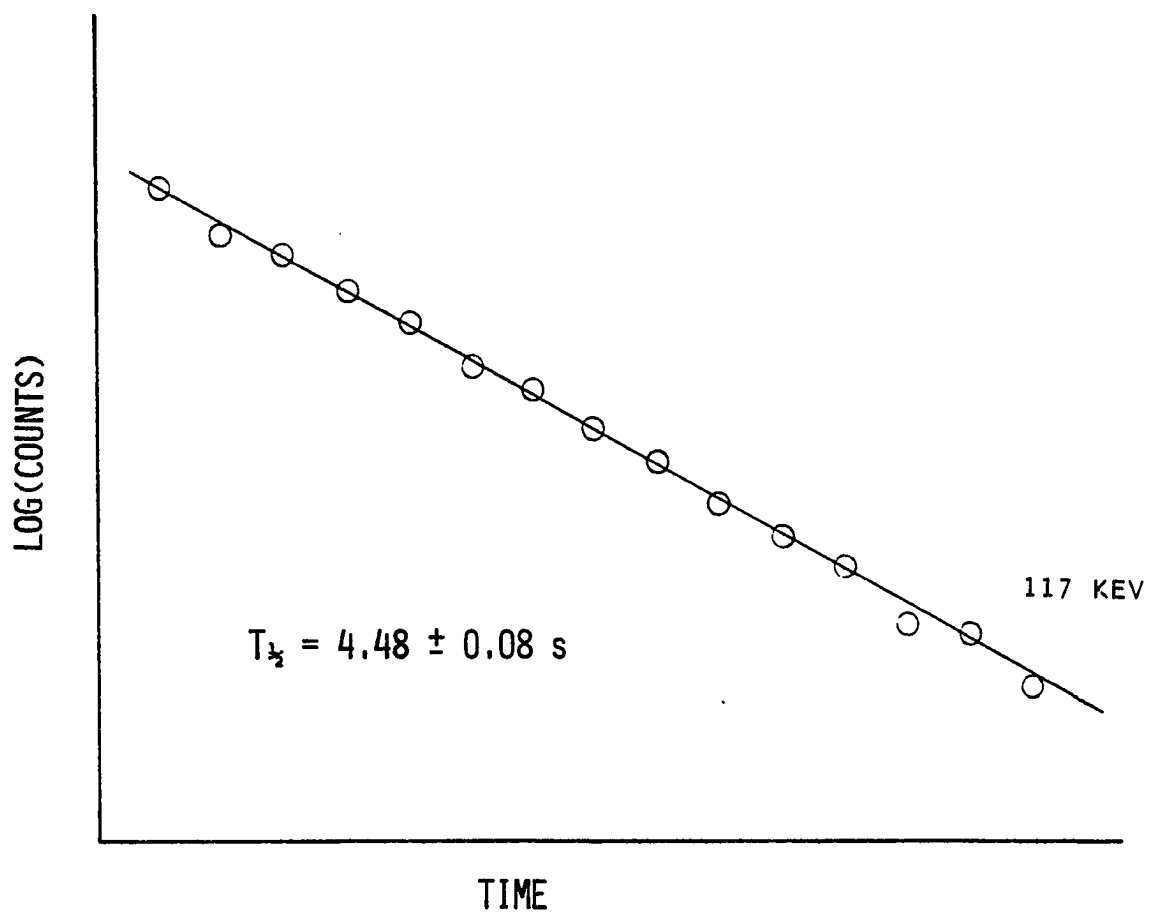


Figure 5.17. Decay Curves of some ^{147}La Transitions

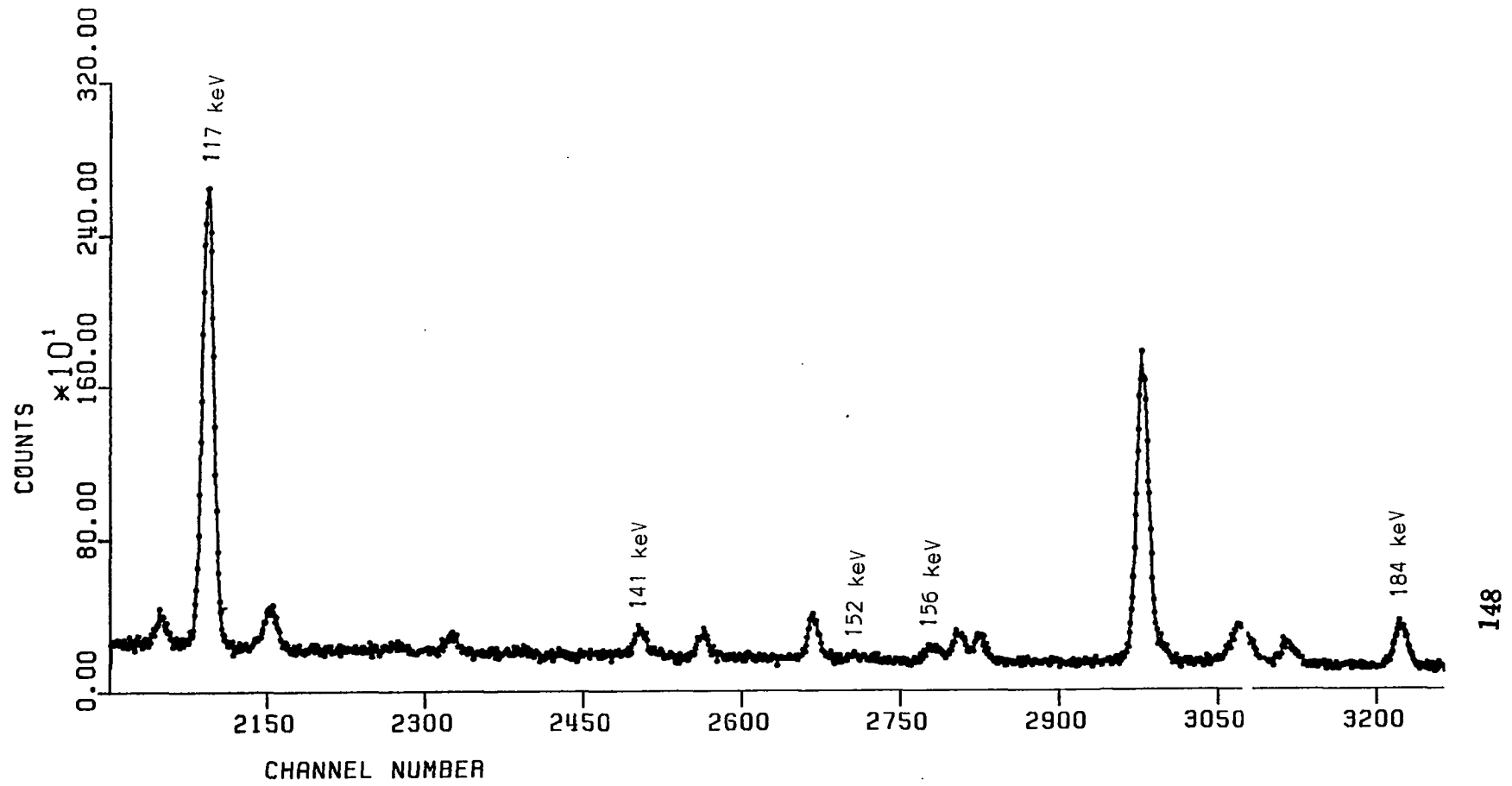


Figure 5.18. Gamma Spectrum from ^{147}La Decay

Table 5.6. The measured energies, intensities of gamma-rays and their placement in decay scheme of ^{147}La . ^aplaced twice in decay scheme. †has not been placed in decay scheme.

| Energy (KeV) | Intensity | Placement |
|--------------------------------|-----------------|-----------|
| 69.50 ± 0.12 | 2.6 ± 0.9 | 186→117 |
| 97.41 ± 0.30 | < 0.5 | 215→117 |
| 117.63 ± 0.01 | 100.0 ± 1.5 | 117→0 |
| 141.66 ± 0.12 | 2.5 ± 0.4 | 495→353 |
| 152.13 ± 0.09 | 2.7 ± 0.4 | 505→353 |
| ^a 156.28 ± 0.13 | 5.4 ± 0.8 | 273→117 |
| | | 558→402 |
| 184.81 ± 0.07 | 4.2 ± 0.7 | 517→332 |
| 186.82 ± 0.02 | 59.6 ± 1.2 | 186→0 |
| 207.10 ± 0.13 | 1.1 ± 0.2 | 608→401 |
| 214.93 ± 0.06 | 24.5 ± 1.2 | 215→0 |
| ^a 215.50 ± 0.03 | 55.1 ± 1.6 | 332→117 |
| | | 402→186 |
| 225.47 ± 0.11 | 2.6 ± 0.5 | 558→332 |
| 235.70 ± 0.01 | 23.1 ± 0.5 | 353→117 |
| 246.13 ± 0.08 | 3.9 ± 0.5 | 432→186 |
| 272.18 ± 0.09 | 1.2 ± 0.4 | 673→401 |
| 273.86 ± 0.05 | 17.7 ± 0.6 | 273→0 |
| 280.01 ± 0.06 | < 0.5 | 495→215 |
| 283.42 ± 0.01 | 23.6 ± 0.5 | 401→117 |
| 292.21 ± 0.10 | 4.4 ± 0.5 | 625→332 |
| 307.93 ± 0.27 | 1.3 ± 0.4 | 495→186 |

Table 5.6, continued

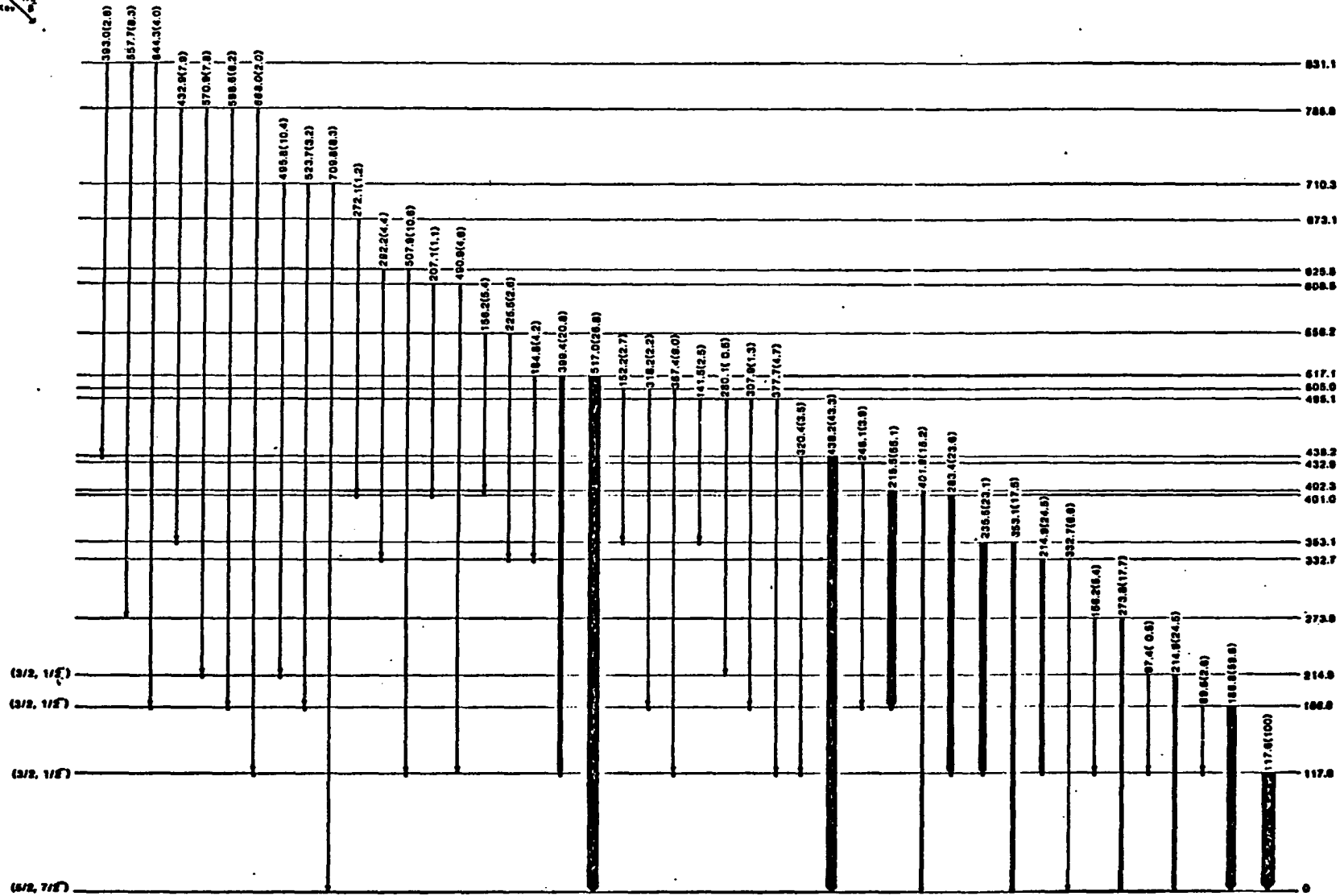
| Energy (KeV) | Intensity | Placement |
|-----------------------------|----------------|-----------|
| 318.24 ± 0.26 | 2.2 ± 0.9 | 505→186 |
| 320.41 ± 0.17 | 3.5 ± 0.8 | 438→117 |
| 332.72 ± 0.08 | 6.6 ± 0.7 | 332→0 |
| 353.17 ± 0.03 | 17.5 ± 0.6 | 353→0 |
| 377.71 ± 0.06 | 4.7 ± 0.4 | 495→117 |
| 387.44 ± 0.05 | 9.0 ± 0.7 | 505→117 |
| 393.04 ± 0.17 | 2.8 ± 0.6 | 831→438 |
| 399.41 ± 0.02 | 20.8 ± 0.7 | 517→117 |
| 401.93 ± 0.03 | 15.2 ± 0.7 | 402→0 |
| 432.91 ± 0.05 | 7.9 ± 0.5 | 785→353 |
| 438.23 ± 0.01 | 43.3 ± 0.6 | 438→0 |
| $^{\dagger}439.91 \pm 0.10$ | 4.3 ± 0.6 | |
| 490.90 ± 0.10 | 4.6 ± 0.6 | 608→117 |
| 495.83 ± 0.05 | 10.4 ± 0.6 | 608→117 |
| 507.91 ± 0.10 | 10.6 ± 0.6 | 626→117 |
| 517.04 ± 0.15 | 26.8 ± 5.7 | 517→0 |
| 523.72 ± 0.10 | 3.2 ± 0.6 | 710→186 |
| 557.70 ± 0.07 | 8.3 ± 0.7 | 831→273 |
| 570.92 ± 0.07 | 7.8 ± 0.8 | 785→215 |
| 598.60 ± 0.11 | 6.2 ± 0.8 | 785→186 |
| 644.37 ± 0.22 | 4.0 ± 0.5 | 831→186 |
| 668.08 ± 0.18 | 2.0 ± 0.5 | 785→117 |
| 709.81 ± 0.15 | 8.3 ± 1.4 | 710→0 |

their half-life, and for those for which the determination of a half-life was not possible the assignment was based on coincidence relationships.

The decay scheme for ^{147}La which has been studied up to 830-keV is shown in Figure 5.19. Coincidence information was obtained by setting gates on more than 50 transitions. Table 5.7 presents the coincidence information extracted from almost ten million coincidence events. Figure 5.20 shows the coincidence spectrum of the 117-keV gate as an example. This data was taken when the cycle was optimized for ^{147}Ba activity, which made the analysis of the data very difficult for ^{147}La . A separate experiment set to optimize the ^{147}La activity was attempted, but because of time limitations and low counting rate this run did not provide enough coincidence events to be useful. An individual low-energy experiment optimized for ^{147}La activity was also performed.

A decay scheme for ^{147}La below 830 keV is proposed (see Figure 5.18) in which 98% of the gamma transitions have been placed. As mentioned earlier a preliminary decay scheme of ^{147}La for energies below 700 keV has been proposed.¹⁹ All the levels in the previous work were confirmed in this work, and eleven more energy levels were added. At the time this work was presented at the 4th International Conference on Nuclei Far from Stability, new work on the $A=147$ chain was also presented by F. Schussler *et al.*⁶⁷ The present work is in agreement with Schussler *et al.*⁶⁷ except for two levels at 359 and 677 keV, which are not supported in this work. The

$^{147}_{57}\text{La}_{90}$
 $T_{1/2} = 4.8 \text{ Dec}$
 $Q_\beta = 47602120 \text{ KeV}$



$^{147}_{57}\text{Ce}_{90}$

Figure 5.18. Decay Scheme of ^{147}La

Table 5.7. The Coincidence relationships of the gamma-rays studied in decay of ^{147}La .
 [] indicates possible coincidence.

| Coincidence Gate (KeV) | Coincidence (KeV) |
|------------------------|---|
| 69.5 | 117, 215, 246, 320, |
| 97.4 | 117, [280], |
| 117.6 | 69, 97, 141, 156, 184, 207, 215, 225, 235, 245, 272, 282, 292, 320, 377, 387, 393, 399, 433, 491, 507, 520, 571, 668, |
| 141.6 | 117, |
| 152.13 | 117, 235, 353, |
| 156.6 | 117, 186, [215], 402, |
| 184.8 | 117, 215, |
| 186.8 | 215, 246, 307, 318, [320], 439, 523, 586, 598, 644, |
| 207.1 | 117, 215, 283, |
| 214.9 | 117, 184, 225, 280, 290, 495, 570 |
| 215.5 | [69], 186 |
| 225.4 | 117, 215, |
| 235.7 | 117, 141, 433, 438, |
| 246.1 | 69, 186, |
| 272.1 | 117, 283 |
| 273.8 | 557, |
| 280.1 | [97], 215, |
| 283.4 | 117, 207, 272, |
| 292.2 | 215, |
| 307.9 | 186, |

Table 5.7, continued

| Coincidence Gate (KeV) | Coincidence (KeV) |
|------------------------|--------------------|
| 318.2 | 186, |
| 320.4 | 117, |
| 332.7 | 184, 292 |
| 353.1 | [141], 432 |
| 377.7 | 117, |
| 387.4 | 117, |
| 393.0 | 117, [320], 438, |
| 399.4 | 117, |
| 401.9 | 156, |
| 432.9 | 117, 235, 353, |
| 438.2 | [393], |
| 439.9 | 117, |
| 490.9 | 117, |
| 495.8 | [97], 215 |
| 507.9 | 117, |
| 517.0 | |
| 523.7 | [69], 186, |
| 557.7 | [117], [156], 273, |
| 570.9 | [97], 117, 215, |
| 598.6 | [69], 186, |
| 644.3 | [69], 186, |
| 668.0 | 117, |

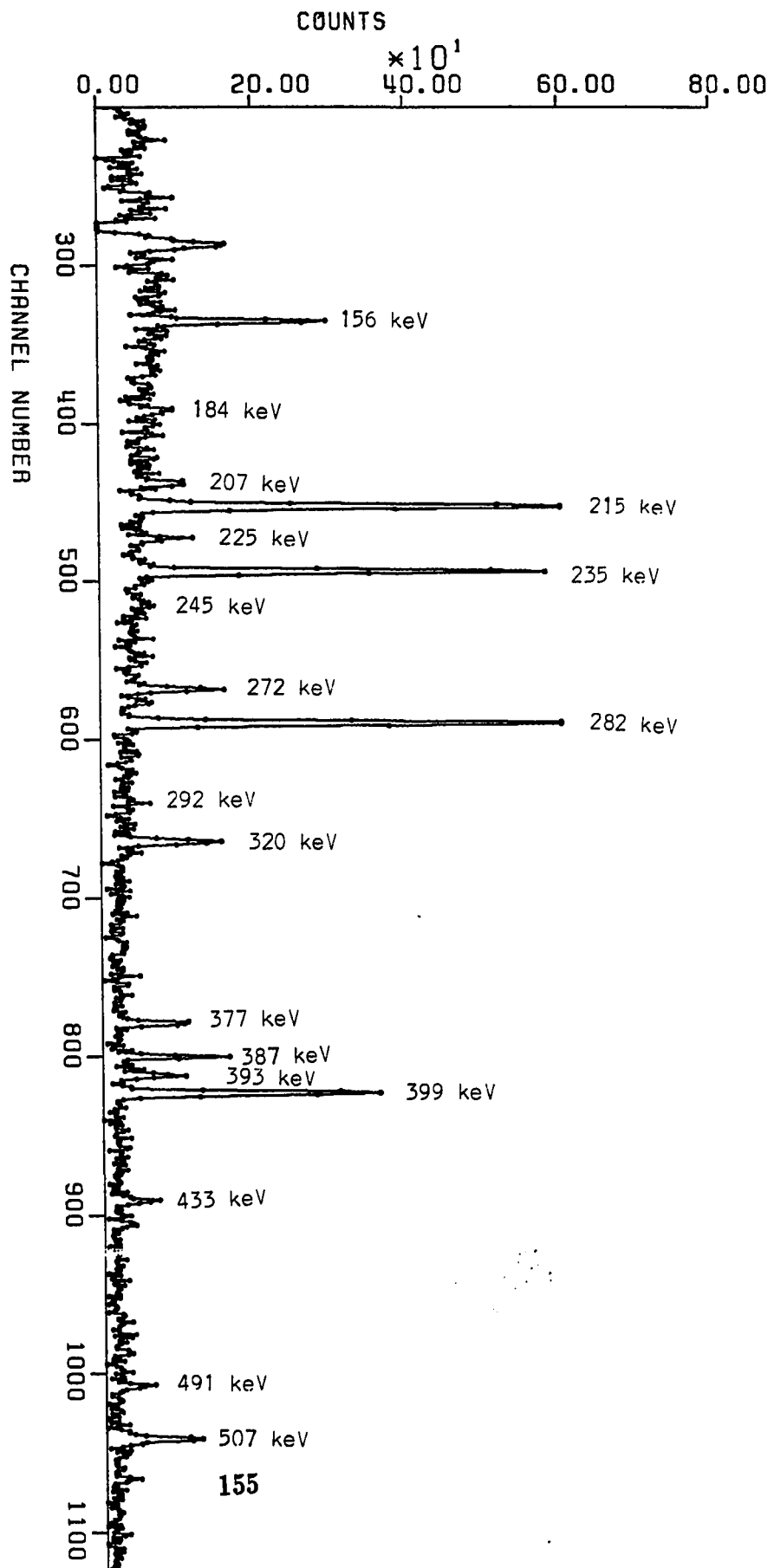


Figure 5.19. Spectrum in Coincidence with the 117-keV
Transition in ^{147}La

present work is also in agreement with reference 19 except for the placement of the 161- and 495-keV gamma transitions. The levels at 401 and 402 keV which could not be resolved in the previous work¹⁹ have been resolved. Since there are no direct measurement of I^π of either ^{147}La or ^{147}Ce which makes a definite spin assignment for any other level impossible, there is no basis for a discussion of spin assignments in this nucleus.

CHAPTER VI

DISCUSSION

6.1. Introduction

The experimental results presented in the previous chapter provide some important information and knowledge about three important odd- A nuclides. This information enables the systematics of two transition regions to be extended. In the discussion below the systematics of Yttrium isotopes are compared with those of Strontium and Zirconium. For the Ba and Ce nuclei systematics of Barium and Cerium isotopes and $N=89$ isotones in this region are compared. Finally a comparison of results from the present experiments will be compared with shell model, Nilsson model and IBM calculations for these regions.

6.2. The Onset of Deformation in $A \sim 100$ Region

^{89}Y falls into the new region of deformation around $A \sim 100$ discovered a few years ago. This region lies in the limiting region of proton number between magic numbers 28 and 50 ($28 < Z < 50$) and neutron number between 50 and 82 ($50 < N < 82$). The proton shell model states

between 28 and 50 are $p_{3/2}$, $f_{5/2}$, $p_{1/2}$, $g_{9/2}$, and the neutron states between 50 and 82 are $g_{7/2}$, $d_{5/2}$, $h_{11/2}$, $d_{3/2}$, $s_{1/2}$ (see Figure 2.7).

The spectroscopy of even-even nuclei⁶³ reveals a different behavior for this region of deformation. The transition from spherical to deformed shape is not a smooth transition, it is rather sudden (see Figure 6.1). A drastic lowering of the 2_1^+ level in ^{88}Sr , ^{100}Zr and ^{102}Mo indicates a sudden change in nuclear shape. The onset of deformation in this region of $Z=38$ to 42 occurs between $N=58$ to 60. It is believed that different nuclear shapes coexist for ^{88}Sr and ^{100}Zr in this narrow transitional region.^{42,68} It is of great interest to study an odd- A nucleus such as ^{89}Y whose neutron numbers lie exactly on the border of this shape transition boundary. As mentioned in Chapter I and Section 2.2.1, the n - p interaction is responsible for the deforming tendency. Deformation occurs when neutron and proton simultaneously fill spin-orbit partner orbitals with very good spatial overlap, in this case $1g_{7/2}$ and $1g_{9/2}$. Calculations have been carried out by Federman and Pittell for Zr and Mo isotopes based on a unified shell model theory explained in Chapter II.

To date there have been no theoretical predictions made for ^{89}Y . The information available is solely experimental, and discussion involves a comparison with the systematics of neighbouring nuclei. Figure 6.2 shows the systematics of odd- A Yttrium isotopes ^{85}Y , ^{87}Y , and ^{89}Y . Immediately evident is the considerable lowering of the excited states of ^{89}Y which

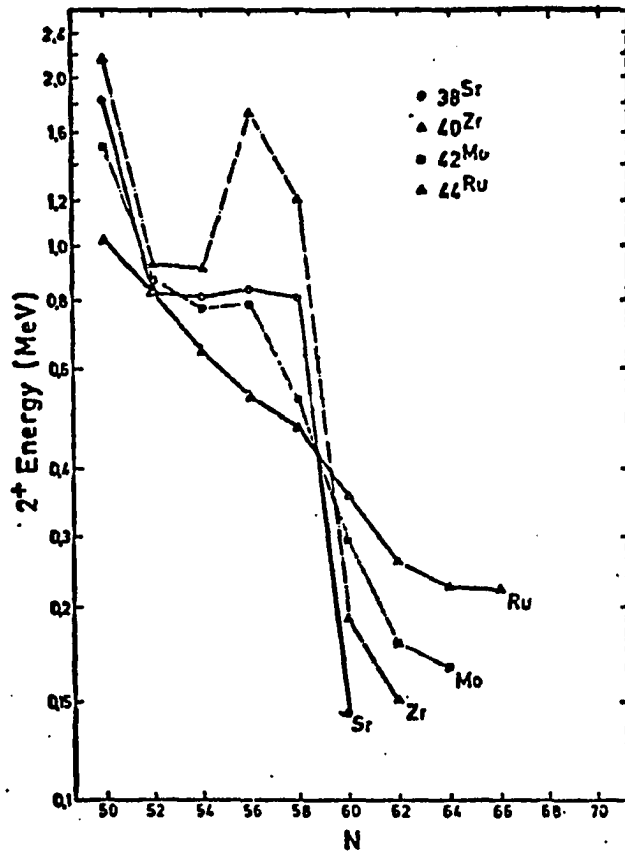


Figure 6.1. Systematics of E_{2^+} versus Neutron Number in the $A \approx 100$ Region

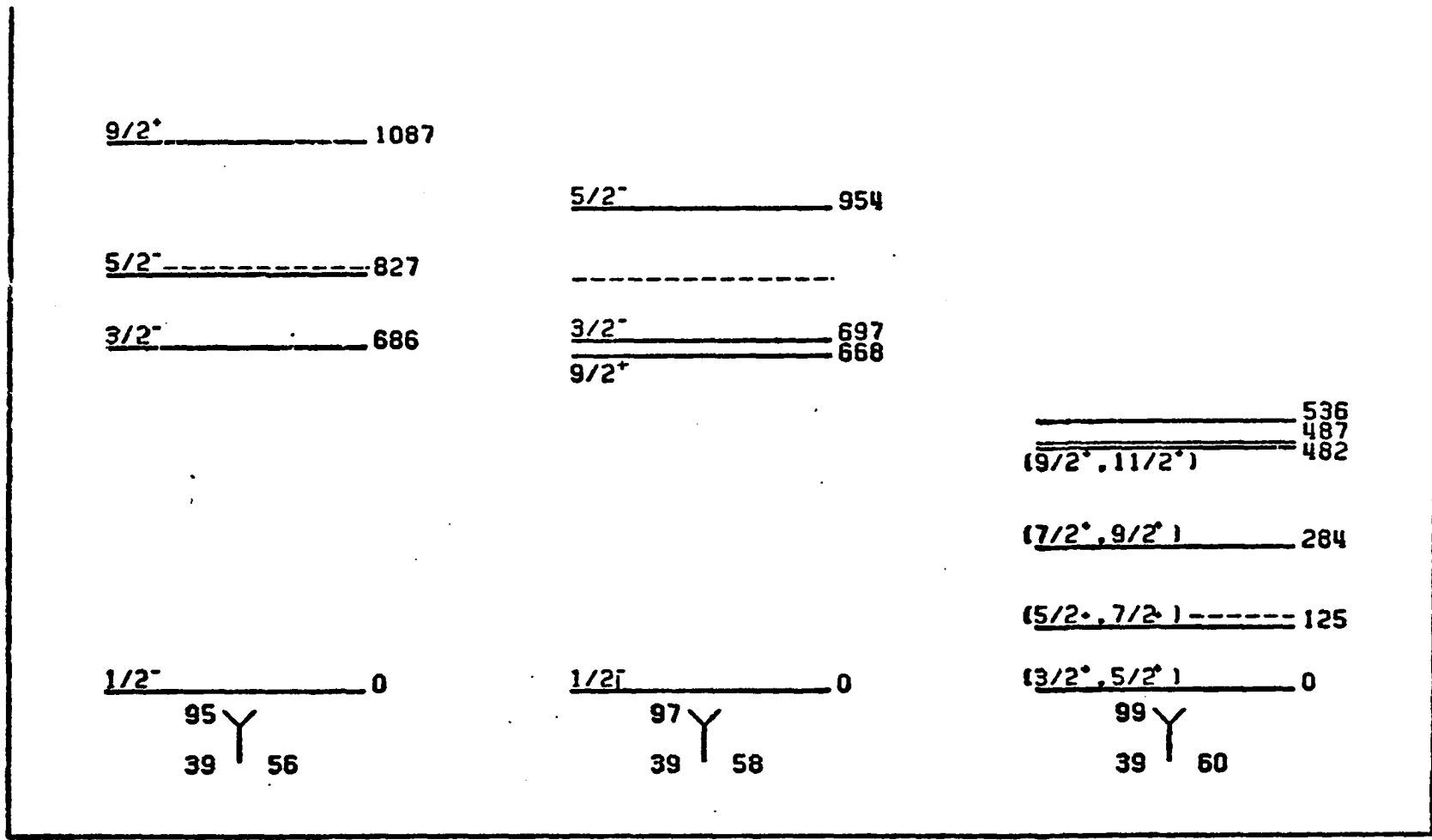


Figure 6.2. Level Systematics for Odd-A Yttrium Isotopes

generally indicates a transition toward a deformed shape. The deformation of ^{99}Y can be seen from the different features of its decay scheme compared to the lighter odd Yttrium isotopes. The SPSM would predict a $p_{1/2}$ orbital for the 39th proton, which would imply a ground state spin and parity of $1/2^-$. This is the case in ^{95}Y and ^{97}Y , but ^{99}Y with $5/2^+$ ground-state shows a completely different character. To understand the origin of the $5/2^+$ ground state of ^{99}Y it is necessary to examine the positive parity $1g_{9/2}$ in ^{95}Y and ^{97}Y . The $1g_{9/2}$ level in ^{95}Y lies above 1 MeV but $1g_{9/2}$ level in ^{97}Y comes down and lies below 700-keV. As mentioned in Chapter II, when neutrons are added the probability of occupation of the $1g_{7/2}$ neutron orbit and $1g_{9/2}$ proton orbit increases. Clearly as the number of neutron goes to 60 the $1g_{9/2}$ proton orbit becomes a large part of the ^{99}Y ground state as can be seen from the data. The $5/2^+$ assignment can be understood from the fact that the ^{98}Sr core has become deformed and so the ideas of the Nilsson model must be applied. The appropriate Nilsson diagram for this region is shown in Figure 6.3. To obtain a $5/2^+$ state for the 39th proton a deformation parameter greater than 0.26 is required as indicated in Figure 6.3. The relevant Nilsson orbital would be $5/2^+$ [422] orbital, which then would be the ground state assignment for ^{99}Y .

The low-lying negative parity levels in ^{95}Y can be understood by viewing ^{95}Y as a $p_{1/2}$ proton coupled to the ^{94}Sr core. The 2_1^+ level of ^{94}Sr is indicated in Figure 6.2 by a dashed line. Coupling the $p_{1/2}$ proton to a

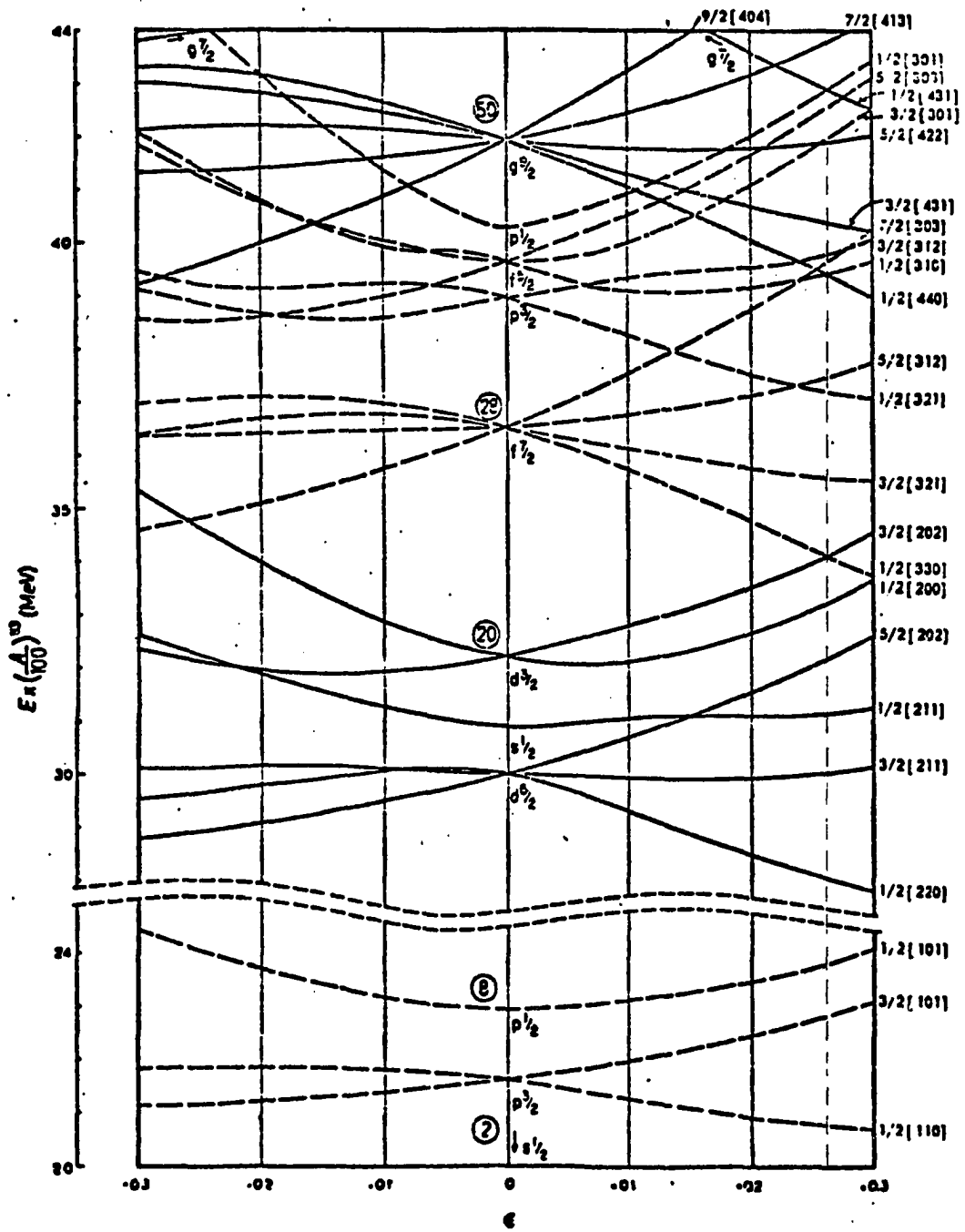


Figure 6.3. Nilsson Diagram for Protons or Neutrons with $Z < 50$

one-phonon core vibration would give two states of $I^\pi = 3/2^-$ and $5/2^-$. Similarly ^{87}Y can be viewed as ^{86}Sr core coupled to a $p_{1/2}$ proton. The dashed line in Figure 6.2 shows the energy of the 2_1^+ one-phonon level of ^{86}Sr . The $3/2^-$ and $5/2^-$ levels in the spectrum are again the result of this coupling.

Figure 6.4 shows the systematics of two of the $N=60$ isotones for odd A nuclei. The magnetic and quadrupole moments have been measured for ^{87}Rb .⁷⁹ The large quadrupole moment that was obtained indicates a large deformation for the ground state of ^{87}Rb . A unique Nilsson orbit of $3/2^+$ [431] for the 37th proton has been assigned to the ground state of this nucleus. This is completely consistent with the assignment of $5/2^+$ [422] in ^{89}Y .

The level spacing of the three first excited states in ^{89}Y suggests the existence of a rotational band built on the ground state. If this is correct this would be the first rotational band observed in an odd mass nucleus in the $A \sim 100$ regions. In a recent report Monnard *et al.*⁴⁶ present evidence for a ground-state rotational band in ^{89}Y . This investigation was based on the decay of a μs isomer with very high spin. The ground-state rotational band have been observed up to very high spin ($19/2^+$). The energies of the band levels have been well reproduced using the rotating nucleus formula:²¹

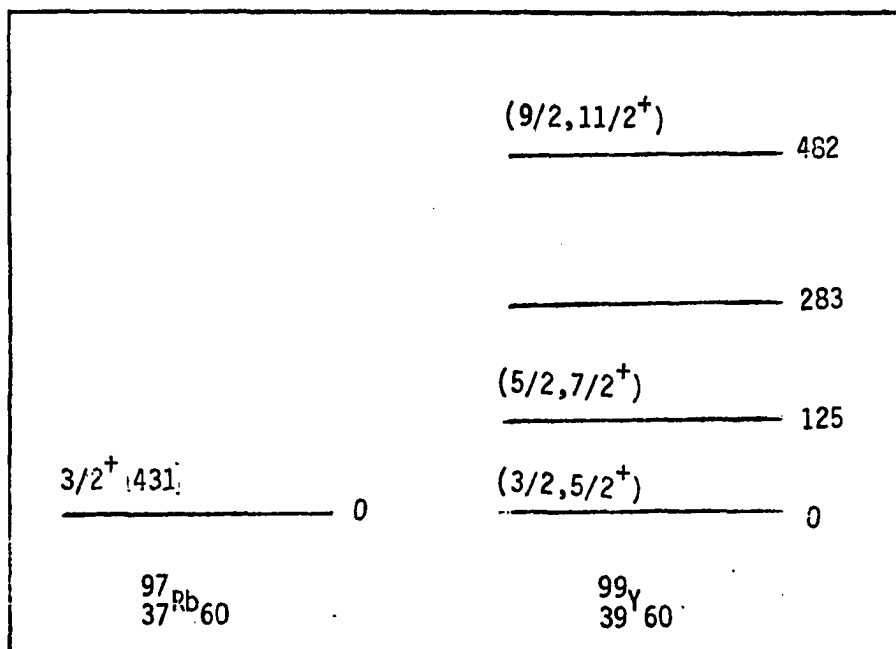


Figure 6.4. Level Systematics for Odd-A Nuclei with $N=60$

$$E(I, k) = E_0 + AI_x^2 + BI_x^4 + A_{2k}(-1)^{I+k} \frac{(I+k)!}{(I-k)!}$$

where $I_x^2 = I(I+1) - k^2$. The fit was made for both $k=3/2$ and $k=5/2$ ground-state, and the best fit was obtained with $k=5/2$ (see Figure 6.5). In Figure 6.5 this fit has been compared with the experimental data. The origin of the spin and parity assignment for the ^{90}Y ground state comes from this work.

6.3. The Onset of Deformation $A \sim 150$ Regions

The Barium and Cerium isotopes studied in this work have proton numbers between the magic numbers 50 and 82 ($50 < Z < 82$) and neutron numbers N between the magic numbers 82 and 126 ($82 < N < 126$). The proton shell model states between 50 and 82 are $g_{7/2}$, $d_{5/2}$, $h_{11/2}$, $d_{3/2}$, and $s_{1/2}$. The neutron states between 82 and 126 are $f_{7/2}$, $h_{9/2}$, $f_{5/2}$, $p_{3/2}$, $i_{13/2}$, $p_{1/2}$. These nuclei lie at the edge of the rare-earth region which includes nuclides from $A=150$ to 190 and has been very well studied near the line of stability. Different collective models have successfully described the phenomena in the rare-earth region, but shell model calculations in this region are impossible to perform and to interpret, because of the number of parameters involved.

The onset of deformation is indicated by a drop in the energy of the 2_1^+ level and an increase in the energy ratio of the 4_1^+ to the 2_1^+ level

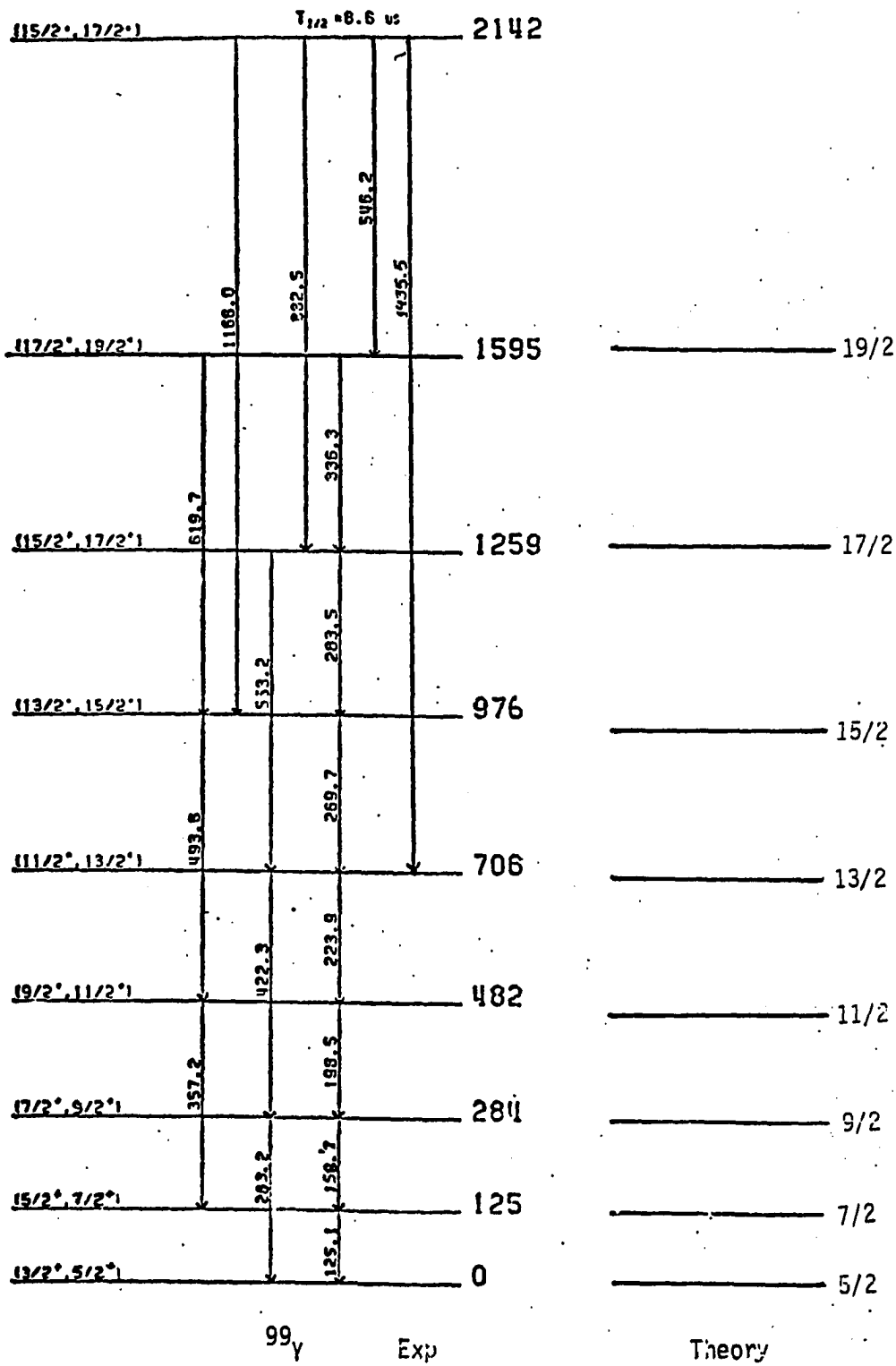


Figure 6.5. Experimental and Calculated Ground-State Rotational Band in the ^{99}Sr Lohengrin-Josef Data

for even-even nuclei. For nuclei with $64 < Z < 58$ this onset is observed to occur as N goes from 88 to 90. However, for Ba ($Z=56$) isotopes the onset of nuclear deformation appears to be between $N=86$ and 88. Therefore, Ce ($Z=58$) with $N=89$ is situated in the transition region and Ba ($Z=56$) with $N=89$ is on the edge of the deformed region. Several $N=89$ isotones have been extensively studied.^{40,41} The nuclei ^{149}Nd , ^{151}Sm , and ^{153}Gd have been studied through β decay or particle reactions. However, not much data existed on the decay of ^{145}Cs until the present work. A preliminary level scheme has been reported for ^{147}Ce from the β decay of ^{147}La , but this was not a detailed investigation.⁴¹ There have been no theoretical calculations performed for either ^{145}Ba or ^{147}Ce . The following discussion therefore is based on a comparison of systematics of odd- A barium and odd- A cerium isotopes and $N=89$ isotones. Figures 6.6, 6.7 and 6.8 show the systematics of odd- A barium, odd- A cerium and the $N=89$ isotones respectively. A comparison of the $N=89$ isotones (Figure 6.8) from ^{153}Gd to ^{149}Nd shows a very low-energy (less than 50-keV) excited state in all of these nuclides. A search for the similar very-low-energy transitions was made for both ^{145}Cs and ^{147}La . No low-energy gamma-ray associated with ^{147}La decay was identified. A 22-keV transition associated with the decay of ^{145}Cs was identified, but it has not been placed in the decay scheme.

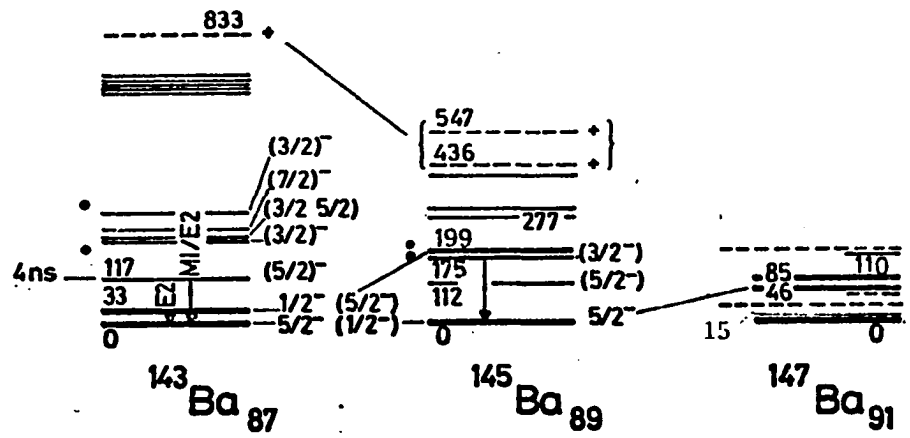


Figure 6.6. Systematics for Odd-A Ba Isotopes

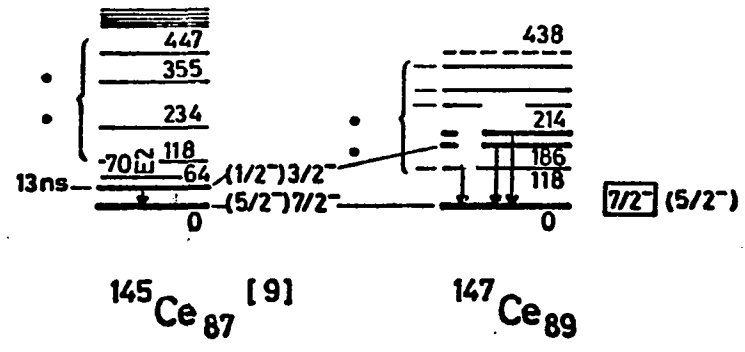


Figure 6.7. Systematics of Odd-A Cerium Isotopes

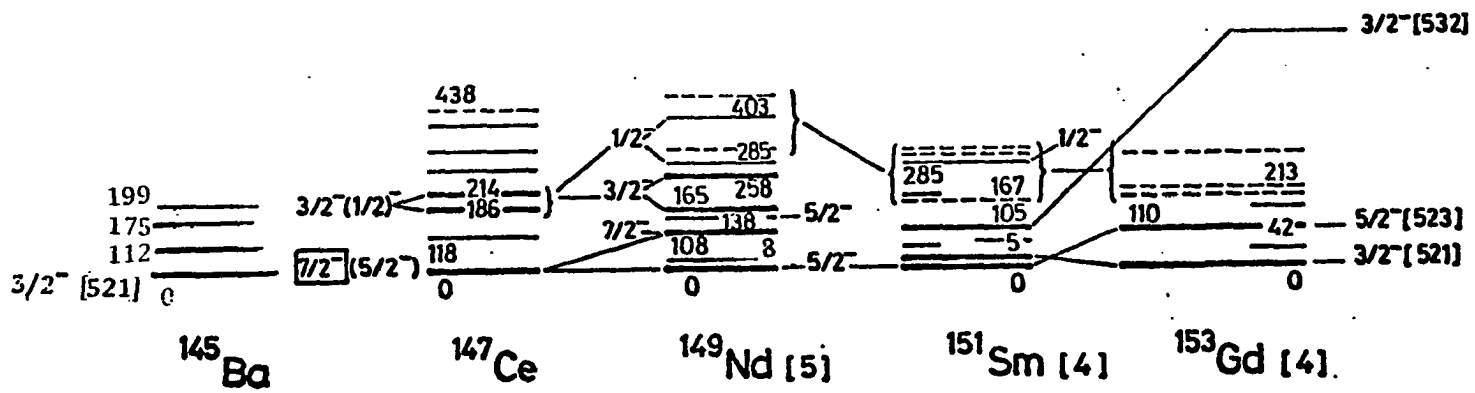


Figure 6.8. Systematics for $N=89$ Isotones

More experimental data are needed to tie down the relationship of the 22-keV transition with the other transitions in ^{145}Cs decay.

No direct measurement of the ground-state spin has been made for ^{147}Ce . Systematics of odd- A cerium isotopes (Figure 6.7) indicate the possibility of $I^\pi = 7/2^-$ or $5/2^-$ for ground state of this nucleus. The systematics of the $N=89$ isotones, however, favors the $I^\pi = 5/2^-$ assignment for the ground state. The Nilsson diagram for neutron number between 82 and 126 (Figure 6.9) may be used as a guide to understanding the possible spin assignment for ^{147}Ce . If the ground state is $5/2^-$ a deformation parameter less than 0.1 can be assigned to this nucleus. In this case two negative intrinsic states ($1/2^-$ and $3/2^-$) should be seen among the low-lying levels. However, if the ground state is $7/2^-$, it would appear that ^{147}Ce is spherical or slightly deformed.

Conversion-electron experiments have been performed on ^{147}La by Schussler *et al.*⁶⁷ and an E_2 multipolarity has been assigned to the 186- and 215-keV transitions by their K/L ratios. This would lead to $I^\pi = \frac{1}{2}^-$ for both of these levels when the ground state $I^\pi = \frac{5}{2}^-$. If the ground-state spin and parity is considered to be $\frac{7}{2}^-$, the spin and parity for the two excited states mentioned above would be $\frac{3}{2}^-$. Also seen from the Nilsson diagram, the absence of positive parity states at low energy is another feature which indicates that the ^{147}Ce is spherical or only very weakly deformed (Figure 6.9). These results are quite in agreement with what one

might expect from the smooth transition from spherical to deformed nuclei in this region. But to make this claim a fact, more experimental data is needed, especially spin and parity determinations.

The ground-state spin of ^{145}Ba has been measured by the collinear laser spectroscopy technique, and spin of $3/2$ was assigned to the ground state.⁵⁰ From the Nilsson diagram (Figure 6.9) it is clear that a negative parity is the only choice for a nucleus with the $N=89$ and a ground-state spin equal to $3/2$. A deformation parameter of 0.1 up to 0.15 and a unique Nilsson orbit of $3/2^- [521]$ can be assigned to this nucleus. The ground state spin of ^{145}Cs was measured also, using on-line atomic resonance, and $I^\pi = 3/2^+$ was assigned to the ground state of this nucleus.²⁷ A conversion-electron experiment has been performed on ^{145}Cs , and multipolarities have been deduced for some of the transitions.⁵⁵ An $M1$ multipolarity was assigned to the 112- 175- 199- 241-keV transitions according to their K/L ratios, and an E_1 multipolarity for the 435-keV transition based on the absence of K conversion electrons for this gamma transition. The $I^\pi=3/2^-$ assignment for the ground state of ^{145}Ba and the above multipolarities lead to a $(1/2 - 5/2)^-$ spin and parity assignment for the 112- 175- 199- 416-keV levels and a $(1/2 - 5/2)^+$ assignment for the 435-keV level. The deduced beta branchings to these levels are consistent with first forbidden transitions. To understand the structure of ^{145}Ba

better and to tie down the deformation for this nucleus, angular correlation experiments are needed.

6.4. Conclusion

The three neutron-rich nuclei ^{99}Y , ^{145}Ba , ^{147}Ce have been studied in this work. Gamma singles, gamma multiscale, and gamma-gamma coincidence experiments were performed using the activity from an on-line fission product mass separator. The energy levels and gamma transitions from most of the energy levels for these nuclei have been established for the first time. Evidence for deformation was observed in ^{99}Y . Shell-model calculations which explain the origin of deformation in these regions were discussed and were used to explain the experimental data. For the new strongly deformed region around $A \approx 100$ the theory accounts qualitatively for the main features of what has been observed, but still more data is needed, especially atomic hyperfine structure measurements to obtain the ground state spins of ^{99}Sr and ^{99}Y . Angular-correlation measurements would also yield needed spin information which could be used to tie down the Nilsson assignments of this odd- A nucleus. Angular correlation experiments for these nuclei is not presently feasible due to low counting rate.

The level scheme of ^{145}Ba was established for the first time, and the experimental data for ^{145}Ba and ^{147}Ce extend the knowledge

of systematic trends of $N=89$ isotones to more neutron-rich nuclei. The spin and parity of $I^\pi = 3/2^-$ for the ground state of ^{145}Ba implies a slight deformation for this nucleus.

Theoretical calculations have been performed in transitional $N=89$ nuclei. It has been shown that the level energies can be successfully described in the particle-rotor model with Nilsson single-particle orbit.⁵⁶ Also a calculation using the Interacting Boson Model (IBM) has been made using the IBM for even-even Sm isotopes in the transitional region by Scholton.⁶¹ The experimental energy levels are reproduced very well. The IBM is capable of describing the main features of the even-even nuclides in the transitional region around $A \sim 150$, even in its simplest form (IBM1) where there is no distinction made between neutron and proton bosons. It is hoped that these calculations will be extended to even-even nuclei in the $A \simeq 100$ region. The IBFM has been applied to some odd- A nuclei (such as ^{101}Rh and ^{149}Eu to ^{155}Eu) by Schelton,³⁷ and the unique parity levels in these nuclei were very well reproduced. The author had planned to carry out some of these calculations, but the time limitation did not allow it. It is hoped that the work which is presented here will be continued to include measurements of multipolarities and spins and parities of low-lying states in these nuclides. Theoretical interpretation of the result of the present work would be possible only when such experimental data are available.

REFERENCES

- ¹ F. Ajzenberg-Selove, *Nucl. Phys.* **A190**, 1 (1972)
- ² S. Amiel, G. Engler, Y. Nir-El and M. Shmid, *Nucl. Inst. and Meth.* **139**, 305 (1976)
- ³ S. Amiel, Y. Nir-El, M. Shmid, A. Venezia and I. Wismontsky, *Proc. Int. Conf. on Electromagnetic Isotope Separator*, 412 (Skövde, Sweden, 1973)
- ⁴ A. Arima and F. Iachello, *Ann. Phys.* **111**, 201 (1978)
- ⁵ A. Arima and F. Iachello, *Ann. Phys.* **99**, 253 (1976)
- ⁶ A. Arima and F. Iachello, *Ann. Rev. Nucl. Part. Sci.* **31**, 75 (1981)
- ⁷ A. Arima and F. Iachello, *Phys. Rev. Lett.* **35**, 1069 (1975)
- ⁸ A. Arima, F. Iachello, *Phys. Rev. Lett.* **40**, 385 (1978)
- ⁹ A. Arima, T. Ohtsuka, F. Iachello and I. Talmi, *Phys. Lett.* **66B**, 205 (1977)
- ¹⁰ F. Ajzenberg-Selove, *Nucl. Phys.* **A190**, 1 (1972)
- ¹¹ P. O. Aronsson, G. Skarnemark and M. Skarestad, *J. Inorg. Nucl. Chem.* **36**, 1689 (1974)

- ¹² D. A. Arseniev, A. Sobiczewski and V. G. Soloviev, *Nucl. Phys.* **A139** (1969)
- ¹³ N. Auerbach and I. Talmi, *Nucl. Phys.* **64**, 458 (1965); D. H. Gloeckner, *Nucl. Phys.* **A253**, 301 (1975)
- ¹⁴ I. Bergstrom, *Proc. of the International Symposium on Why and How We Should Investigate Nuclides Far from the Stability Line*, W. Forsling, C. S. Herrlan and H. Ryder, editors (Almquist and Wiksell, Stockholm) *Arkiv fur Fysik* **36** (1966)
- ¹⁵ H. G. Börner, W. F. Davidson, J. Almeida, J. Blachot, J. A. Pinston, and P.H.W. VanAssche, *Nucl. Inst. Meth.* **186**, 165 (1981)
- ¹⁶ Yardley Beers, *Introduction to the Theory of Error*, (1957) p. 46
- ¹⁷ Philip R. Bevington, *Data Reduction and Error Analysis for the Physical Sciences*, (1969) p. 36
- ¹⁸ J. Blachot, H. P. Bocquet, E. Monnard, B. Pfeiffer, F. Schussler, H. Lawin, T. A. Khan, W. D. Lauppe, G. Sadler, H. A. Selic, K. Sistemich *et al.*, *KFA-IKP* 10/77 (1977) p. 49
- ¹⁹ J. Blachot and G. Fiche, *At. Data Nucl. Data Tables* **20**, 241 (1977)
- ²⁰ A. Bohr and B. R. Mottelson, *Mat.Fys.Medd.Dan.Vid.Selsk.* **27**, 16 (1953)
- ²¹ A. Bohr and B. R. Mottelson, *Nuclear Structure*, **2** (New York, Amsterdam, Benjamin Inc., 1975) 31
- ²² M. E. Bunker and C. W. Reich, *Rev. Mod. Phys.* **43**, 348 (1971)

- ²³R. F. Casten and J. A. Cizewski, *Nucl. Phys.* **A309** (1978)
- ²⁴E. R. Cheifetz, C. Jared, S. G. Thompson and J. B. Wilhelmy, *Phys. Rev. Lett.* **25**, 38 (1970)
- ²⁵R. E. Chrien, M. L. Stelts, V. Manzella, R. L. Gill, F. K. Wohn and J. C. Hill, *Inst. Phys. Conf. Ser. No. 51*, 44 (1980)
- ²⁶S. DeBenedetti, *Nuclear Interaction* (Robert E. Krieger Pub. Co., Huntington NY, 1974) 115
- ²⁷C. Ekström, L. Robertsson, G. Wannberg and J. Heinemeier, *Phys. Scr.* **19**, 516 (1979)
- ²⁸G. Engler, Y. Nir-El, M. Shmid and S. Amiel, *Phys. Rev. C* **19**, 1948 (1979)
- ²⁹ P. Federman and S. Pittel, *Phys. Lett.* **69B**, 385 (1977)
- ³⁰ P. Federman, S. Pittel and R. Campos, *Phys. Lett.* **82B**, 9 (1979)
- ³¹P. Federman and S. Pittel, *Phys. Lett.* **77B**, 29 (1978)
- ³²P. Federman and S. Pittel, *Phys. Rev.* **C20**, 820 (1979)
- ³³ Fourth Int. Conf. on Nuclei Far from Stability (Helsingor, Denmark, 1981)
- ³⁴R. L. Gill, M. L. Stelts, R. E. Chrien, V. Manzella, H. Liou and S. Shostak, *Nucl. Inst. Meth.* **186**, 243 (1981)
- ³⁵G. Gneuss and W. Greiner, *Nucl. Phys.* **A171** (1971) 449
- ³⁶B. Harmatz and W. B. Ewbank, *Nucl. Data Sheets* **25**, 113 (1978)

- ³⁷ F. Iachello, *Interacting Boson-Fermion System in Nuclei* (Plenum Press, New York, London, 1981) 285
- ³⁸ F. Iachello and A. Arima, *Phys. Lett. B* **53**, 309 (1974)
- ³⁹ J. D. Jackson, *Classical Electrodynamics* (John Wiley and Sons, Inc., 1962)
- ⁴⁰ R. Katajanheimo and E. Hammaren, *Phys. Scr.* **19**, 497 (1979)
- ⁴¹ R. Katajanheimo, *Phys. Scr.* **22**, 321 (1980)
- ⁴² T. A. Khan, W. D. Lauppe, K. Sistemich, H. Lawin, G. Sadler and H. A. Selic, *Z. Phys.* **A283**, 105 (1977)
- ⁴³ E. Koglin, G. Jung, G. Siegert, R. Decker, K. D. Wunsch and H. Wollnik, *Z. Phys.* **A288**, 319 (1978)
- ⁴⁴ K. Kumar, *Nucl. Phys.* **A231**, 189 (1974)
- ⁴⁵ C. M. Lederer and V. S. Shirley (Eds.), *Table of Isotopes*, Seventh Edition (Wiley, 1978)
- ⁴⁶ G. Lovhoiden, J. R. Lien, S. El-Kazzaz, J. Rekstad, C. Ellegaard, J. R. Bjerregaard, J. Knudsen and P. Kleinheinz, *Nucl. Phys. A* **339**, 477 (1980)
- ⁴⁷ M. Mayer and J. Jensen, (John Wiley and Sons Inc., New York, 1955) 58
- ⁴⁸ J. R. McConnell and W. L. Talbert, Jr., *Nucl. Inst. Meth.* **128**, 277 (1975)

- ⁴⁹E. Monnard, J. A. Pinston, F. Schussler, B. Pfeiffer, H. Lawin,
G. Battistuzzi, K. Shizuma and K. Sistemich, *Z. Phys. A*
306, 183 (1982)
- ⁵⁰R. Neugart, *Nucl. Inst. Meth.* **186**, 165 (1981)
- ⁵¹ S. G. Nilson and K. Danske, *Vidensk.Selsk.Mat.Fys.Medd.* **9**,
No. 16 (1955)
- ⁵²J. M. Norman, W. L. Talbert, Jr., and D. M. Roberts, *Ames Report*
IS-1893 (1968)
- ⁵³ EG&G ORTEC Manual for Ge(Li) detector
- ⁵⁴T. Otsuka, A. Arima, F. Iachello and I. Talmi, *Phys. Lett.* **76B**, 139 (1978)
- ⁵⁵T. Otsuka and A. Arima, *Phys. Lett.* **77B**, 1 (1978)
- ⁵⁶T. Otsuka, Ph.D. Thesis, University of Tokyo, Japan (1979)
- ⁵⁷B. Pfeiffer, E. Monnard, J. A. Pinston, F. Schussler, G. Jung, J. Munzel
and H. Wollnik, *Proc. 4th Int. Conf. on Nuclei Far From Stability*
(Helsingør, Denmark, 1981)
- ⁵⁸S. Pittel, P. D. Duval and B. R. Barret, *Bull. of the APS* (Oct. 1982)
- ⁵⁹ M. A. Preston and R. K. Bhaduri, *Structure of the Nucleus*
(Addison-Wesley Pub. Co. Inc., 1975) 370
- ⁶⁰M. S. Rapaport, G. Engler, A. Gayer and I. Yoresh, *Z. Phys.* **A305**,
359 (1982)
- ⁶¹J. Rekstad, E. Osnes and G. Lovhoiden, *Phys. Lett.* **62B**, 15 (1976)
- ⁶²J. J. Sakurai, *Advanced Quantum Mechanics* (Addison-Wesley, 1967)

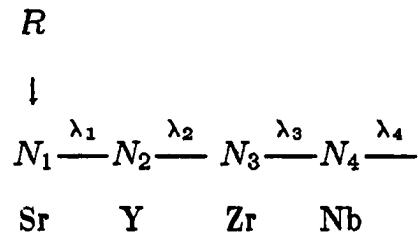
- ⁶³W. C. Schick, Jr., "PEAKFIND," *Ames Report IS-3636* (1975)
- ⁶⁴W. C. Schick, Jr., "SKEWGAUS," *Ames Report IS-3460* (1974)
- ⁶²O. Scholton, F. Iachello and A. Arima, *Ann. Phys.* **115**, 325 (1978)
- ⁶³O. Scholton, *Proc. 1st Sym. on Interacting Bosons in Nuclear Physics*,
Erice, Sicily 1, 17 (1978)
- ⁶⁴F. Schussler, B. Pfeiffer, H. Lawin, E. Monnard, J. Münzel, J. A. Pinston
and K. Sistemisch, *Proc. 4th Int. Conf. on Nuclei Far From
Stability*, Helsingor (1981) 589
- ⁶⁸F. Schussler, J. A. Pinston, E. Monnard, A. Moussa, G. Jung, E. Koglin,
B. Pfeiffer, R.V.F. Janssens and J. Van Klinken, *Nucl. Phys.* **A339**,
415(1980)
- ⁶⁹H. A. Selic, G. Sadler, T. A. Khan, W. D. Lauppe, H. Lawin, K. Sistemich,
E. Monnard, J. Blachot, J. P. Bocquet and F. Schussler, *Z. Phys.*
A289, 197 (1979)
- ⁷⁰R. K. Sheline, I. Ragnarsson and S. G. Nilsson, *Phys. Lett.*
41B, 115 (1972)
- ⁷¹M. Shmid, Y. Y. Chu, G. M. Gowdy, R. L. Gill, H. Liou, M. L. Stelts,
R. E. Chrien, R. F. Petry, H. Dejbakhsh, C. Chung and D. S.
Branner, *Proc. 4th Int. Conf. on Nuclei Far From Stability*
(Helsingor, Denmark, 1981) 576
- ⁷²M. Shmid, Y. Nir-El, G. Engler and S. Amiel, *Nucl. Inst. and Meth.*
144, 60 (1977)

- ⁷³ M. Shmid, private communication
- ⁷⁴ M. Shmid, to be published
- ⁷⁵ K. Siegbahn, *Alpha-Beta and Gamma-Ray Spectroscopy* (North Holland Pub. Co.: Amsterdam, 1968)
- ⁷⁶ R. M. Steffen and K. Alden, *The Electromagnetic Interaction in Nuclear Spectroscopy*, Ch. 13, Ed. W. D. Hamilton (North Holland Pub. Co., Amsterdam, 1975)
- ⁷⁷ W. L. Talbert, Jr., *Proceedings of the Isotope Separator On-Line Workshop*, Brookhaven National Lab, 4 (1977)
- ⁷⁸ I. Talmi, *Rev. Mod. Phys.* **34**, 704 (1962)
- ⁷⁹ Thibault *et al.*, *Phys. Rev. C* **23**, 2720 (1981)
- ⁸⁰ Third Int. Conf. on Nuclei Far From Stability (Cargese, France, 1976)
- ⁸¹ B. L. Tracy, J. Chaumont, R. Klapisch, J. M. Nitschke, A. M. Poskanzer, E. Roeckl and C. Thibault, *Phys. Lett.* **34B**, 277 (1971)
- ⁸² K. Wünsch, H. Gunther, G. Sieger and H. Wollnik, *J. Phys. A: Math. Nucl. Gen.* **6**, L93 (1973)
- ⁸³ L. Wilets and M. Jean, *Phys. Rev.* **102**, 788 (1956)
- ⁸⁴ F. K. Wohn, *Ames Report IS-4270* (1977)

APPENDIX A

The buildup and decay of the activity deposited on the moving tape collector is as follows:

For the case of ^{90}Sr , if we ignore the production and decay of ^{90}Rb (which is not an unrealistic approximation) and consider only one primary product with a production rate of R , then one can write



The initial conditions on this decay chain are:

$$\boxed{N_1(t=0) = N_2(t=0) = N_3(t=0) = 0}$$

The rate of change of the number of Sr nuclei deposited on the tape is then:

$$\frac{dN_1}{dt} = R_1 - N_1\lambda_1 \tag{1}$$

for which a solution of the form

$$N_1 = (a_1 e^{-\lambda_1 t} + b_1) \tag{2}$$

is suggested. From the initial conditions, $a_1 + b_1 = 0$ or $a_1 = -b_1$.

Substituting Eq. (2) into Eq. (1):

$$-\lambda_1 a_1 e^{-\lambda_1 t} = R_1 - \lambda_1 a_1 e^{-\lambda_1 t} - \lambda_1 b_1$$

Since this equation must hold for all times, a_1 and b_1 must satisfy the relations

$$a_1 = -\frac{R_1}{\lambda_1}, \quad b_1 = \frac{R_1}{\lambda_1}$$

Substituting these into equation (2) gives

$$N_1 \lambda_1 = R_1 (1 - e^{-\lambda_1 t}) \quad (3)$$

where

$$N_1 \lambda_1 = A_1 \quad \text{activity of } {}^{89}\text{Sr}$$

For the second member in the chain:

$$\frac{dN_2}{dt} = N_1 \lambda_1 - N_2 \lambda_2 \quad (4)$$

and the solution is of the form

$$N_2 = (a_2 e^{-\lambda_1 t} + b_2 e^{-\lambda_2 t} + c_2) \quad (5)$$

The initial conditions give $a_2 + b_2 + c_2 = 0$. Substituting (5) into (4) yields

$$-a_2 \lambda_1 e^{-\lambda_1 t} - b_2 \lambda_2 e^{-\lambda_2 t} = R_1 - R_1 e^{-\lambda_1 t} \lambda_1 - a_2 \lambda_2 e^{-\lambda_1 t} - b_2 \lambda_2 e^{-\lambda_2 t} - c_2 \lambda_2$$

from which a_2 , b_2 and c_2 may be obtained as above. This gives

$$N_2\lambda_2 = \frac{R_1\lambda_2}{\lambda_2-\lambda_1}(e^{-\lambda_2 t} - e^{-\lambda_1 t}) + R_1(1 - e^{-\lambda_2 t})$$

$$N_2\lambda_2 = A_2 \quad \text{activity of } {}^{90}\text{Y}$$

The rate of change of the third member of the chain (${}^{90}\text{Zr}$) is

$$\frac{dN_3}{dt} = N_2\lambda_2 - N_3\lambda_3 \quad (6)$$

and the trial solution is:

$$N_3 = (a_3 e^{-\lambda_1 t} + b_3 e^{-\lambda_2 t} + c_3 e^{-\lambda_3 t} + d_3) \quad (7)$$

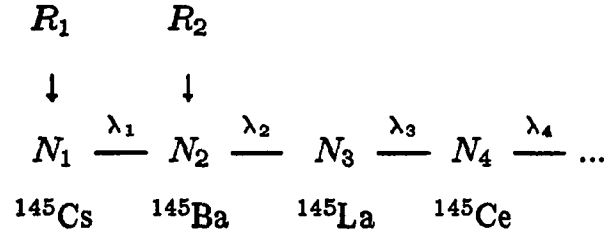
for which initial condition is $a_3 + b_3 + c_3 + d_3 = 0$.

Substituting Eq. (7) into Eq. (6) and solving for the coefficients as before gives

$$N_3\lambda_3 = \frac{R_1\lambda_2\lambda_3}{(\lambda_2-\lambda_1)(\lambda_3-\lambda_1)}(e^{-\lambda_3 t} - e^{-\lambda_1 t}) - \frac{R_1\lambda_2\lambda_3}{(\lambda_2-\lambda_1)(\lambda_3-\lambda_2)}(e^{-\lambda_3 t} - e^{-\lambda_2 t}) + \frac{R_1\lambda_3}{(\lambda_3-\lambda_2)}(e^{-\lambda_3 t} - e^{-\lambda_2 t}) + R_1(1 - e^{-\lambda_3 t})$$

$$N_3\lambda_3 = A_3 \quad \text{activity of } {}^{90}\text{Zr}$$

The situation is different for the $A=145$ chain, because two members of the chain were produced in the primary beam. If R_1 and R_2 are the initial rates of production of the first two isobars,



The solution for ${}^{145}\text{Cs}$ is the same as that for ${}^{90}\text{Sr}$:

$$N_1\lambda_1 = R_1(1 - e^{-\lambda_1 t})$$

$$N_1\lambda_1 = A_1 \quad \text{activity of } {}^{145}\text{Cs}$$

For the Ba nuclei

$$\frac{dN_2}{dt} = R_2 + N_1\lambda_1 - N_2\lambda_2 \quad (8)$$

The solution can be written as

$$N_2 = (a_2 e^{-\lambda_1 t} + b_2 e^{-\lambda_2 t} + c_3) \quad (9)$$

and the general solution is

$$N_2\lambda_2 = \frac{R_1\lambda_2}{(\lambda_2 - \lambda_1)}(e^{-\lambda_2 t} - e^{-\lambda_1 t}) + (R_1 + R_2)(1 - e^{-\lambda_2 t})$$

$$N_2\lambda_2 = A_2 \quad \text{activity of } {}^{145}\text{Ba}$$

For third member of isobaric chain ${}^{145}\text{La}$ the rate of change can be written

$$\frac{dN_3}{dt} = N_2\lambda_2 - N_3\lambda_3 \quad (10)$$

and the trial solution is:

$$N_3 = (a_3 e^{-\lambda_1 t} + b_3 e^{-\lambda_2 t} + c_3 e^{-\lambda_3 t} + d_3. \quad (11)$$

Substituting (11) into (10)

$$\begin{aligned} N_3 \lambda_3 = & \frac{R_1 \lambda_2 \lambda_3}{(\lambda_2 - \lambda_1)(\lambda_3 - \lambda_1)} (e^{\lambda_3 t} - e^{-\lambda_1 t}) \\ & - \frac{R_1 \lambda_2 \lambda_3}{(\lambda_2 - \lambda_1)(\lambda_3 - \lambda_2)} (e^{-\lambda_3 t} - e^{-\lambda_2 t}) + \\ & \frac{(R_1 + R_2) \lambda_3}{(\lambda_3 - \lambda_2)} (e^{-\lambda_3 t} - e^{-\lambda_2 t}) + (R_1 + R_2)(1 - e^{-\lambda_3 t}) \end{aligned}$$

$$N_3 \lambda_3 = A_3 \quad \text{activity of } ^{145}\text{La}$$

APPENDIX B

In this appendix the list of programs which have been used for analysis of data and short description of each one is given. The computer program PEAKFIND is design to find (determine the peak centroid) and fit peaks in spectra. The peak finding procedure is to examine the smoothed second difference between adjacent channels in the spectrum to locate the peaks. The condition for identification of a peak have deliberately been made very loose, so that the program can find everything that might possibly be a peak.

The the fitting procedure in PEAKFIND is similar to that which is used in the FORTRAN program SKEWGAUS. Only the fitting procedure in SKEWGAUS will be discussed here. The fitting of an analytic function to a peak in the semiconductor detector spectrum is complicated because the shape of these peaks is influenced by different factors. For example the statistical fluctuation in the number of charge pairs formed in the detector tends to create a Gaussian peak shape. Noise in the detector and electronics has a similar effect. Incomplete charge collection in the detector tends to produce a tail on the low energy side of the peak. The fitting function in both programs is Gaussian, and an exponential tail has been smoothly

joined on the lower side. This function is found to provide a shape for the peak very close to that of experimental data. The function used for fitting is shown in Figure B.1. The function has seven variables:

h - peak height (counts)

χ_0 - centroid (channels)

FWHM - full width at half maximum of Gaussian (channels)

τ - distance from centroid to junction of the exponential tail (channels)

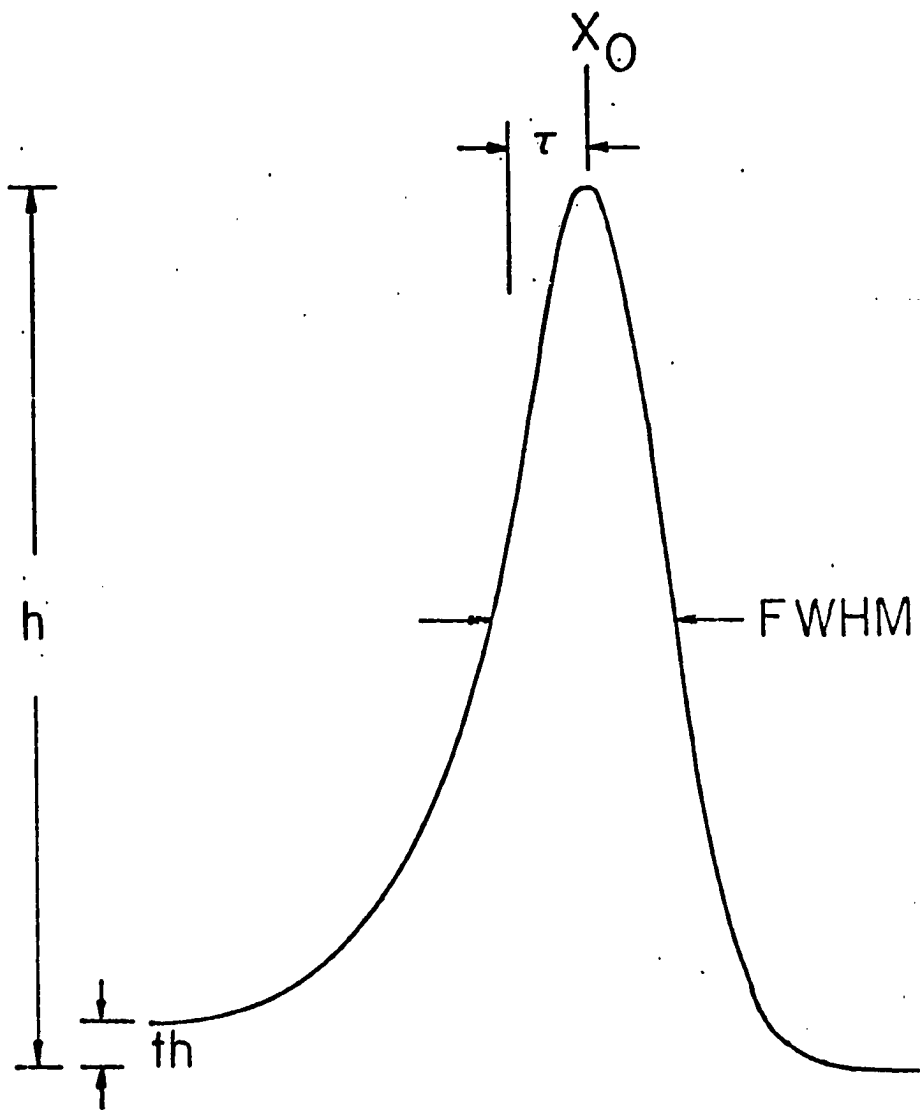
t - ratio of tail height to peak height (dimensionless)

a - lower skewness parameter (dimensionless)

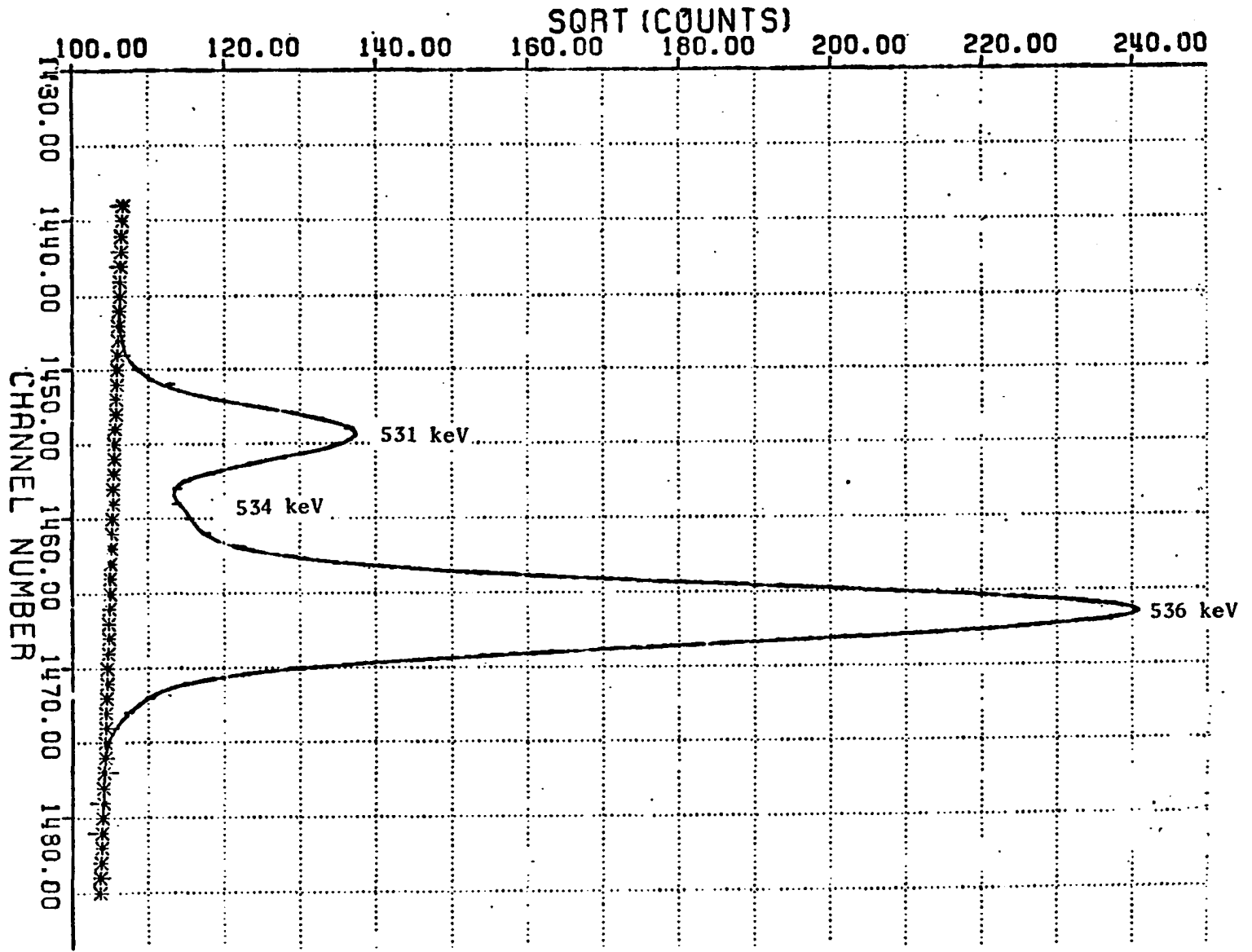
b - upper skewness parameter (dimensionless)

For most of peaks the three last parameters can be set equal to zero and still get a very good fit to data. Most of the time it is necessary to include two or more peaks in a single fit region (especially in a complicated spectrum such as Cs and Ba) because the peaks are not separated well enough to be fit individually. The fit function then becomes a sum of up to 13 terms of the form for a single fit function. A multi-peak fitting is shown in Figure B.2.

The computer code DRUDGE uses the output file of SKEWGAUS which contains peak centroid, peak area and peak heights and errors associate with each quantity, as an input file. The centroid and area are used



B-1. Function Used for Peak Fitting



B-2. An Example of Peak Fitting for 530-537 keV Region in ⁹⁹Sr Beta Decay

in this program to determine the energy and intensity. In this program the non-linearity of the system is taken into account.

Another computer code ATP which also has fitting capability has been developed at BNL. This program was used to determine the peak centroid and area, but the function that was used for fitting was not as complicated as the one used at in SKEWGAUS.

The computer code GMPLLOT has been developed at OU for the purpose of plotting the data. Another plotting code PNLX has been used at BNL.

The computer code DLE has been used to scan the coincidence data. This program was available only at BNL.

For scanning GMS data a computer code DLK was available at BNL. This program also did gain shift and summing of the spectra.

A decay program was available at BNL, and one also was developed at OU. A linear least square straight line was fitted to the logarithm of the data points.

A few computer programs were developed at OU to read and convert the data created at BNL on the PDP 11/20 to a suitable format for the VAX.